공학박사 학위논문

Biomass Enhancement in *Chlamydomonas reinhardtii* using Steady C/N Ratio Microfluidic Perfusion Bioreactor, Vibrational Stress Priming, and Malate Synthase Expression

미세유체 관류 배양기의 C/N 비율 유지, 진동 자극 프라이밍, 말릭산 합성 효소의 발현을 통한 *Chlamydomonas reinhardtii*의 생체량 증대

2018년 8월

서울대학교 대학원

협동과정 바이오엔지니어링

백 상 민

Biomass Enhancement in *Chlamydomonas reinhardtii* using Steady C/N Ratio Microfluidic Perfusion Bioreactor, Vibrational Stress Priming, and Malate Synthase Expression

by

Sang-Min Paik

Advisor : Professor Noo Li Jeon, Ph.D.

August, 2018

Interdisciplinary Program for Bioengineering

Graduate School

Seoul National University

ABSTRACT

Biomass Enhancement in *Chlamydomonas reinhardtii* using Steady C/N Ratio Microfluidic Perfusion Bioreactor, Vibrational Stress Priming, and Malate Synthase Expression

Sang-Min Paik

Interdisciplinary Program for Bioengineering

The Graduate School

Seoul National University

Microalgae, a photosynthetic microorganism, has recently attracted attention as an effective resource for both renewable energy and food security. This is because sequestration of more CO_2 and composition of more nutrition than terrestrial plants help microalgae mitigate climate change and secure food shortage in the future. Therefore, efficient process operation on microalgae cultivation is of importance. In

this dissertation, three strategies were developed and applied to enhance microalgal biomass productivity with less time and cost at large-scale.

The first one is cultivation with steady unbalanced C/N ratio. Microalgae-derived secondary metabolites include antioxidants (lutein, astaxanthin, etc) and neutral lipids (TAG), most of which are useful substances. These substances are produced in cells cultivated in a nutrient-depleted environment. In order to improve total productivity, increase in microalgal biomass should be accompanied well with increase in intracellular content. Thus, traditional nutrient depletion method can no longer be viable drastically constraining cellular growth. Recently, cultivation with unbalanced C/N ratio has been reported to increase biomass at a certain level simultaneously with TAG content increase. However, because batch process also has depleted nutrient over time, this method has the same limitations for enhancement of total products yield as traditional methods. In this study, continued supply of low concentrations of nutrients with the maintenance of unbalanced C/N ratio was proposed to enhance secondary metabolites production A microfluidic continuous perfusion system was designed and tested to culture microalgae, *Chlamydomonas reinhardtii*, under constant nutrient concentration slightly lower than normal condition with high C/N ratio. When cultured in 7.5%/7.5% of NH_4^+ /PO_4^{2-}, *C. reinhardtii* showed a 2.4-fold increase in TAG production with a 3.5-fold increase

in biomass compared to level obtained under an only NH_4^+ depleted condition. This is because nutrients continue to be supplied in small quantities without depletion of nutrients. Maintaining the unbalanced C/N ratio can improve the total TAG productivity by increasing the biomass.

The second is cellular stress response preparedness against turbulence in bioreactors. Turbulence agitates all the nutritional components for cellular proliferation. However, severe hydrodynamic shear fields by the turbulence decreases cell viability that detrimentally influence maximum yieldable biomass. Vibrational wave treatment has been used to increase proliferation of microalgae. When directly applied at large scale, however, it costs much setting up massive vibration generating system, and turbulence can offset positive effects of vibration on microalgae proliferation. Stress priming is the phenomenon that primed cells with activated stress response by milder stress can prepare themselves for harsh stress and exhibit greater survival rate. In this study, vibration pretreatment (between 10–30 Hz and 0.15–0.45 G) was used to prime the cells for enhanced biomass. When exposed to 10 Hz at 0.15 G for 72 h and inoculated in baffled flasks of large shear fields (0.292 Pa for the average wall shear force (aveWSF) and 184 s^{-1} for the average shear strain rate (aveSSR)), microalgae showed 27% increase in biomass as well as 39% increase in corresponding amount of heterologous protein (*i.e.* GFP-3HA). The

level of *TRP11* transcript was increased both at vibration treatment and at shaking cultivation. Ca^{2+}-signaling pathway closely relates with stress response. In plants, calmodulin (CaM)-binding transcription factor (CAMTA) is involved in expression of CBF/CREB1 master transcriptional regulator under stressful conditions. Although Ca^{2+}-signaling pathway in *Chlamydomonas* has not yet been studied in detail, our results show that stress primed microalgae with vibrations can lead to improved proliferation that results in increased biomass production at industrial scale bioprocesses.

Last but not at least, cellular metabolism itself could be additionally activated by malate. Malate has a close relation to biomass increase. High uptake of malate leads to biomass increase, reducing non-growth associated coefficient (maintenance energy). In addition, in plants, efficient distribution of intracellular malate to organelles was also elucidated to relate to biomass. Redox balance, especially in chloroplast, is carried out with reducing equivalents such as NADPH. Because its pool should be tightly regulated to maintain its capacity, intermediate metabolite, malate, play a role as an high potential energy carrier without disturbing reducing equivalents pool, and the malate is exported to other organelles. In this study, transgenic *Chlamydomonas* expressing malate synthase in chloroplast was developed. Stable expression of malate synthase enables malate production in

chloroplast and distribution of more malate could be carried out in the transgenic cells. Transgenic *Chlamydomonas* under glyoxylate treatment showed 19% more increase in microalgal biomass than wild-type. By RNA analysis, the levels of malate dehydrogenase (*MDH4*) in TCA cycle, acetyl-CoA synthetase (*ACS3*), and isocitrate lyase (*ICL1*) and malate synthase (*MAS1*) of glyoxylate shunt, were significantly more expressed, which was consistent with reported metabolic flux analysis of heterotrophic cultivated cells. More meticulous analysis are necessary, but, in the transgenic microalgae with malate synthase overexpression, the metabolism is likely to more rely on energy production via TCA cycle and glyoxylate cycle than on photosynthesis, resulting in increase in microalgal biomass.

Keywords : Microalgae, Microalgal Biomass, Triacylglycerol, Microfluidic Perfusion Bioreactor, Stress Priming, Malate Synthase

Student Number **:** 2013-30302

CONTENTS

LIST OF FIGURES

LIST OF TABLES

LIST OF ABBREVIATIONS

ACH	Aconitate hydratase
ACS	Acetyl-CoA synthetase
ATP	Adenosine triphosphate
aveSSR	Average shear strain rate
aveWSF	Average wall shear force
BODIPY	Boron-dipyrromethene
BSA	Bovine serum albumin
CAV	Voltage- dependent calcium channel
CBB	Coomassie brilliant blue
CBLP	Chlamydomonas β subunit-like polypeptide
cDNA	Complementary DNA
CFD	Computational fluid dynamics
CIS	Citrate synthase
CSR	Cellular stress response
D.W.	Distilled water
DMSO	Dimethyl sulfoxide
DNA	Deoxyribonucleic acid
dNTP	Deoxynucleotide
DTNB	5,5′-Dithio-bis-(2-nitrobenzoic acid)
EDTA	Ethylenediaminetetraacetic acid
EtOH	Ethanol

FITC	Fluorescein isothiocyanate
F_v/F_m	Maximum efficiency of PSII
GFP	Green fluorescent protein
HA	Human influenza hemagglutinin
HS	High salt
Hz	Hertz
ICL	Isocitrate lyase
IPTG	Isopropyl β-D-1-thiogalactopyranoside
IMAC	Immobilized metal affinity chromatography
LB	Lysogeny broth
LC/MS	Liquid chromatography/mass spectrometry
MAS	Malate synthase
MDH	Malate dehydrogenase
MeOH	Methanol
MME	Malic enzyme
mRNA	Messenger RNA
MSC	Mechanosensitive channel
NADPH	Nicotinamide adenine dinucleotide phosphate
NTA	N-terminal activation domain
OD	Optical density
PAGE	Polyacrylamide gel electrophoresis
PBS	Phosphate-buffered saline
PCI	Phenol:chloroform:isoamylalcohol
PCR	Polymerase chain reaction

PDMS	Polydimethylsiloxane
PEG	Polyethylene glycol
PET	Polyethylene terephthalate
PIC	Protease inhibitor cocktail
PLL	Poly-l-lysine
psbD	Photosystem II D2 protein
qRT-PCR	quantitative real time polymerase chain reaction
rbcL	Rubisco (ribulose-1,5-bisphosphate carboxylase/oxygenase) large subunit
RNA	Ribonucleic acid
RP	Recombinant protein
SDS	Sodium dodecyl sulfate
TAP	Tris-acetate-phosphate
TCA cycle	Tricarboxylic acid cycle
TNB	5-thio-2-nitrobenzoic acid
tRNA	Transfer RNA
TRP	Transient receptor potential channel
TSP	Total soluble protein
VOF	Volume of fluid
WB	Western blotting

Chapter 1

Research Background and Objective

Today's rapid population increase [1] has increased pressure for higher food productivity; however, crop yields are reported to decrease by 10-20%. Constraints from climate change and social regulation of livestock rearing also have hindered food producers from meeting global demand for food [2]. Plant-based foods have been proposed as an alternative to regular animal food consumption [3] because they require less water and have more nutrients than that of meat-based foods. In view of sustainable development goals (SDGs), however, plant farming has limitations because it needs more arable land and longer periods of cultivation which is not sustainable anymore [4].

Photosynthetic microalgae have recently been proposed as a resource for food security. They sequester more carbon dioxide, grow at high rates, contain abundant nutrition, produce value-added co-products, and can thrive in marginal lands, all of which are environmentally sustainable [3]. Therefore, microalgae can contribute to securing the food supply for the world while maintaining carbon neutrality. In this dissertation, three strategies were introduced to yield more microalgal biomass: *i)* continuous low concentration of nutrients at steady high C/N ratio, *ii)* vibrational stress priming against turbulence by agitators, and *iii)* chloroplastic malate synthase expression-associated metabolism.

Recently, demands for secondary metabolites such as antioxidants, antibiotics, and nutritional additives have markedly increased. These secondary metabolites, however, are produced in the cellular stationary phase, and in that phase, nutrients may become mostly depleted, and cells cannot proliferate. This trade-off relationship between cell growth and secondary metabolite productivity consequently results in a decrease in the total amount of metabolites produced. This nutrient depletion is the major drawback for the total yield of secondary metabolites [5-7].

Turbulence in large-scale bioreactors is necessary to agitate all the required components in the media for cellular proliferation such as oxygen/carbon dioxide and nutrients to increase the biomass. Apparatuses like stirring panels, agitators, or a baffled block in large-scale bioreactors also help prevent microbes from clustering or settling down. However, the turbulence can give rise to hydrodynamic shear force fields leading to lower a cellular viability, which means that cells should be able to endure such harsh conditions [8].

Malate can function both as a growth inducer and as a redox balance mediator. Extracellular malate promotes growth-associated parameters exhibiting biomass increase. Intracellular malate can balance redox states of chloroplast or mitochondria by transferring energy from reducing equivalents such as NADPH or

NADH that are essential metabolites for catabolism or anabolism [9,10], because these pools should be tightly regulated to maintain its capacity in each organelle. From an engineering view point, such malate could enhance microalgal biomass.

The objectives of this study were as follows.

- To demonstrate that a continuous, stable flow of low concentration nutrient medium at steady high C/N ratio enhances the total secondary metabolites productivity
- To verify that vibrational stress priming based on the innate characteristics of the microalgae contributes to turbulence endurance and biomass increase
- To develop transgenic microalgae expressing malate synthase in chloroplast to upregulate primary metabolisms

Chapter 2

Literature Review

2.1 Earthcare with Sustainable Development Goals (SDGs)

2.1.1 Global Warming

Many climate change researchers have said that the use of fossil fuels since industrial revolution in the 19th century has promoted global warming. Fossil fuels are energy-potential buried carbon sources. Burning fossil fuels not only generates much heat energy but also emits a substantial amount of carbon dioxide (CO_2) as an oxidized byproduct. The accumulation of anthropogenic CO_2 recently reached 400 ppm. Because CO_2 has thermodynamic features in confining heat, it accelerates global warming over time and induces many social and environmental issues including increased global temperatures, rising sea levels, and changing climates in the form of extreme weather such as droughts, heat waves, heavy snowfall and heavy rainfall with floods as well as ocean acidification. The collapsed carbon balance and climate change have gained a large inertia. IPCC [11] and UNFCCC [12] that in the case that the global temperature increases by over 2 ℃, nothing could solve these issues, and the consequences will persist for decades, centuries, or even tens of thousands of years to come. This has made people focus on various methods to reduce the level of CO_2.

2.1.2 Population Increase and Food Insecurity

The United Nations Department of Economic and Social Affairs (UN DESA) [13] published a report saying that the global population could be as high as 10 billion by 2050. In the Global Agricultural Productivity (GAP) report [1], the rapid population increase is expected to cause serious issues in food security. To ensure an adequate food supply for the world, food production should be boosted by 70% [2]. Even though the global food demand has continued to increase, numerous growing constraints due to climate change and human activity have hindered food producers from meeting the demand. Moreover, recently, regulations limiting animal food consumption have been ongoing. This is because meat consumption could lead to unavoidable negative issues related to human health and the environment [4].

2.1.3 Plant-Based Food for Sustainable Development Goals (SDGs)

To solve both global warming and food insecurity caused by the increase in the population, sustainable development is needed to harmonize human society with nature. Green technology is regarded as technology with sustainable development goals (SDGs). Among these technologies, there are energy technology (renewable

energy), environment technology (bioremediation), and agriculture technology. Unlike others, CO_2-utilized food production from agriculture technology can contribute to secure the food supply for the world while maintaining carbon neutrality.

In view of the SDGs, photosynthetic crops have been given much attention as an alternative to animal-based food. Photosynthesis is a mechanism where atmospheric carbon dioxide (CO_2) is converted to glucose and water under light. Plants have a similar protein composition and larger quantity of carbohydrates than that of meats. Therefore, plant-based foods have been proposed as an alternative to regular animal food consumption [3,14-18] (Table 2.1). Considering today's rapid population increase and the consequent food security problem, however, it is likely that plant farming could have limitations and is not sustainable anymore [4].

Table 2.1. Comparison of chemical composition of macronutrients, productivity and water for feeding in commodities and microalgae on a dry matter basis (%). [3, 14-18]

Species	Proteins (%)	Carbohydrates (%)	Lipids (%)	Productivity (t ha^{-1} yr^{-1})	Water (L g^{-1} protein)
Meat	43 - 74	0 – 1.0	12 - 34	1.0	105,000
Rice	7 - 8	77 – 80	0.6 – 2.0	1.5	12,500
Soybean	36 - 37	30	18 – 20	4.5	9,000
Microalgae	27.1 – 48.2	24.6 – 34.3	7.9 – 14.3	25	2,100

2.2 Microalgae

2.2.1 Microalgae as Food Resource

Photosynthetic microalgae have recently been proposed as a resource to solve the problem that the world will face in supplying enough food and animal feed. Microalgae have abundant macronutrients and micronutrients (*i.e.*, the necessary vitamins, iron, and dietary elements); they grow fast enough such that all countries could get more plant-based products but with less labor and costs; they can be farmed with a high productivity of 20-40 g m^{-2} d^{-1} and potentially use only 300 times smaller areas of arable land than that of plants and a small amount of fresh water (Table 2.2); they can help to mitigate climate change with a 10 to 30 times higher CO_2 capture capacity (180 g CO_2 to 100 g biomass) than that of plants, all of which are environmentally sustainable [3,16,17,19-21].

2.2.2 Microalgae Cultivation Process

There are two types of industrial scale microalgal production systems: an open raceway pond (ORP) and a closed photobioreactor (PBR). A PBR is a batch bioprocess that controls cultivation variables (*i.e.*, temperature, pH, inorganic or

organic CO_2, and macronutrients including nitrogen (N) and phosphate (P) sources or microelements concentration) [21] (Table 2.3). The PBR can be operated based on a specific mathematical model that predicts the best yield and productivity of the microalgal biomass or microalgal metabolites when scaling up the process. This is why optimizing the microalgal culture environment in batch processes can be not only more useful but also more profitable in the microalgal industry. When it comes to lipid production from microalgae, while ORP produces a biomass of 6.8 ± 3.0 g m^{-2} d^{-1} with a lipid content of 20 ± 5% and costs 109$ gal^{-1}, PBR produces a biomass of 9.3 ± 2.0 g m^{-2} d^{-1} with a lipid content of 40 ± 10% and costs 77$ gal^{-1}, which is economic competitive [16,17,21] (Table 2.4).

Table 2.2. Photosynthetic productivities and solar conversion efficiencies. [3, 16-17, 19-21]

Species/process	Productivity (% of theoretical maximum)	Solar-to-product energy conversion efficiency (%)	Land area needed (M ha)
Theoretical productivity of photosynthesis	100	8-10	
Lab or small-scale green microalgal productivity	27 - 54	3.0	
Chlorella (commercial, average rates of production)	22 - 27	2.0	
Spirulina (*Arthrospira*) (commercial, average rates of production)	4.5 - 9.0	0.5	2.0 - 4.5 (microalgae)
Miscanthus giganteus (field trial)	11 - 22	1-2	
Switchgrass (field trial)	1.8 - 3.6	0.2	24 - 846 (crops)

Table 2.3. Nutrient functions during microalgae cultivation. [21]

Nutrition	Main ingredients	Function	Suitable content range
Carbon source	CO_2, HCO_3^-, CO_3^{2-}, etc.	Provide C to the whole cell, etc.	1 - 10 g/L
Nitrogen source	NO_3^-, Urea, AA, N_2, etc.	Provide N to the whole cell, etc.	10 - 2000 mg/L
Phosphorus	Hydrophosphate, phosphate, etc.	Provide P to every reaction in cells, etc.	10 - 500 mg/L
Sulphur	Sulphate, etc.	Provide S to proteins and reactions, etc.	1 - 200 mg/L
Inorganic salts	K, Ca, Na, Mg, etc.	Maintain cell structure and activity, etc.	0.1 - 100 mg/L
Trace elements	Fe, Zn, Mn, Pb, Cd, etc.	Be coenzyme factors, etc.	0.01 - 10 mg/L
Vitamin	978 m^2/pond; 12 m wide, 82 m long, 0.30 m deep	Aid to cell division, etc.	0.01 - 1000 µg/L

Table 2.4. Comparison of open raceway ponds (ORP) and photobioreactors (PBR). [16,17,21]

	Open raceway ponds (ORP)	Photobioreactors (PBR)
Annual biomass production (kg)	100,000	100,000
Volumetric productivity (kg m^{-3} d^{-1})	0.117	1.535
Areal productivity (kg m^{-2} d^{-1})	0.035	0.048 / 0.072
Biomass concentration in broth (kg m^{-3})	0.14	4
Dilution rate (d^{-1})	0.25	0.384
Area needed (m^2)	7,828	5,681
Oil yield (m^3 ha^{-1})	99.4 / 42.6	136.9 / 58.7
Annual CO_2 consumption (kg)	183,333	183,333
Number of units needed	8	6
System geometry	978 m^2/pond; 12 m wide, 82 m long, 0.30 m deep	132 parallel tubes/unit; 80 m long tubes; 0.06 m tube diameter

2.2.3 Chlamydomonas reinhardtii

Chlamydomonas reinhardtii is a single-cell green microalga of 10 μm in diameter. It has two flagella for swimming, hydroxyproline-rich glycoproteins in its cell wall besides cellulose, a light-sensing eyespot, and a large cup-shaped chloroplast with pyrenoid.

Other microalgae besides *C. reinhardtii* have higher biomass productivities and efficient lipid biosynthesis [17,23] (Table 2.5). *C. reinhardtii*, however, is well studied as a model microalga due to its faster growth rate, easier cultivation and evident genetic manipulation. *C. reinhardtii* can not only grow autotrophically on light but also grow in the dark when supplied with organic carbon especially acetate. Recently, with its generally regarded as safe (GRAS) status [24], *C. reinhardtii* has gained interest as a cellular green factory for producing nutraceuticals, biopharmaceuticals and biofuel as well as biochemicals.

Laboratory *C. reinhardtii* is listed in Table 2.6 [25,26].

Table 2.5. Biomass productivities, lipids content, and productivities of different microalgae strains. [17,23]

Microalgae species	Biomass productivity ($g\ L^{-1}\ day^{-1}$)	Lipid content (% dcw)	Lipid productivity ($mg\ L^{-1}\ day^{-1}$)
Ankistrodesmus falcatus	0.34	16.49	56.07
Ankistrodesmus fusiformis	0.24	20.66	49.58
Botryococcus braunii	0.25	44.97	112.43
Botryococcus terribilis	0.2	49	98
Chlamydomomas reinhardtii	0.24	22.10	
Chlamydomonas sp.	0.24	15.07	36.17
Chlorella vulgaris	0.73	28.07	204.91
Dunaliella tertiolecta	0.098 - 0.12	16.7 - 71.0	
Monoraphidium contortum	0.307	22.2	
Nannochloropsis sp.	0.17 - 1.43	12.0 - 53.0	37.6 - 90.0
Scenedesmus obliquus	0.16	16.73	26.77
Tribonema minus	0.17	50.23	

Table 2.6. Genotypes of *Chlamydomonas reinhardtii* strains. [25,26]

Strains	Alternate Names	Genotype	References or Source
CC-124	137c mt-	*mt- nit1 nit2*	*Chlamydomonas Center*
CC-125	137c mt+	*mt+- nit1 nit2*	*Chlamydomonas Center*
CC-503		*mt+ cw92*	*Chlamydomonas Center*
CC-620	R3+ (Subclones of 137c wild type)	*mt+ nit1 nit2*	*Chlamydomonas Center*
CC-621	NO- (Subclones of 137c wild type)	*mt- nit1 nit2*	*Chlamydomonas Center*
CC-2653	Spreitzer 18-7G-12		*Chlamydomonas Center*
CC-4349	Goodenough cw15	*mt-*	*Chlamydomonas Center*
CC-4348	BAFJ5 or sta6	*mt+ nit1 nit2 cw15 arg7-7 sta6-1::ARG7*	*Chlamydomonas Center*

2.3 Metabolic Engineering in *Chlamydomonas reinhardtii*

2.3.1 Advantageous Transgenic Microalgae over Other Chemotrophic Microbes

Recent industrial bioprocesses using bacteria (*e.g.*, *Escherichia coli*, *Corynebacterium glutamicum*, and *Lactobacillus spp.*) and yeasts (*e.g.*, *Saccharomyces cerevisiae*) have been well established with their metabolic engineering over several decades [27]. In contrast to their large number of applications at an industrial scale, among microalgae, only *C. reinhardtii* has been reported to be successfully transformed. The advantages of transgenic *C. reinhardtii* over those chemotrophic microbes could provide an opportunity to expedite their utilization at an industrial scale; *i)* transgenic microalgae can grow both under phototrophic and heterotrophic conditions; *ii)* they can especially express specific genes which yeast cannot express (*i.e.*, genes related to flagellar function, photosynthesis and photoreception), and *iii)* they can be engineered to express mammalian proteins such as hormones or antibodies with high quality [5].

2.3.2 Chloroplast Transformation

Since its first report about successful genetic transformation at both nucleus and chloroplast, *C. reinhardii* has been mainly focused for development of transgenic microalgae with stable heterologous gene expression. The main characteristics and potential uses of nuclear and chloroplast transformation are summarized in Table 2.7 [5]. In order that transgenic *C. reinhardtii* should be feasible to come up with its widespread utilization for industrial and pharmaceutical applications through metabolic engineering, chloroplast transformation should be performed for recombinant protein (RP) production from *C. reinhardtii* chloroplasts. This is reported to be economically viable owing to RP titers of several percent total soluble protein (TSP) and reliable targeted genetic manipulation by homologous recombination [28,29,54] (Table 2.8).

The chloroplast of *C. reinhardtii* contains its own genome, which is called the plastome. It is a circular form of a DNA molecule approximately 200 kb in size and encompasses about 80 identical copies of itself [54]. That is why stable chloroplast transformation requires that all the copies of the plastome change to the recombinant form, which is achieved by site-specific homologous recombination between homologous DNA sequences present in the target plastome and the

construct [55]. This ensures integration of the transgenes into the plastome, resulting in high expression levels with no gene silencing [6,54].

Recently, chloroplast DNA mutants that have defects in photosynthetic genes and rescuing vectors for their original functions have been utilized to develop transgenic *C. reinhardtii* expressing chloroplast-localized transgenes. These microalgal mutants are typically unable to grow under autotrophic condition, but when transformed with the rescuing vectors, they can restore their photosynthesis by replacing its abnormal genes with original genes [54,56] (Table 2.9). This complementation system has led to its proposed use for screening chloroplast transgenic microalgae without antibiotics as selection markers.

Table 2.7. Characteristics of nuclear and chloroplastic transformations. [5]

	Nuclear	Chloroplastic
Cell compartment of expression	Extracellular, cytosol and chloroplast, among others	Chloroplast
Recombination machinery for integration of exogenous DNA	Mostly non-homologous	Homologous
Gene silencing	Probable	Not probable
Inheritance of integrated gene	Mendelian	Maternal
Level of expression (gene copy number)	Low to intermediate	High
Co-transformation of different markers	High	High
Versatility to express genes from different organisms	Intermediate to low	High
Glycosylation pattern of proteins	Similar to plants and animals	None

Table 2.8. Examples of recombinant proteins (RP) from chloroplast transformation. [28,29,54]

Promoter /Terminator	Selection Markers	Antibiotics	Recombinant Protein Produced	References
atpA/rbcL	*aadA*	spectinomycin (Spc)	VP1-CTB; Protein VP1 from foot and mouth disease virus (FMDV) fused to cholera toxin B (CTB)	[30]
rbcL/rbcL atpA/rbcL	*aadA*	spectinomycin (Spc)	HSV-lsc; Large single chain (lsc) antibody directed against glycoprotein D protein from Herpes simplex virus (HSV)	[31]
atpA/rbcL	*aadA*	spectinomycin (Spc)	TRAIL; Tumor necrosis factor-related apoptosis-inducing ligand	[32]
psbD/psbA	*aadA*	spectinomycin (Spc)	M-SAA; Mammary-associated serum amyloid	[33]
atpA/rbcL	*aadA*	spectinomycin (Spc)	CSFV-E2; Classical swine fever virus (CSFV) structural protein E2	[34]
rbcL/rbcL	*aadA*	spectinomycin (Spc)	hGAD65; Human glutamic acid decarboxylase	[35]
psbA, atpA psbD/rbcL	*aadA*	spectinomycin (Spc)	IBDV-VP2; Infectious burial disease virus VP2 protein	[36]

Table 2.8. Examples of recombinant proteins (RP) from chloroplast transformation. [28,29,54] (Continued)

Promoter /Terminator	Selection Markers	Antibiotics	Recombinant Protein Produced	References
psbA, atpA /rbcL	*aadA*	spectinomycin (Spc)	IHNV-G; Infectious haematopoietic necrosis virus	[36]
psbA, atpA /rbcL	*aadA*	spectinomycin (Spc)	IPNV-VP2; Infectious pancreatic necrosis virus	[36]
psbA, atpA /rbcL	*aadA*	spectinomycin (Spc)	IPNV-VP2 SBC; Infectious pancreatic necrosis virus	[36]
psbA, atpA /rbcL	*aadA*	spectinomycin (Spc)	p57; Quorum sensing-regulated gene (LecA)	[36]
psbA, atpA /rbcL	*aadA*	spectinomycin (Spc)	PCV2; Porcine circovirus type 2	[36]
psbA, atpA /rbcL	*aadA*	spectinomycin (Spc)	VP-2C	[36]
psbA, atpA psbD/rbcL	*aadA*	spectinomycin (Spc)	VP28	[36]

Table 2.8. Examples of recombinant proteins (RP) from chloroplast transformation. [28,29,54] (Continued)

Promoter /Terminator	Selection Markers	Antibiotics	Recombinant Protein Produced	References
psbA/rbcL	*aadA*	spectinomycin (Spc)	HC-83K7C; Heavy chain human monoclonal antibody against anthrax protective antigen 83 (PA83)	[37]
psbA/psbA	*aadA*	spectinomycin (Spc)	LC-83K7C; Light chain human monoclonal antibody against anthrax PA83	[37]
rbcL,atpA /rbcL	*aadA*	spectinomycin (Spc)	CTB-D2; D2 fibronectin-binding domain of *Staphylococcus aureus* fused to the cholera toxin B subunit	[38]
psbA, atpA /rbcL	*aphA6*	kanamycin (Kan)	Erythropoietin; a hormone that promotes the formation of red blood cells by the bone marrow	[39]
psbA, atpA /rbcL	*aphA6*	kanamycin (Kan)	10FN3; The tenth human fibronectin type three domain	[39]
psbA, atpA /rbcL	*aphA6*	kanamycin (Kan)	14FN3; Domain 14 of human fibronectin	[39]
psbA, atpA /rbcL	*aphA6*	kanamycin (Kan)	Interferon β; a cytokine in the interferon family used to treat multiple sclerosis (MS)	[39]

Table 2.8. Examples of recombinant proteins (RP) from chloroplast transformation. [28,29,54] (Continued)

Promoter /Terminator	Selection Markers	Antibiotics	Recombinant Protein Produced	References
psbA, atpA /rbcL	*aphA6*	kanamycin (Kan)	Proinsulin	[39]
psbA, atpA /rbcL	*aphA6*	kanamycin (Kan)	VEGF; Human vascular endothelial growth factor	[39]
psbA, atpA /rbcL	*aphA6*	kanamycin (Kan)	HMGB1; High mobility group protein B1	[39]
atpA,psaA, psbA,psbD /rbcL	*aadA*	spectinomycin (Spc)	acrV2 and vapA2; antigens from the fish pathogen *Aeromonas salmonicida*	[40]
atpA/rbcL	*aadA*	spectinomycin (Spc)	*Escherichia coli* phytase gene (*appA*)	[41]
psbA/psbA	*aphA6*	kanamycin (Kan)	Pfs25 and Pfs28; surface proteins from Plasmodium falciparum	[42]
psbA/psbA	*aphA6*	kanamycin (Kan)	αCD22PE40; monomeric immunotoxin consisting on the single chain antibody that recognizes the CD22, fused to domains II and III of exotoxin A (PE40) from *Pseudomonas aeruginosa*	[43]

Table 2.8. Examples of recombinant proteins (RP) from chloroplast transformation. [28,29,54] (Continued)

Promoter /Terminator	Selection Markers	Antibiotics	Recombinant Protein Produced	References
psbA/psbA	*aphA6*	kanamycin (Kan)	αCD22HCH23PE40; dimeric version of αCD22PE40	[43]
psbA/psbA	*aphA6*	kanamycin (Kan)	CtxB-Pfs25; Plasmodium falciparum surface protein 25 fused to the β subunit of the cholera toxin from *Vibrio cholera*	[44]
psbA/psbA	*aphA6*	kanamycin (Kan)	αCD22Gel; single chain antibody targeting the CD22 receptor from B-cells, fused to the eukaryotic ribosome inactivating protein, gelonin, from *Gelonium multiflorm*	[45]
psbA/psbA	*aphA6*	kanamycin (Kan)	αCD22CH23Gel; dimeric version of αCD22Gel	[45]
psaA/rbcL	Marker -free	TN72 strain, psbH rescued	Cpl-1 and Pal; the endolysin specific to the major human pathogen *Streptococcus pneumoniae,*	[46]
psaA/rbcL	Marker -free	TN72 strain, psbH rescued	Cytosine deaminase (CD); catalyses conversion of cytosine to uracil and ammonia for pyrimidine salvage, but can also convert the synthetic compound 5-fluorocytosine (5-FC) to the toxic product 5-fluorouracil (5-FU)	[47]

Table 2.8. Examples of recombinant proteins (RP) from chloroplast transformation. [28,29,54] (Continued)

Promoter /Terminator	Selection Markers	Antibiotics	Recombinant Protein Produced	References
16S,atpA /rbcL psbA,psbD /psbA	Marker -free	Fud7 strain, psbA rescued	MPT64; a protein releasedfrom Mycobacterium tuberculosis and relevant for diagnostic pur-poses	[48]
rbcL/rbcL 16S-atpA/rbcL psbA/psbA 16S-psbA/rbcL	*aadA*	spectinomycin (Spc)	Luxiferase	[49]
psbD/psbA	Marker -free	TN72 strain, psbH rescued	Luxiferase	[49]
atpA/rbcL 16S-atpA/rbcL psbA/psbA 16S-psbA/rbcL	*aadA*	spectinomycin (Spc)	14FN3	[49]

Table 2.8. Examples of recombinant proteins (RP) from chloroplast transformation. [28,29,54] (Continued)

Promoter /Terminator	Selection Markers	Antibiotics	Recombinant Protein Produced	References
atpA/atpA, rbcL,psbA rbcL/rbcL, psbA psbA/psbA psbD/psbA	*aadA*	spectinomycin (Spc)	GFP; Green Fluorescent Protein	[50]
rbcL/rbcL	Marker -free	CC-2653 strain, rbcL rescued	ADH; alcohol dehydrogenase from *Saccharomyces cerevisiae*	[51]
HSP70A-RBCS2/	*aadA*	spectinomycin (Spc)	LPAAT; lysophosphatidic acid acyltransferase	[52]
psbD/rbcL	Marker -free	CC-2653 strain, rbcL rescued	GFP; Green Fluorescent Protein	[53]
psbD/rbcL	Marker -free	CC-2653 strain, rbcL rescued	MS; Malate Synthase	In this thesis

Table 2.9. Examples of mutants where chloroplast genes essential for photosynthesis are missing. [54,56]

Missing Genes	Full Name of Genes	Description
rbcL (CC-2653)	Ribulose bisphosphate carboxylase large subunit	Unable to assemble the RbcL large subunit of Rubisco Cannot fix CO_2 and require acetate for growth Nonsense mutations in the *Chlamydomonas* chloroplast gene that codes for the large subunit of ribulose-bisphosphate carboxylase/oxygenase
psbA (CC-4147)	Photosystem II protein D1	Unable to assemble the psbA/D1 reaction center protein of photosystems-II Cannot perform photosystem-II photochemistry Require acetate for growth
psbD (CC-4385)	Photosystem II protein D2	Unable to assemble the psbD/D2 reaction center protein of photosystems-II Cannot do photosystem-II photochemistry Require acetate for growth
petA (CC-4384)	Apocytochrome f precursor; component of cytochrome b6/f complex	Unable to assemble the cytochrome f part of the cytochrome b-f complex Cannot transport electrons between photosystem-II and photosystem-I
atpA, atpB	ATP synthase CF1 alpha chain; ATPase alpha subunit	Unable to assemble the ATP synthase CF1 subunit Cannot synthesize ATP Require acetate for growth
psbH (CC-5168) (cw15 ΔpsbH)	Photosystem II reaction center protein H	Destabilizes photosystem II complex Cannot do photosystem-II photochemistry Require acetate for growth

2.3.3 Metabolic Engineering for Improving the Microalgal Biomass

While there have been many studies on increasing secondary metabolites productivity (*e.g.*, astaxanthin, lutein, TAG, etc.), few studies have reported on engineering growth-associated primary metabolism.

2.3.3.1 Reduction of Antenna Size

Typical photobioreactor at industrial scale is capable to operate a large amount of suspension cultivation at batch. A high pigment optical density by large antenna systems of *C. reinhardtii* at outmost layers, however, results in light scattering effect that reduces light accessibility of lower part of microalgal cells. Generation of strains with size-reduced antenna was summarized in Table 2.10 [57]. It was shown that their photosystems were composed of 10 to 33% minimum molecules and avoided over-saturation.

2.3.3.2 NPQ (Non-Photochemical Quenching) Deactivation

Photon conversion efficiency (PCE) is closely related with microalgal biomass

productivity. When exposed to full sunlight intensity, *C. reinhardtii* at the outer most layers becomes over-saturated, where about 75% of the energy captured by the LHC antenna complex is not converted to biomass but dissipated as heat and fluorescence. Additionally, the light excitation flux exceeds the CO_2 fixation rate, inducing a pH drop in the thylakoid lumen and NPQ activation (de-excitation of chlorophyll molecules in PSII via qE and qT mechanisms) [66].

NPQ mutants were studied to reduce the energy loss but showed a reduction in high-light tolerance without improving the growth. They likely got over-excited, where the half-life of a singlet Chl ($^1Chl^*$) increases, and spin inversion is more likely to result in a triplet Chl ($^3Chl^*$). The $^3Chl^*$ is known as a photosensitizer causing harmless triplet O_2 to become a reactive oxygen species (ROS), which contributes to damaging the photosystem [67].

2.3.3.3 Metabolism Manipulation

Although central carbon metabolism has been recently unveiled (Figure 2.1) [68], there have been few studies about primary metabolism engineering and its positive effects on microalgal biomass enhancement.

Table 2.10. The phenotypic characteristics of different truncated antenna mutants. [57]

Mutants	Genetic mod.	Chl total (%)	Chl a/b ratio (%)	Growth rate increase (%)	PSII antenna size (%)	PSI antenna size (%)	References
tla1	Random DNA insertion	37.5	270		65	50	[58]
Rl6	RNAi-mediated knock-down	30	231		74	50	[59]
tla3	Random DNA insertion	16	444		38	52	[60]
as1/as2	Random DNA insertion		237/130		~20/~80		[61]
stm3LR3	RNAi-mediated knock-down of all LHCBM genes	32	208	185			[62]
stm6Glc4L01	RNAi-mediated knock-down of LHCBM1/2/3 genes	50	114	165			[63]
stm6Glc4T7	Site-directed mutagenesis	80	106	153	83-90		[64]
tla4	Random DNA insertion		<400	158	74	56	[65]

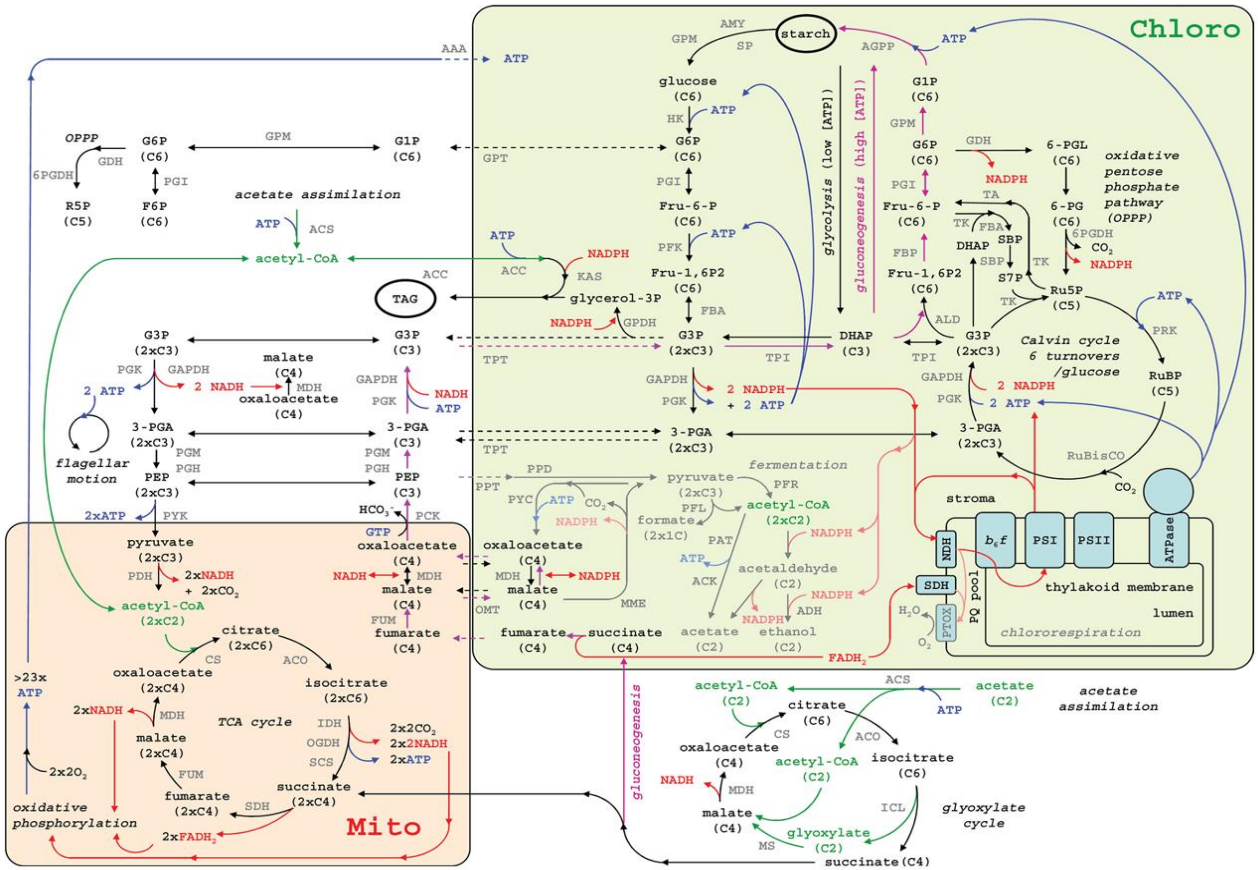

Figure 2.1 Central carbon metabolism in *Chlamydomonas reinhardtii.* [68]

2.4 Mechanotransduction in *Chlamydomonas reinhardtii* and its Application

2.4.1 Ca^{2+} Signalling Mechanisms in Plants

Cells ensure their survival by responding to diverse environmental stimuli, where Ca^{2+} has a significant role as a second messenger, amplifying and propagating intracellular signals. Because a low concentration of cytosolic Ca^{2+} (~100 nM) causes a large inward concentration gradient, activation of Ca^{2+} ion channels by stimuli results in a rapid influx of extracellular Ca^{2+} ions into cells and the elevation of cytosolic Ca^{2+} ($[Ca^{2+}]_{cyt}$). Ca^{2+} influx, efflux, and decoding are sophisticatedly regulated for eliciting downstream responses [69].

Ca^{2+} influx related ion channels such as the MscS like channel respond to stress stimuli by opening pores and permitting Ca^{2+} influx, which depolarizes the membrane potential. Ca^{2+} efflux proteins such as Ca^{2+} ATPases or Ca^{2+}/H^{+} exchangers release out $[Ca^{2+}]_{cyt}$ to its resting level [70]. The changes in cytosolic Ca^{2+} by influx or efflux lead to various Ca^{2+}-binding proteins that elicit downstream stress responsive signaling pathways [71,72], which include calmodulin (CaM),

calcium-dependent protein kinases (CDPKs), calcineurin B-like (CBL), or calcium sensor proteins and their CBL-interacting protein kinases (CIPKs) [69].

After microarrays identified the stress-dependent Ca^{2+} responses, the promoter regions of Ca^{2+}-regulated genes were shown to contain common abscisic acid-responsive element (ABRE)-related *cis*-elements [73]. The ABRE was also elucidated to be a part of the promoter of CBF/DREB1 transcription factors that function as master regulators of abiotic stress responses [74]. This means that Ca^{2+}-regulated gene transcription and abiotic stress responses are directly interconnected. In recent studies, it was unveiled that calmodulin binding transcription factors (CAMTA) was the direct transcription factor bridging the interconnection by immediately translating Ca^{2+} signatures to transcriptional regulation, which is regulated by CAMs (Figure 2.2) [75,84].

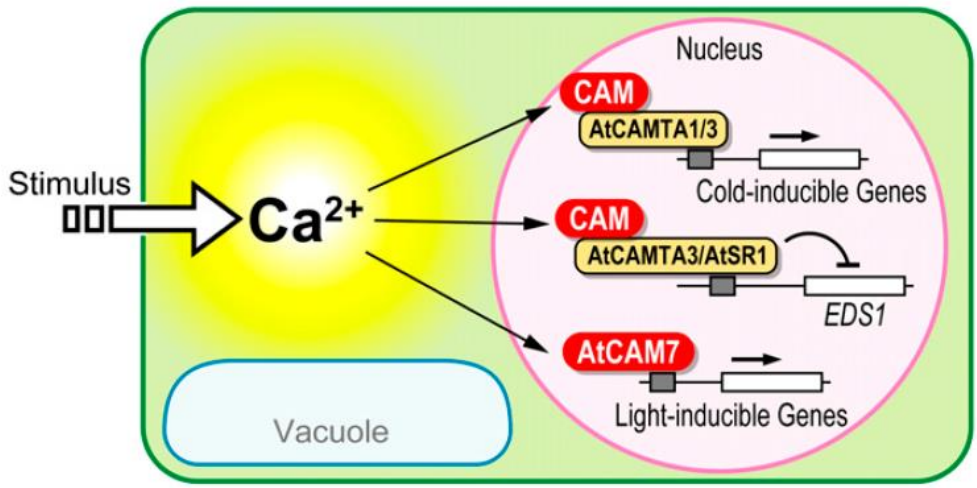

Figure 2.2 Schematics of interconnection of abiotic stress and Ca^{2+}-regulated transcription. [75]

2.4.2 Mechanotransduction in Chlamydomonas reinhardtii

Chlamydomonas reinhardtii responds to rapid changes in light, osmotic stress and nutrient availability by diverse signaling pathways. Emerging evidence suggests that Ca^{2+}-dependent signaling mechanisms are central to many cellular stress responses in *C. reinhardtii* [69]. Compared to higher plants, however, there is relatively little understanding of the nature of the Ca^{2+} dependent stress signaling mechanisms in *C. reinhardtii*.

Specifically, studies on the interconnection between mechanotransduction and the Ca^{2+} signaling pathway in *C. reinhardtii* remain in their infancy [69]. Some key mechanoreceptors or ion channels have been identified providing insight into the underlying mechanosensitive signaling pathway. They were demonstrated to be mainly localized at the flagella detecting collisions to obstacles. This is because the cell body is covered by a rigid cell wall, and flagella are the only part outside the cell body [76]. TRP11, an ortholog of transient receptor potential (TRP) channels [77], is the mechanosensitive receptor that has a role in generating the membrane potential at the first collision [76]. The initial Ca^{2+} influx by TRP11 promotes the depolarization of the flagella membrane and activates CAV2, the α1 subunit of a voltage-dependent calcium channel [78]. CAV2 triggers the action potential by

amplifying the Ca^{2+} influx to change the flagella bending pattern to avoid the collision. CAV2 is comprised of four homologous repeat domains (D1 to D4) with six transmembrane segments (S1 to S6) for each, which are conserved. S5 and S6 generally make up the pore of CAV2 [79]. P-loops connecting S5 and S6 at the extracellular side have glutamine residues (EEEE motif), which is essential as a Ca^{2+} selectivity filter [76].

Besides the mechanosensitive channels at the flagella, MSC1, a member of the MscS-like proteins, spans intracellular membranes such as the nucleus or chloroplast. While *E. coli* MscS is almost non-selective, MSC1 is selective essentially for monovalent anions as permeable ions [76]. Ascending and descending ramps of mechanical stimuli showed that MSC1 opens for a large stimulus intensity but closes for a small stimulus intensity, which means that the gating kinetics of MSC1 is hysteretic. In addition to that, MSC1 RNAi showed an abnormal localization of chlorophyll, suggesting that MSC1 is involved in organizing the shape of the chloroplast membranes [76].

2.4.3 Mechanical Stimulus for Biomass Increase

There have been several studies on the positive effect of mechanical stimulus on biomass increase (Table 2.11). Their methods, however, have difficulty applying to industrial-scale bioreactors with high facility cost for generating such mechanical stimuli as ultra-sonic wave or massive vibrational force.

Table 2.11. Examples of the positive effects of mechanical stimuli on biomass increase. [80-84]

Organisms	Frequency (hz)	Intensity /Acceleration	Vibration Time	Vibration Period	References
e.coli K-12	250-16,000 :8,000 (biomass)	80dB (growth rate)		48 hrs	[80]
hASCs	25, 35, 45	0.3 G	15 min	14 days	[81]
hASCs	50, 100	3 G	3 hr	1, 7, 14 days	[82]
Anabaena variabilis (flask)	40,000 (ultra sonic bath)	0, 200, 350, 500 W	10 min	3 days	[83]
Arabidopsis thaliana	250, 500, 1000, 2000, 3000		1 hr	2 days	[84]

2.5 Triacylglycerol (TAG) Production in *Chlamydomonas reinhardtii*

2.5.1 Potential Triacylglycerol (TAG) Following Transesterification

A triacylglycerol (or triglyceride, TAG) is a tri-ester of glycerol and three fatty acids. Triacylglycerol is reacted with alcohol, especially methanol, in an alkali-catalyzed reaction known as transesterification or alcoholysis, producing one glycerol and three methyl esters of fatty acids (FA) (Figure 2.3) [16]. The three fatty acids are generally different, the chain of which comprises 16, 18, or 20 carbon atoms- natural fatty acids found in eukaryotes typically consist of even numbers of carbon atoms, reflecting fatty acid biosynthesis from the two-carbon acetyl CoA [16].

Alkali-catalyzed transesterification is about 4000 times faster than the acid catalyzed reaction [85] and more cost-feasible than lipase-mediated treatment. Consequently, alkalis such as sodium and potassium hydroxide are commonly used as commercial catalysts at a concentration of about 1% by the weight of the oil [16].

This transesterification is carried out at 60°C under atmospheric pressure, preventing methanol from boiling off at 65 °C. Operation at a higher temperature and pressure is also possible but costs expensive. The reaction mixture is separated

into two liquid phases of methanol and oil. By repeated washing with water for the removal of glycerol and methanol, the fatty acids could be recovered [16].

Glycerol and fatty acids from TAG are used as a precursor for various commodities in healthcare and for various industrial uses [86] including the following: substances to prevent dryness of the skin, food, or costumes with moisturizing properties, castor oil to help restore the skin's natural moisture balance, and biodiesel as an alternative to fossil fuels.

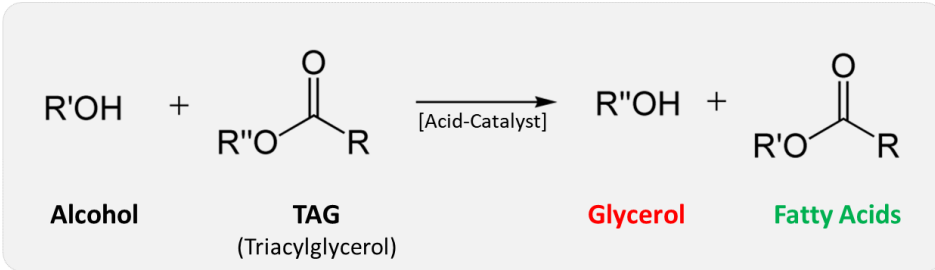

Figure 2.3 Transesterification of TAG for glycerol and fatty acids production.

[16]

2.5.2 Lipid Synthesis Molecular Mechanism

C. reinhardtii responds to environmental cues by accumulation of intracellular lipid droplets (LDs). Nitrogen deprivation is the most common trigger for oil accumulation among the other physical stressors such as high light, salinity increase, or temperature change [87]. Transcriptome analysis of nitrogen-starved *C. reinhardtii* helped give insights into the TAG synthetic mechanisms [88,89]. Nitrogen deprivation was reported to downregulate photosynthesis and protein synthesis individually or simultaneously and to drive acetate flux into fatty acid synthesis not to gluconeogenesis [87]. In addition to that, the nitrogen-responsive regulator, NRR1, was identified as the only transcriptional up-regulator of TAG accumulation- the *nrr1* mutant showed a reduction in the oil content by more 50% [90].

Biosynthesis of fatty acids and triacylglycerols are summarized in Figure 2.4, 2.5 and 2.6, respectively [19].

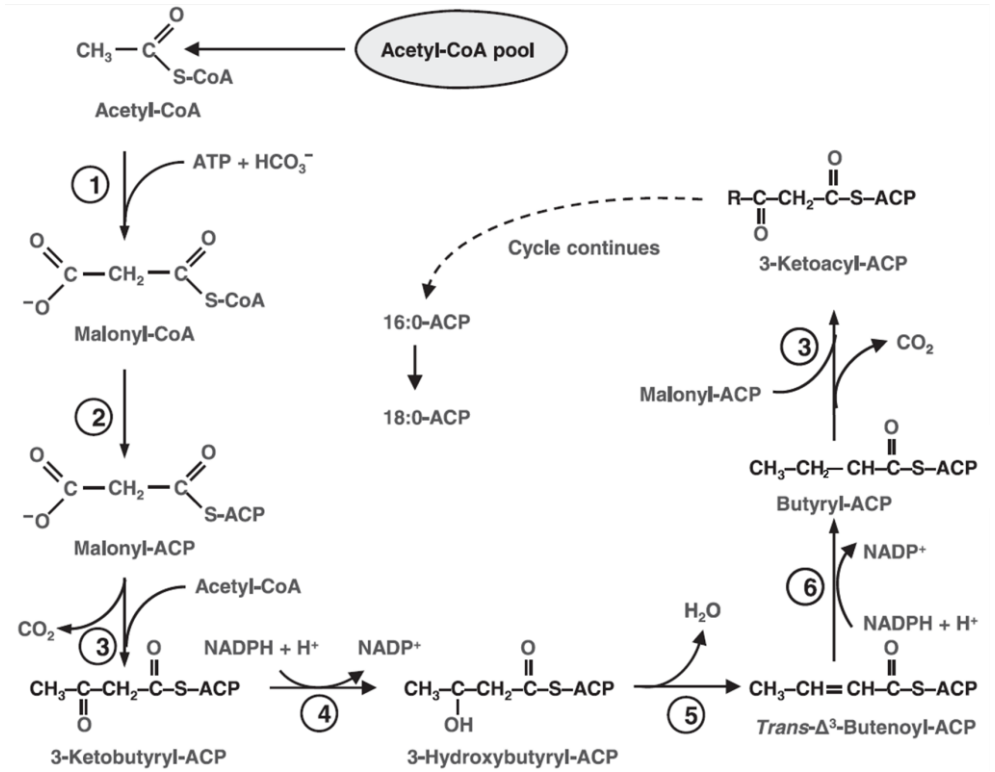

Figure 2.4 Fatty acid synthesis pathway in chloroplasts [19]. (1, 3) acetyl CoA carboxylase, (2) malonyl CoA:ACP transferase, (4) 3-ketoacyl ACP reductase, (5) 3-hydroxyacyl ACP dehydrase, and (6) enoyl ACP reductase.

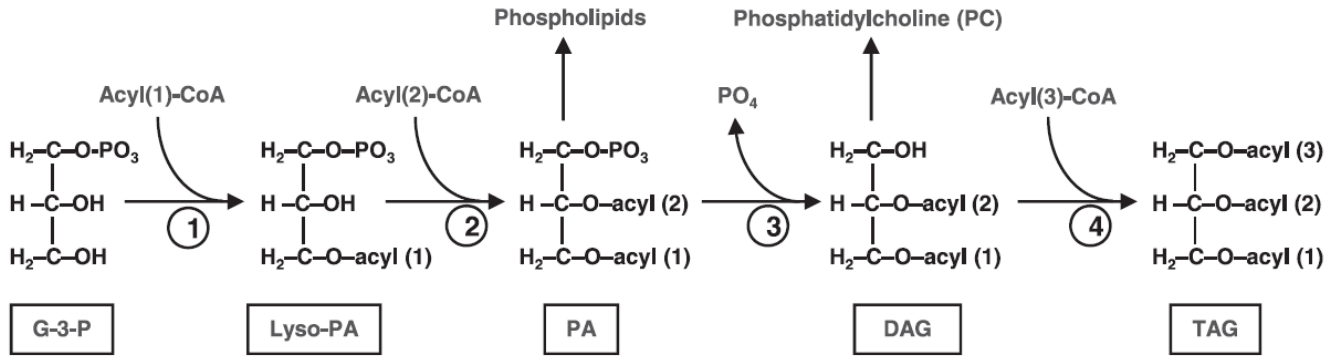

Figure 2.5 Simplified TAG biosynthesis pathway in microalgae [19]. (1) Cytosolic glycerol-3-phosphate acyl transferase, (2) lyso-phosphatidic acid acyl transferase, (3) phosphatidic acid phosphatase, and (4) diacylglycerol acyl transferase.

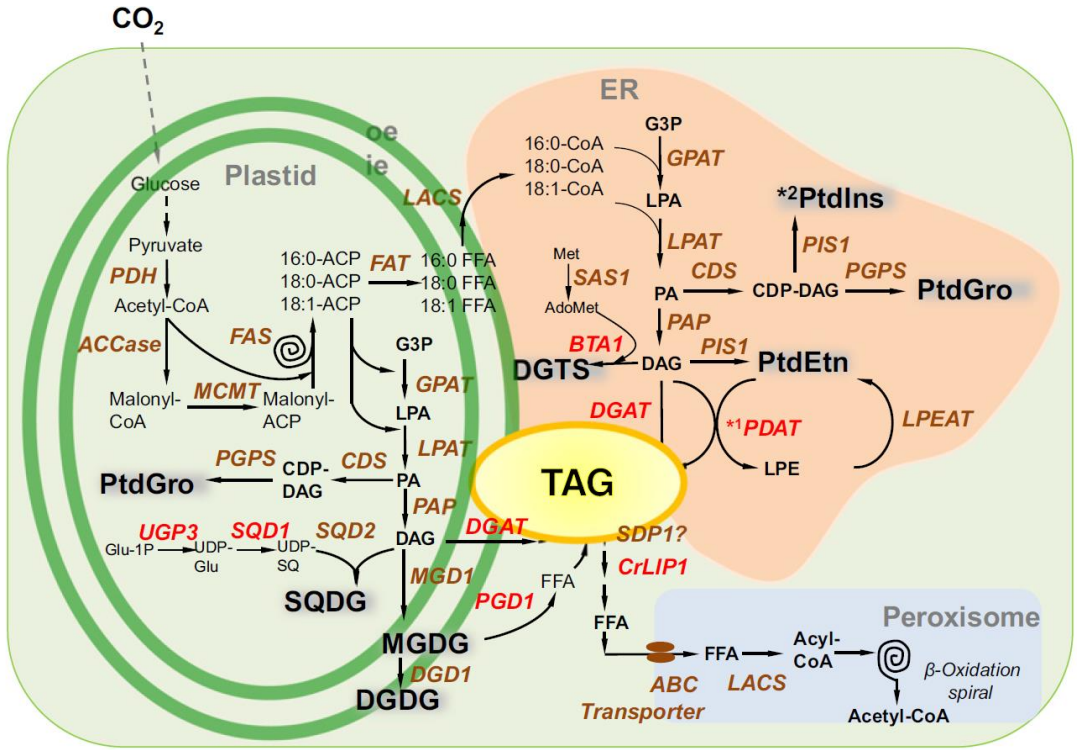

Figure 2.6 Reactions known or thought to be involved in glycerolipid metabolism in *Chlamydomonas reinhardtii.* [87]

2.5.3 Genetic Engineering of Lipid Metabolism

Several transgenic strategies have been studied to enhance the lipid content in higher plants [6]. Because many of the genes in the lipid metabolism of plants are homologous to the sequenced microalgal genomes, these strategies have been also applied especially to industrial microalgae (*Nannochloropsis salina*, *Dunaliella tertiolecta*, and *Chlorella vulgaris*). Several recent studies are summarized in Table 2.12 [6,91].

In that 90% of the fatty acids comprising TAG is mostly derived from chloroplast, it can be seen that most of the studies targeted chloroplast-related genes [87]. In order to inactivate the fatty acid synthesis-related genes in nucleus, nuclear transformation has been performed either through random mutagenesis or through RNA silencing [6].

As mentioned earlier that nuclear transformation has the limitation of phenotype maintenance, there is a need to confirm whether gene silencing disturbs transgene expression and whether these species still maintain their transformant phenotypes with high lipid productivity.

Table 2.12. Examples of genetic engineering of lipid metabolism. [6,91]

Hosts	Sources	Genetic Methods	Results	References
Acetyl-CoA carboxylase (Acc1) gene				
Navicula saprophila	*Cyclotella cryptica*	Overexpression	2–3 × ACC activity, no change in lipid content	[92]
Diacylglycerol acyl-transferase (DGAT2) gene				
Chlamydomonas reinhardtii	*Brassica napus*	Overexpression	1.5 times increase in the lipid content and change the lipid profile	[93]
Phaeodactylum tricornutum	*Phaeodactylum tricornutum*	Overexpression	Increase the neutral lipid content by 35%	[94]
Phosphoenolpyruvate carboxylase (PEPC1) gene				
Chlamydomonas reinhardtii		Knocking-out	Increase the TAG level by 20%	[95]
Phosphoenolpyruvate carboxykinase (PEPCK) gene				
Phaeodactylum tricornutum		Knocking-out	1.5 times increase in the lipid content and increase the TAG accumulation about 1.1 times	[96]

Table 2.12. Examples of genetic engineering of lipid metabolism. [6,91] (Continued)

Hosts	Sources	Genetic Methods	Results	References
Acetyl-CoA carboxylase (Acc1) gene				
Cyclotella cryptica	*Cyclotella cryptica*	Overexpression	2-3 fold increase in ACCase activity	[97]
Brassica napus	*Arabidopsis thaliana*	Overexpression	6% increase	[98]
Solanum tuberosum	*Arabidopsis thaliana*	Overexpression	5-fold increase in a tissue that normally is very starch rich and lipid poor	[99]
3-ketoacyl-acylcarrier protein synthase III (KASIII) gene				
Nicotiana tabacum	*Spinacia oleracea*	Overexpression	No increase	[100]
Arabidopsis thaliana	*Cuphea hookeriana*	Overexpression	No increase	[100]
Brassica napus		Overexpression	No increase	[100]

Table 2.12. Examples of genetic engineering of lipid metabolism. [6,91] (Continued)

Hosts	Sources	Genetic Methods	Results	References
Glycerol-3-phosphate dehydrogenase (G3PDH) gene				
Brassica napus	*Saccharomyces cerevisiae*	Overexpression	40% increase	[101]
Glycerol-3-phosphate acyltransferase (GPAT) gene				
Arabidopsis thaliana	*Carthamus tinctorius*	Overexpression	10 - 21% increase	[102]
Arabidopsis thaliana	*Escherichia coli*	Overexpression	15% oil content increase	[102]
Lysophosphatidic acid acyltransferase (LPAT) gene				
Brassica napus	*Saccharomyces cerevisiae*	Overexpression	Increases of 8 to 48% in seed oil content	[103
Arabidopsis thaliana	*Saccharomyces cerevisiae*	Overexpression	Increases of 8 to 48% in seed oil content	[103]

Table 2.12. Examples of genetic engineering of lipid metabolism. [6,91] (Continued)

Host	Source	Genetic Methods	Results	References
Diacylglycerol acyltransferase (DAGAT) gene				
Glycine max	*Umbelopsis ramanniana*	Overexpression	Increase in oil of 1.5%	[104]
ADP-glucose pyrophosphorylase gene				
Chlamydomonas reinhardtii	*sta6*	Knocking-out	1.5-fold	[105]
Isoamylase genes gene				
Chlamydomonas reinhardtii	*sta7*	Knocking-out	2.0 – 3.5-fold	[105]
Chlorella pyrenoidosa		Knocking-out	Accumulated 20.4% more polyunsaturated fatty acids and 18% less saturated fatty acids	[106]
Acetyl-CoA carboxylase / acyl-CoA synthetase (fadD) gene				
Escherichia coli	*endogenous thioesterase/ plant*	Overexpression Knocking out	20-fold increase	[107]

Table 2.12. Examples of genetic engineering of lipid metabolism. [6,91] (Continued)

Host	Source	Genetic Methods	Results	References
Peroxisomal long-chain acyl-CoA synthetase (LACS) isozymes gene				
Arabidopsis thaliana	-	Knocking-out	This enzyme is involved in β-oxidation pathway of fatty acids that cells depend on for cellular energy and precursors for cellular division.. This mutant showed deleterious effects on cellular growth.	[108]
3-ketoacyl-CoA thiolase (KAT2) gene				
Arabidopsis thaliana	-	Knocking-out	This enzyme is involved in β-oxidation pathway of fatty acids that cells depend on for cellular energy and precursors for cellular division.. This mutant showed deleterious effects on cellular growth.	[109]
Short-chain acyl-CoA oxidase enzymes (ACX3 and ACX4) gene				
Arabidopsis thaliana	-	Knocking-out (Double)	This enzyme is involved in β-oxidation pathway of fatty acids that cells depend on for cellular energy and precursors for cellular division.. This mutant showed deleterious effects on cellular growth.	[110]

Table 2.12. Examples of genetic engineering of lipid metabolism. [6,91] (Continued)

Host	Source	Genetic Methods	Results	References
12:0-biased acyl-ACP thioesterases gene				
Arabidopsis thaliana	*Umbelopsis ramanniana*	Overexpression	10 – 24% 12:0 of total FA	[111]
Escherichia coli	*Umbelopsis ramanniana*	Overexpression	10% of the total unsaturated synthesis in the log phase up to nearly 90% in the early stationary phase	[112]
14:0-biased acyl-ACP thioesterases, gene				
Escherichia coli	*Cinnamomum camphorum*	Overexpression	200-fold increase	[113]
8:0/10:0-biased acyl-ACP thioesterases gene, ACP synthase (KAS) gene				
Canola	*Cuphea hookeriana*	Overexpression Knocking-out	30-40% FA increase	[114]

2.5.4 Economic Triacylglycerol (TAG) Production

Genetic engineering of lipid metabolism has been mainly investigated for oil enhancement, but only the increase in lipid content of microalgae has been reported to limit overall lipid productivity [115]. Considering trade-off between growth and lipid metabolism, proper balance of growth and lipid content should be required for the best economic production [116]. Some research supposed that inducible promoters could control overexpression of lipid synthesis without negative impacts on microalgal growth (e.g. copper-responsive elements in *C. reinhardtii*) [117]. From an economical point of view, however, such strategies have difficulty for cost-effective TAG production [6].

More significantly, optimization of cultivation has been also considered to increase TAG. It is well known that when exposed to stress conditions (*e.g.*, nutrient deprivation), microalgae accumulate lipids in the form of TAGs [20]. What is problematic is that this accumulation occurs at the expense of growth-associated energy, leading to a decrease in microalgal biomass and productivity [6].

Nutrient deprivation for TAG induction is closely connected to the C/N ratio, the ratio of carbon to nitrogen, or Redfield ratio. When microalgae do not have enough nitrogen, they slow down their proliferation and start converting the

excessive amount of carbon sources to energy storage products, such as lipids and/or starch, to balance the C/N ratio [87]. A low amount of remnant carbon and nitrogen sources with a re-steady C/N ratio would be used for growth-associated metabolism. This combinatorial impact on growth and TAG production has been mentioned in several studies (Table 2.13).

Table 2.13. Examples of increased lipid productivity that results from concurrent growth and lipid accumulation

Organisms	Process Types	Nutrient Concentration	Results	References
Chlorella munutissima	Batch	50% NO^{3-} / 60% PO_4^{3-} (0.125 g/l of NO^{3-} / 0.075 g/l of PO_4^{3-})	1.47-fold increase	[118]
Chlamydomonas reinhardtii	Batch	3.7% NH_4^+ (0.7 mM of NH_4^+)	2.1-fold increase	[119]
Chlorella vulgaris	Batch	1 mM $NaNO_3$ and 10 mM KNO_3	1.55-fold increase	[117]
Chlorococcum oleofaciens	Batch	1 mM $NaNO_3$ and 10 mM KNO_3	1.48-fold increase	[117]

Chapter 3

Microfluidic Perfusion Bioreactor with Steady High C/N Ratio for Optimization of Microalgal Lipid Productivity

*Published in Bioresource Technology 2017, **233**, 433-437*

3.1 Introduction

Recently, demands for secondary metabolites such as antioxidants, antibiotics, and nutritional additives have markedly increased, and there is a need for technologies that can meet those demands [5]. Secondary metabolites, however, are produced in the cellular stationary phase, and in that phase, nutrients may become mostly depleted. Consequently, there is no cell growth, which results in a decrease in the total amount of metabolites produced. Although cell-strain development via genetic engineering could increase metabolite productivity per cell, genetically modified organism issues can arise and decreased growth could occur [5,6,7].

A bioreactor process that provides a continuous supply of elementary nutrients is known to effectively increase biomass production and secondary bioproduct yield compared to that obtained from a traditional batch process. Cells in a batch process system consume a finite amount of nutrients that are available in concentrations that decrease with time. Accordingly, when batch processes are operated with high carbon to nitrogen (C/N) ratio for both cellular growth and secondary metabolites production, the ratio becomes not kept over time and finally no nutrients exists due to microbial consumption. In addition to that, the steady state achieved in a continuous supply process contributes to a constant nutrient condition,

under which the cells in the reactor proliferate with constant physiological phenotypes. This one-condition-to-one-phenotype feature can assist in the physiological analysis of cellular characteristics during cultivation [120]. In contrast, time-dependent nutrient changes in batch processes can make it difficult to analyze cellular properties due to the many-conditions-to-one-phenotype feature of batch processing [118,121-124].

Development of microfluidic chips could help realize changes in continuous cultivation processes that can be applied at microscale to milliscale [125]. In order to produce a miniature, precise bioreactor that is capable of presenting the same physiological conditions as those on an industrial scale, the microfluidic chips should be capable not only of continuous processing but also capable of suspension cultivation, a second important factor in bioreactor processes. Suspension-based cultivation increases the cellular contact area available for nutrient uptake while maintaining the cells' physiological properties. It was demonstrated that trapping of *Corynebacterium glutamicum* could precipitate a physiologically undeniable deviation in the state of suspended cells; *i.e.*, 50% decreases in division rate and cell length [126], and it was reported that immobilized *Chlamydomonas reinhardtii*, a microalgal model, exhibited 16% and 28% decreases in photosynthesis and respiratory activities, respectively [127]. In addition, it was described a diffusible

microfluidic chip that could be used to test the effects of a toxin on several marine microalgae and diatoms, including *Phaeodactylum tricornutum* [128-130]. Their device included diffusible chambers confined by semipermeable membranes above a continuous flow with different concentrations, and in which the cells were not immobilized but freely swimming and more sensitive to the toxin concentration.

In this study, a perfusion microfluidic chip is fabricated that meets both the continuous processing and suspension cultivation requirements. The microfluidic chip was applied in a continuous feed system at steady high C/N ratio for production of a secondary metabolite, triacylglyceride (TAG), from *C. reinhardtii*. TAG, a bio-derived neutral lipid, has been regarded as a precursor for biodiesel, an alternative to fossil fuel, and for ricinoleic acid (RA), which has healthcare and industrial uses [86]. Ammonium (NH_4^+) nutrient starvation is the most efficient way to obtain TAG from *C. reinhardtii*, but that approach limits biomass increases, thereby reducing the total lipid quantity produced. We assumed that conditions under which cells could sense being starved but still exert their primary metabolic activities, such as growth, would be the best cultivation condition for achieving maximal TAG production.

3.2 Materials and Methods

3.2.1 Fabrication of Microfluidic Perfusion Bioreactor

The microfluidic continuous cultivating device was fabricated in PDMS (SylGard A, B) by applying soft lithography to produce Module I for nutrient gradient generation and Module II for microalgae growth. Module I had curved serpentine channels and embedded inlet and outlet holes. A glass coverslip was treated with air plasma (150 mTorr, 100 W) for 5 min and then attached to Module I. Subsequently, a polyethylene terephthalate (PET) transwell membrane (BD Biosciences, Cat. No.: 353091) and an upper PDMS piece were stacked in order, and the assembly was heated for 30 min in a 75°C oven for irreversible bonding. The membranes were treated with PLL(20)-g-PEG(2) (0.1 mg/mL) in 10 mM Tris-HCl buffer (pH 6.8) for an hour at room temperature and washed twice with 10 mM Tris-HCl buffer (pH 6.8) to block microalgal cell adhesion [131]. Module II was prepared with two air-plasma-treated PDMS fragments between which other membranes were located. After loading the samples into the provided holes in Module I, Module II was placed on top of Module I to form a growth chamber that could be subjected to continuous perfusion mixed streams. Polyethylene tubing was inserted into the inlet and outlet

holes to make the fluidic connections. The pieces of tubing were then connected to medium-containing syringes installed in a syringe pump (Figure 3.1). Rhodamine solution (SigmaAldrich, Cat. No.: R6626, 0.7 mg/mL) was used to check the concentration gradient, and fluorescein isothiocyanate (FITC)-dextran solution (SigmaAldrich, Cat. No.: FD10S) 25 μg/mL in 10 mM Tris-HCl (pH 8.0) was used to check concentration stability.

3.2.2 Microalgae Cultivation

CC-4349 (*cw15 mt-* strain) from the Chlamydomonas Center was cultivated in tris-acetate-phosphate (TAP) with NH_4^+ liquid medium for 5–7 d until the cells entered the stationary phase. A second inoculation of the suspension diluted the cells to 5×10^4 cells/mL in 30 mL of medium in order to maintain the cells in a healthy state for further cultivation. When cell abundance reached $3–4 \times 10^6$ cells/mL they underwent two deionized water (D.W.) washings, and the washed cells were loaded to Module I. Cell counting was performed by using a hematocytometer.

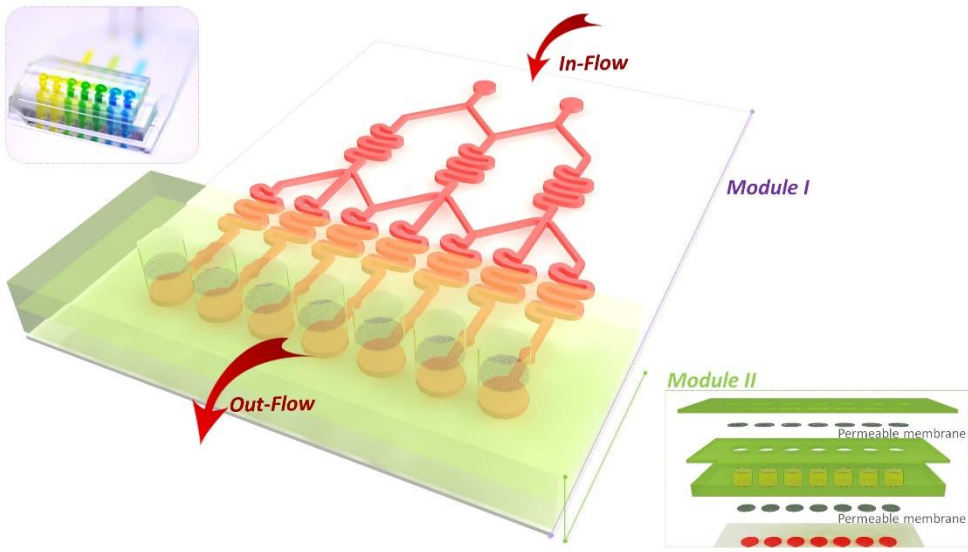

Figure 3.1 Schematic representation of the microfluidic perfusion bioreactor for continuous, stable flows of nutrient medium. The left top box shows the photograph of this device with concentration gradient. Yellow cylindrical spaces in Module II are chambers for microalgal growth.

3.2.3 Triacylglycerol (TAG) Staining and Fluorescent Microscopy

BODIPY 505/515 (4,4-difluoro-1,3,5,7-tetramethyl-4-bora-3a,4a-diaza-s-indacen) (Thermo, Cat. No.: D3921) was dissolved in dimethyl sulfoxide (DMSO) to form a 5 mM stock solution [132]. A microalgal suspension was mixed with 1/1,000 volumes of the stock BODIPY solution and agitated for 30 s. After 10 min incubation in the dark, each sample was washed once with 5× lower volumes of 20 mM Tris-HCl buffer. Images of BODIPY-stained lipid droplets in cells were captured by using an epifluorescence Eclipse Ti inverted fluorescence microscope (Nikon) with a GFP_Quadruple filter. Images were processed with NIS-Elements AR v.4.20.00 for intensity measurement.

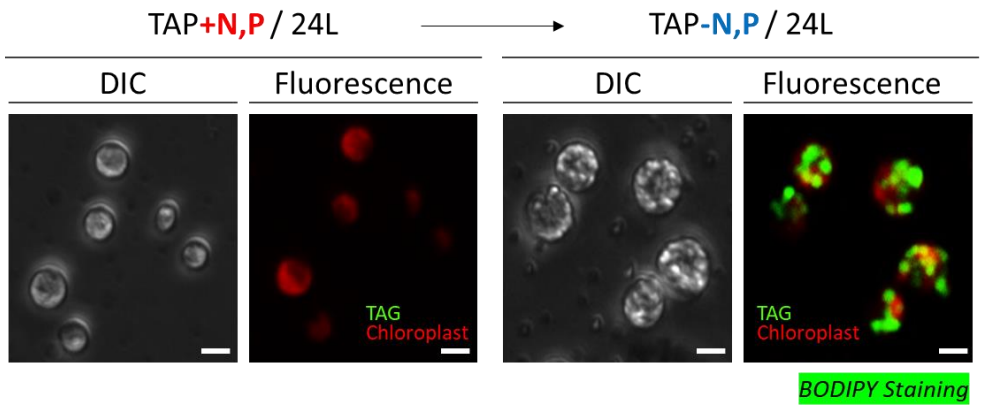

Figure 3.2 BODIPY staining for TAG produced after depletion of both NH^{4}_{+} and PO_4^{2-}.

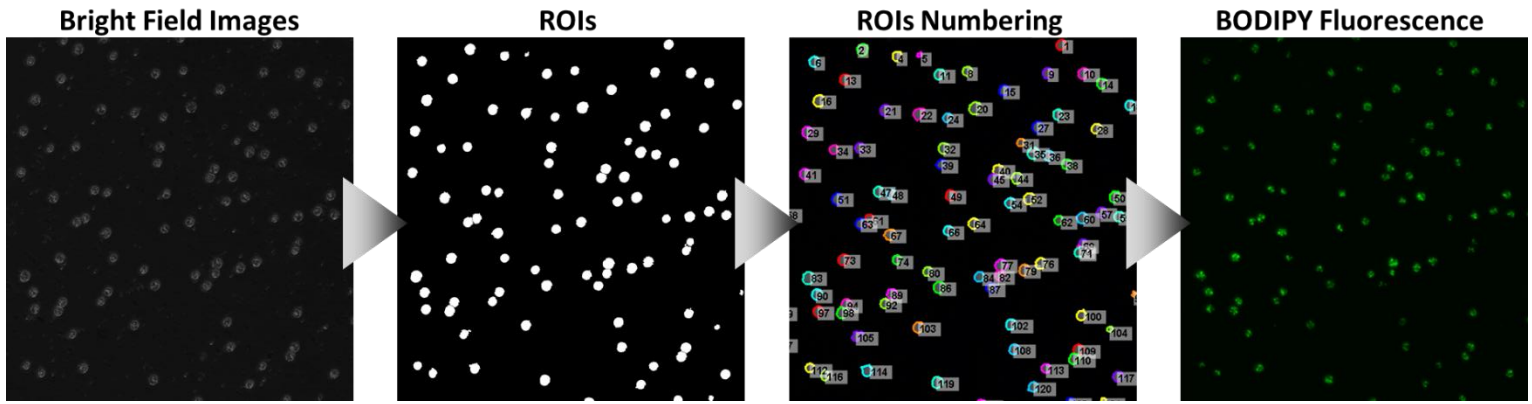

Figure 3.3 Measurement of individual cell areas and its TAG-fluorescent intensity. Each cell was defined as individual ROIs by manipulating boundaries of cells captured in bright field images, which can help calculate fluorescent intensities in each numbered ROI.

3.3 Results and Discussion

3.3.1 Characteristics of Microfluidic Perfusion Bioreactor

Laminar streams of two different solutions were sufficiently mixed by diffusion and a little inertial force in the curved serpentine channels (Figure 3.4 (a) and (b)). To assess the bioreactor's solution-mixing behavior, 0% rhodamine (*i.e.*, D.W.) and 100% rhodamine solutions were introduced separately to the microfluidic chip through one or the other inlets. It was observed that concentrations at the five outlets were linearly generated, which meant that Module I could precisely produce proportionally linear gradients (Figure 3.4 (c)).

Module II included culture chambers sandwiched by top and bottom permeable membranes (Figure 3.5 (d) and (e)). After filling the microfluidic chip with D.W., FITC-Dextran solution was introduced at 10 μl/hr across the chambers. Fluorescence intensity graphs showed that the D.W. was rapidly exchanged (within a couple of minutes) with the FITC-Dextran solution; moreover, the FITC-Dextran content in the chambers remained constant over time (Figure 3.5 (f)).

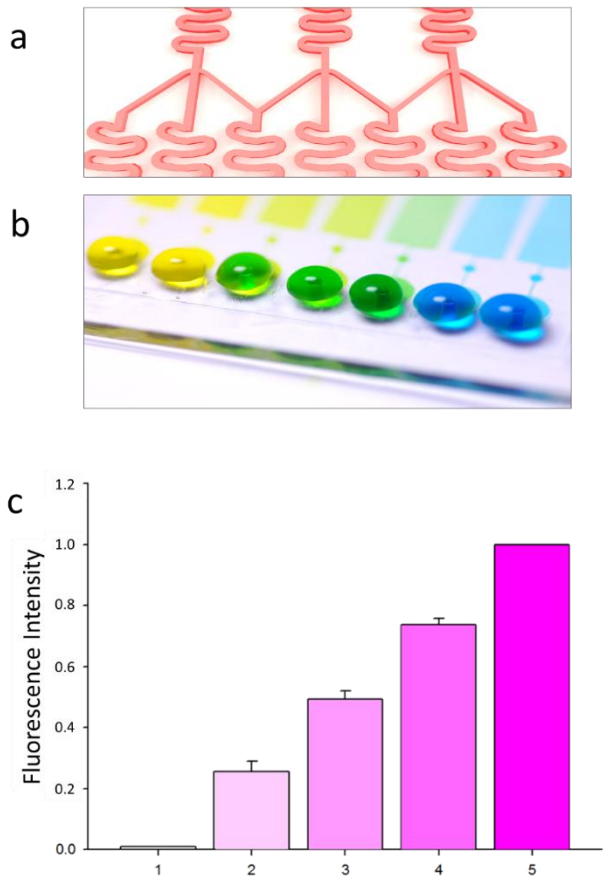

Figure 3.4 Evaluation of characteristics of Module I. (a) Schematic of curved serpentine channels and mixing channels in Module I, (b) photograph of Module I, (c) fluorescent intensity measurement of rhodamine diluted solutions in each hole. Error bars represent standard deviation (SD) from three biological replicates.

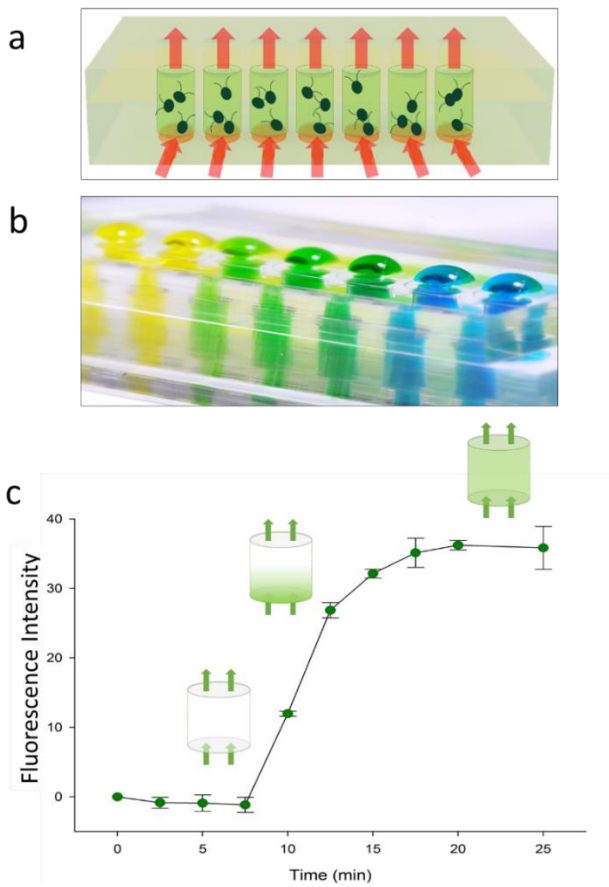

Figure 3.5 Evaluation of characteristics of Module II. (a) schematic growth chambers in Module II and continuous feeds through the chambers, (b) photograph of Module II filled with food dyes, and (c) temporal changes in kinetics of FITC-dextran fluorescent intensity of growth chambers initially filled with deionized water. Error bars represent standard deviation (SD) from three biological replicates.

3.3.2 Synergetic Effect of Phosphate Depletion

This microfluidic chip was applied for assessing TAG production in order to determine whether, along with the effect of NH_4^+, there is a synergistic effect of phosphate PO_4^{2-}, which could be an important factor in the production of TAG. A NH_4^+-deplete medium with five different concentrations of PO_4^{2-} were continuously passed through the growth chamber where CC-4349 in the exponential state under normal conditions (7.5 mM NH_4^+, 1.0 mM PO_4^{2-}) had been loaded. After 120 hr, starved cells in each chamber were collected and stained with BODIPY to detect TAG. A scatter plot graph (N = 313) showed that the slope of the sum fluorescent intensity of the cells was highest under 0% NH_4^+/ 0% PO_4^{2-} conditions (Figure 3.6). In addition, the percentile graph showed that the 50% median bar was 2.43 times higher under 0% NH_4^+/ 0% PO_4^{2-} than under the other conditions.

These results indicate that PO_4^{2-} is a factor that affects TAG production efficiency and that both NH_4^+/PO_4^{2-} starvation can synergistically induce an increase in TAG production. Traditional batch cultivation with 0%/25% of NH_4^+/PO_4^{2-} could also show synergistic effects on TAG yield, but the batch process supposedly involves nutrient depletion over time and the depletion seem to synergistically activate TAG production (Figure 3.7).

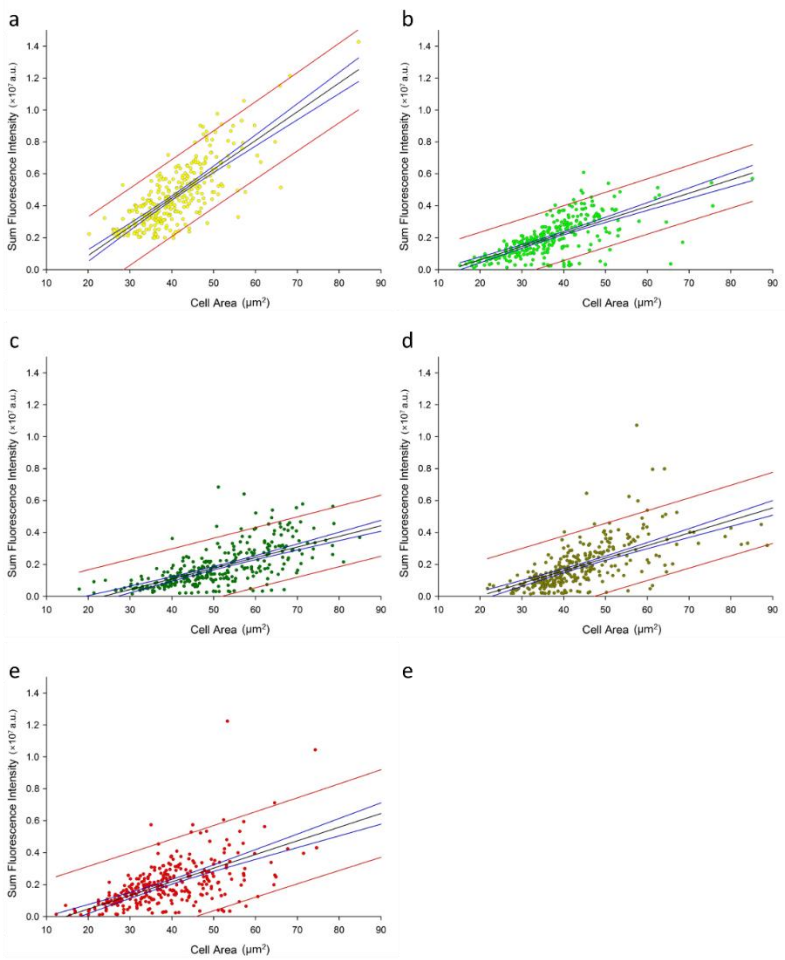

Figure 3.6 Scatter graph plot of each cell area and the sum fluorescent intensities of each tested phosphate and ammonium concentration ((a) 0/0, (b) 0/25, (c) 0/50, (d) 0/75, and (e) 0/100 of [NH_4^+]%/[PO_4^{2-}]%). Each circle represents a single cell (N=313) from three separate biological replicates. Black slope is trend line that indirectly indicates the amount of TAG produced in a cell, and blue slope and red slope show 95% prediction line and 95% confidence line, respectively.

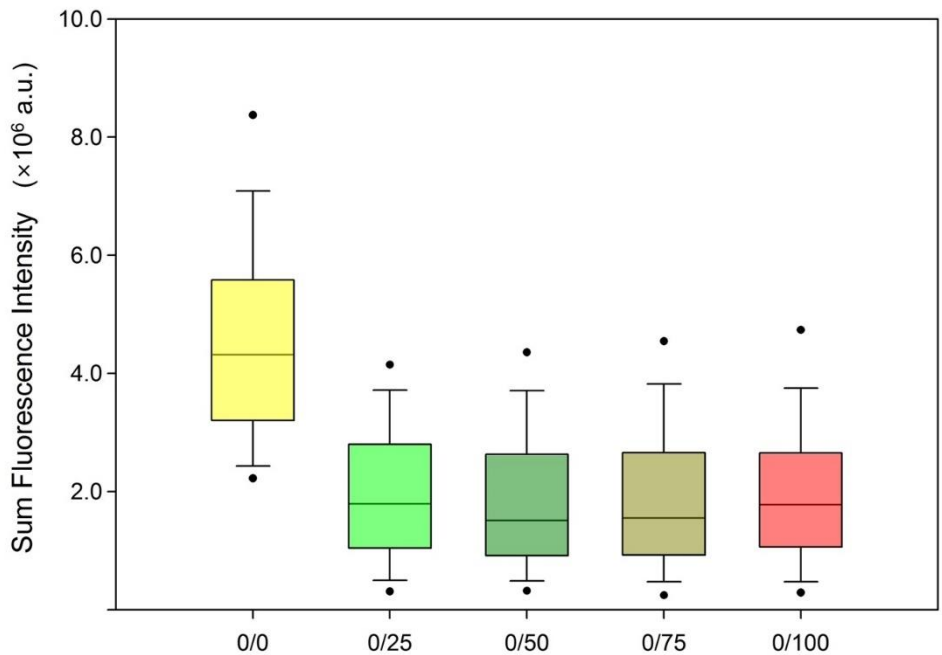

Figure 3.7 Percentile graph presenting TAG fluorescent intensities for five phosphate and ammonium concentration gradients (0/0, 0/25, 0/50, 0/75, and 0/100 of [NH_4^+]%/[PO_4^{2-}]%). The box indicates from 25th percentile to 75th percentile, the line in the middle of the box is for the median, and the upper and lower whisker are for 10th and 90th percentile, respectively.

3.3.3 Effect of Low Concentrations of NH_4^+ and PO_4^{2-}

Based on the evidence of synergistic effects, it was hypothesized that a small amount of NH_4^+/PO_4^{2-} could increase cell growth to a greater extent than that obtained from the only NH_4^+-deplete medium and that additional growth thereby increases biomass. A gradient series of double deficient NH_4^+/PO_4^{2-} media (0%/0%, 2.5%/2.5%, 5.0%/5.0%, 7.5%/7.5%, and 10%/10%) was generated, and sums of TAG fluorescent intensities and final cell numbers were derived. The sums of fluorescent intensities, as well as the fluorescent slopes (Figure 3.8), showed few differences in median values, meaning that the tested range of nutrient conditions had no critical effect on TAG yield. In contrast, concentrations above 5%/5% resulted in higher levels of cell growth than that under the 0%/0% condition. In particular, the cells in 7.5%/7.5% media had a 3.5-fold increase in apparent growth rate. This 7.5%/7.5% of NH_4^+/PO_4^{2-} media combination was regarded as the maximum starvation threshold point that positively affected both TAG yield from starvation and biomass increase from continuous nutrient (Figure 3.9).

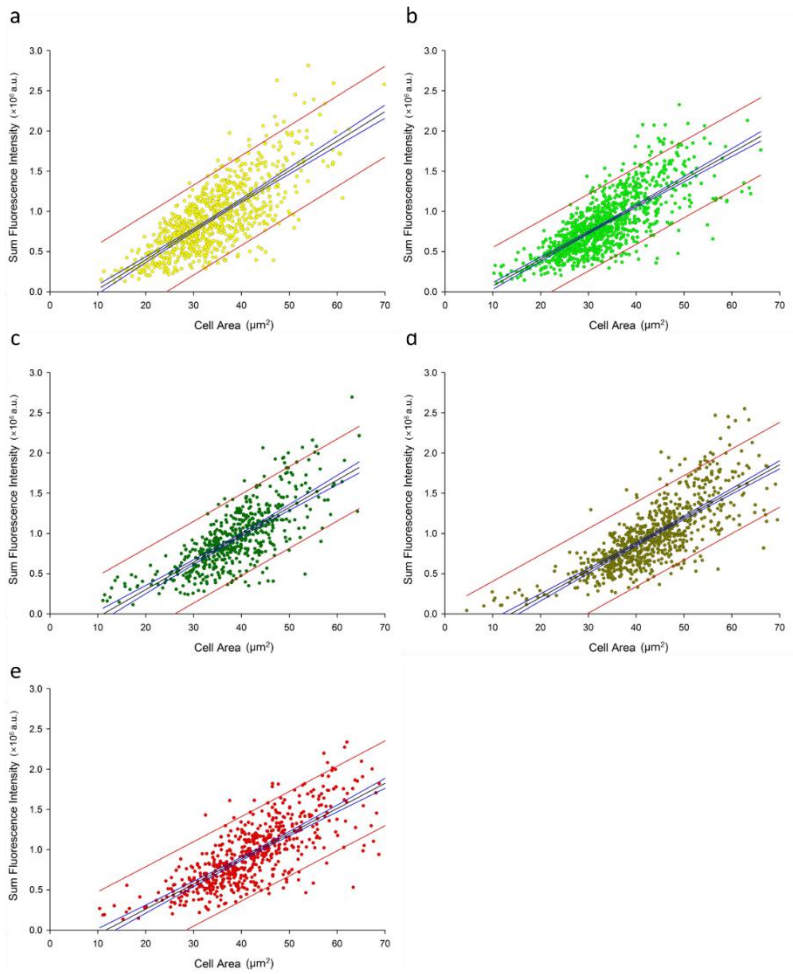

Figure 3.8 Scatter graph plot of each cell area and the sum fluorescent intensities of concurrent nutrient concentrations ((a) 0/0, (b) 2.5/2.5, (c) 5.0/5.0, (d) 7.5/7.5, and (e) 10.0/10.0 of [NH_4^+]%/[PO_4^{2-}]%). Each circle represents a single cell (N=546) from three separate biological replicates. Black slope is trend line that indirectly indicates the amount of TAG produced in a cell, and blue slope and red slope show 95% prediction line and 95% confidence line, respectively.

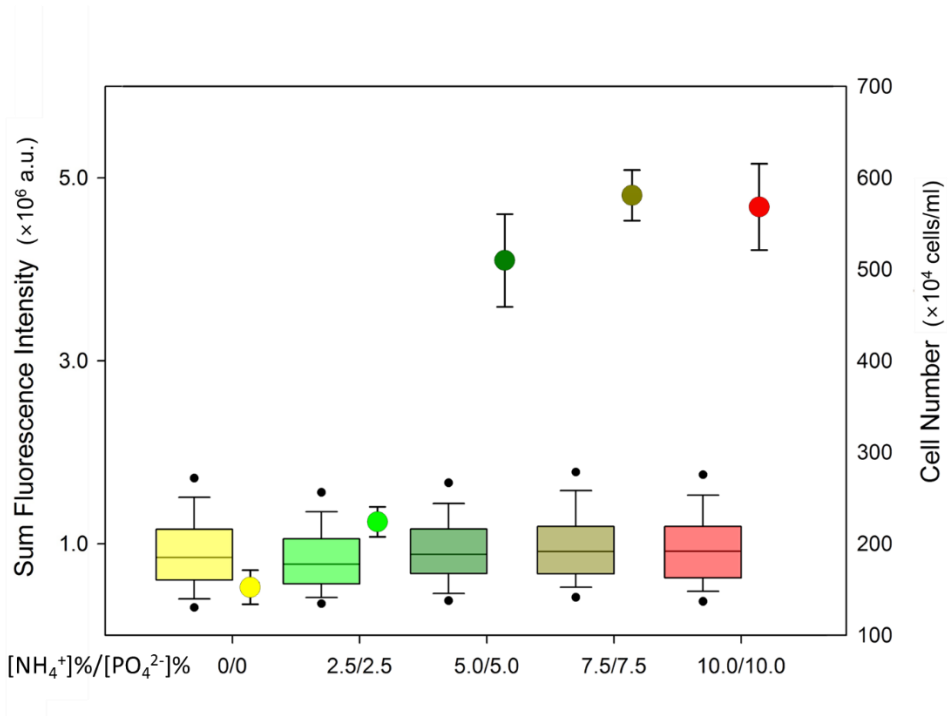

Figure 3.9 Percentile graph presenting TAG fluorescent intensities and a graph of final cell numbers obtained by applying concurrent concentration gradients of phosphate and ammonium (0/0, 2.5/2.5, 5.0/5.0, 7.5/7.5, and 10.0/10.0 of $[NH_4^+]$%/$[PO_4^{2-}]$%). The box indicates from 25th percentile to 75th percentile, the line in the middle of the box is for the median, and the upper and lower whisker are for 10th and 90th percentile, respectively. Error bars represent standard deviation (SD) from three biological replicates.

5%/5% NH_4^+/PO_4^{2-} to 10%/10% NH_4^+/PO_4^{2-} conditions were demonstrated to yield more biomass than the quantity obtained by applying the 0%/0% NH_4^+/PO_4^{2-} condition. It was expected that when cells were supplied with more than 5.0%/5.0% NH_4^+/PO_4^{2-}, the TAG yield would be slightly less than that of the double deplete condition because the cell growth can compete with or refrain from activating secondary metabolite pathways. The yields, nevertheless, were more than expected. There is a study about the starvation and its connection with quorum sensing, a special cellular characteristic that maintains cell numbers, in a cultivated space [133]. This perfusion bioreactor on a microfluidic chip trapped the microalgae between upper and lower permeable membranes in the area in which the nutrient-bearing medium flowed. As time passed, cells continued to grow under the low nutrient concentrations, and under that condition, the chambers became filled with many cells, which triggered quorum sensing and starvation with TAG production. In other words, the greater the cell growth in limited space of the chamber, the more cell starvation, particularly in media with concentrations of 5.0%/5.0% NH_4^+/PO_4^{2-} or higher.

A low amount of nitrogen o phosphorous in batch processes could also contribute to both proliferation and TAG production. But, such processes involves depletion of the nutrients, where cells stop growth-associated metabolism resulting in the low total yield of TAG. In contrast, continuous supply of a low nutrient in

microalgal cultivation could help the cells keep growth-associated metabolism as well as TAG production with remnant carbon sources, maintaining re-steady C/N ratio without nutrient depletion. This cultivation could be competitive in supplementing costs on facilities and process operation by improvement of TAG total yield.

The results suggest that the developed microfluidic device can be utilized as an investigative tool to assist in determining optimized growth/starvation conditions for potential use at the millimeter or larger scale. The device results showed that a greater quantity of TAG can be obtained by changing the cultivation system and cultivation media. A similar cultivation approach on an industrial scale may produce different results with a delicate modelling [124] and, therefore, there is a need to perform further trials on larger scales [134].

3.4 Conclusions

The cells in the perfusion system of steady high C/N ratio produced TAG and also grew although they were being supplied with a nutrient concentration (particularly 7.5%/7.5% NH_4^+/PO_4^{2-}) that was only slightly higher than an absolutely deplete one. This suggests that a continuous, stable flow of a low concentration nutrient medium at steady high C/N ratio can not only starve cells but also encourage them to grow at a minimum growth rate.

Chapter 4

Vibration-Induced Stress Priming During Seed Culture to Increase Microalgal Biomass in High Shear Field-Cultivation

*Published in Bioresource Technology 2018, **254**, 340-346*

4.1 Introduction

In order to increase the microalgal biomass, some research groups have studied the effect of ultrasound on microalgal growth rates [83, 135] because mechanical stimulus is known as one of the key factors to produce more biomass as well as metabolites which can be used as nutrients. Although the microalgae grew faster, the equipment necessary for ultrasound could not be achieved on an industrial scale. It has been pointed out that the costs for the microalgae process are too high, and the process has yet to be efficiently managed [136]. In this regard, it is not cost-effective to set up a vibration generating system on a large industrial scale. In addition, its vibrational effect could be offset by the vigorous turbulence in the bioreactors.

To enhance biomass productivity, it is necessary to use a realistic approach that uses the innate characteristics of the microbes. Cellular stress response (CSR) consists of a wide range of molecular changes that cells undergo in response to environmental stress. Microbes are exposed to many environmental factors such as temperature changes, osmolality variations, and nutrient deprivation. These stressors cause the microbes to physiologically change through various signal transduction networks which can negatively affect their survival and reproduction. Afterwards, these cells reprogram their metabolism and adapt to their environment achieving

proper cellular growth, proliferation, and development under the stressors. Priming is a special cellular phenomenon of CSR: cells that have previously experienced a temporary milder stress (priming) have an enhanced stress response to a second stress event (triggering) [137-141]. The primed state comes with a transient metabolic cost shifting the metabolism from growth to production of protective compounds, but primed microbes are more beneficial in terms of survival in a stress environment than non-primed ones. In plants, a caterpillar chewing-treatment made *Arabidopsis thaliana* respond more actively than the non-treated ones in a severe vibrational actuator treatment [142]. In addition, fungi that already experienced milder heat also showed their priming effect on progeny colonial growth in extreme heat conditions [143]. These results were supported by a stress response metabolite analysis, in which stress priming was found to activate the general stress response which helps the cells to prepare themselves.

Although this priming effect is helpful for living organisms' survival and their biomass, stress priming of *Chlamydomonas reinhardtii* (a model photosynthetic microalgae) and mechanical stimulation that the microalgae experience in bioprocesses have not been considered together. According to molecular biology for microalgal mechanotransduction, several mechanoreceptors were just found to be involved in its mechanotransductory pathway: *TRP11* encodes a flagellar

mechanoreceptor protein [77], *CAV2* a flagellar voltage-dependent calcium channel, *ADF1*, which is a TRP family Ca^{2+} channel [78], and *MSC1* an intracellular mechanosensitive ion channel involved in the organization of the chloroplast membrane [76, 144]. Collisions deform the microalgal cell body. Thus, *C. reinhardtii* activates intracellular Ca^{2+} concentration-dependent collision-avoiding reactions which result in several behavioral responses (*i.e.*, mechanoreception, flagella excision, phototaxis, and photophobic response). The mechanical stimulus during the collisions excites the cellular membrane potential to express mechanosensitive channels like the TRP family, especially TRP11 and TRP15, by which an influx of Ca^{2+} is triggered. When the membrane depolarization exceeds a threshold level, an action potential is generated at the flagella by the voltage-dependent calcium channels, CAV2. In order to increase microbial biomass, a realistic approach is necessary that uses the innate characteristics of the microbes, and this mechanotransduction pathway could be activated to prime cells to increase microalgal biomass when they are cultivated in industrial-scale bioreactors with harsh mechanical stresses.

In this study, *Chlamydomonas reinhardtii* was pretreated with a lab-scale up/down vibration generating system and cultivated in baffled flasks which had a shear stress force similar to that of large-scale bioreactors, and the changes in RNA

expression of mechanosensitive channels were analyzed. It was assumed that *C. reinhardtii* could 1) recognize a mild compressional/tensional mechanical stimulus generated from the vibration system and 2) become primed so that they could withstand a similar extent of shear stress from industrial bioreactors leading to an increased proliferation and biomass productivity.

4.2 Materials and Methods

4.2.1 Microalgae Cultivation

CC-124 (*mt- nit1 nit2* strain) from *Chlamydomonas Center* was cultivated in tris-acetate-phosphate (TAP) with NH_4^+ liquid medium under continuous low irradiance (50 μE) for 5–7 days until the cells just entered the stationary phase [145]. A second inoculation of the suspension diluted the cells to 1/2,500 in 5 mL of fresh medium to maintain the cells in a healthy state for further experiments. When the cellular state reached the late exponential phase again, the cells were diluted again with fresh TAP+N medium to 3×10^6 cells/ml. Then, 200 μl of the resuspended cells were spread onto 1.5% TAP+N agar plates (7.5 ml of a mixture of TAP+N and agar had been poured in Ø60 petri dishes and dried at room temperature for 5 days). The cells were treated for 72 h with up/down vibration from a vibration system (SONICWORLD/SONIX SW-R3.03) using different frequencies of 10, 30, and 100 Hz at 0.5 G, or different magnitudes of 0.15, 0.30, and 0.45 G at 10 Hz. Each resultant G-force was profiled with an accelerometer (Nagano, G-MEN DR20) (Figure 4.1). After the vibration pretreatment, they were collected and inoculated in

30 ml of TAP+N medium in baffled flasks at a concentration of 5×10^4 cells/ml for about 10 days (Figure 4.2).

4.2.2 Baffled Flask

250 ml Erlenmeyer flasks (Duran, Cat. No.: 21 216 36) were symmetrically equipped with four side baffles positioned at 90 degrees and four bottom baffles offset from the side baffles, and their heights were all 15 mm. These eight deep baffles were designed to enhance vigorous agitation providing almost the same hydrodynamic shear force field as in industrial bioreactors. The shaking frequency was set at 245 rpm (Figure 4.3).

4.2.3 RNA preparation and Analysis

The microalgal cells were lysed with buffer containing 10 mM Tris-HCl (pH 8.0), 200 mM NaCl, 1% SDS, and 10 mM EDTA. Following the traditional acidic phenol-chloroform method, 1 µg of extracted mRNA was used to synthesize cDNA using reverse transcriptase (Thermo Scientific, Cat. No.: EP0441) with an oligo dT_{15} (IDT) primer and dNTPs. Then, 5 µl of cDNA (diluted 1:5) were amplified by SYBR Green

I master mix (Roche Applied Science, Cat. No.: 04 707 516 001) using 5 pmol of each specific primer with 50 cycles of 95°C for 20 s, 60°C for 20 s, and 72°C for 20 s on a Lightcycler 480 II System (Roche Applied Science). Relative levels of specific mRNA to CBLP (*Chlamydomonas* β subunit-like polypeptide) were represented as normalized target/reference ratios.

4.2.4 CFD Simulation for the Shear Force Analysis

The CFX module of ANSYS student ver. 18.2, CFD (Computational Fluid Dynamics) software, was used to simulate and characterize the fluid flows in the baffled flasks. The simulations were performed as previously reported [146]. Briefly, the gas–liquid interface was set as the free surface. The two-phase flow using the volume of fluid (VOF) model and the water turbulence using the RNG k-ε turbulence model were applied to simulate the movement of the fluid in orbital rotated flasks. In addition, to describe the orbital shaken flasks more precisely, not only the gravity but also the centrifugal force was considered to achieve a more realistic simulation of the fluids in the baffled flasks. The orbital rotating centrifugal force is calculated as follows:

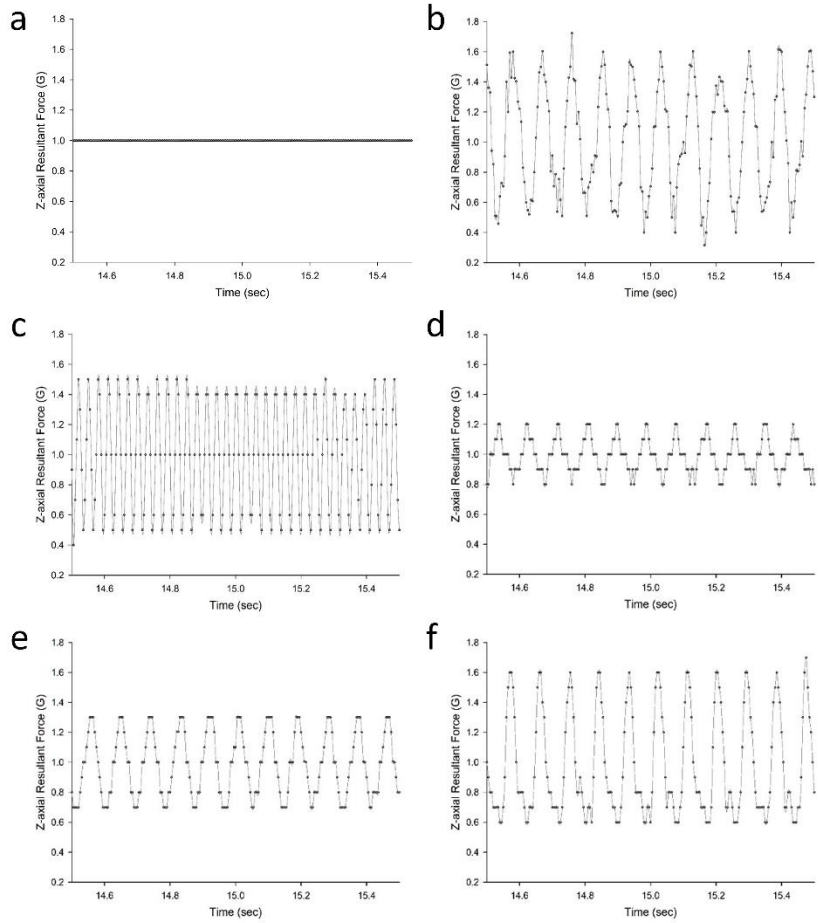

g *Curve Fit formulated as* $f = y_0 + \boldsymbol{A}\sin(2\pi\frac{t}{\boldsymbol{B}} + c)$

#	*Frequency (Hz)*	*Amplitude (G)*	*A (G)*	*B (1/Hz)*
a	0	0	0±0	INF
b	10	0.50	0.5008±0.0017	0.0903±5.0185E-007
c	30	0.50	0.4948±0.0010	0.0301±3.3679E-008
d	10	0.15	0.1463±0.0008	0.0904±8.5926E-007
e	10	0.30	0.2960±0.0008	0.0903±3.8577E-007
f	10	0.45	0.4488±0.0026	0.0903±8.6859E-007

Figure 4.1 Vibrational wave curve fit analysis for the measurements of frequencies and amplitudes of each condition. Z-axial resultant force (G) was recorded by an accelerometer from 0 to 30 sec. These graphs show the G-force record data from 14.5 to 15.5 sec.

Figure 4.2 Schematic representation of the two steps for microalgal stress priming. the vibration generation system for stress priming (top right) and the baffled flask shaking incubator for high shear stress (middle). This steps were compared with the steps from a seed plate (top left) as a control.

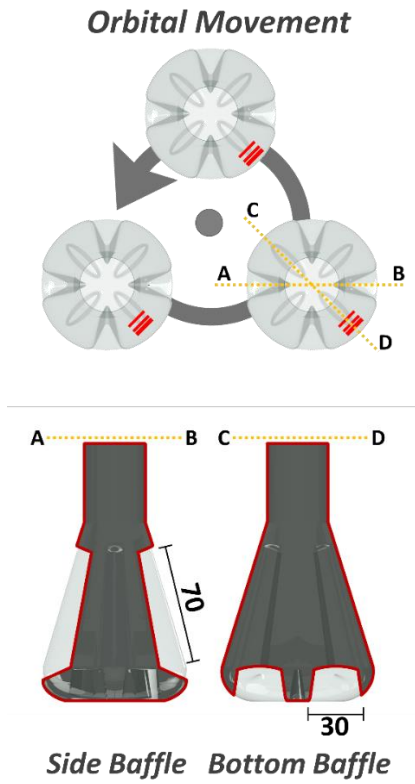

Figure 4.3. Schematic of the orbital movement of the baffled flasks and a section view showing the side baffles and bottom baffles.

Table 4.1 Primer sets used in real-time PCR for the analysis of vibration effects

Gene	Forward Primer	Reverse Primer
CBLP	CTTCTCGCCCATGACCAC	CCCACCAGGTTGTTCTTCAG
TRP11	GGCAGGACCGCGACGACTT	AGCACCGCCACCATCAGCTC
CAV2	GTCACGCTCGACAAGTTCA	TGCACATCCACCCAGTTC
ADF1	GTGGGAGTCCAACCACTACTACC	GCCGCTCCAAGAACCTCATG
MSC1	GATCGCTGCCAAGGTGAA	CTGCACCAGCATCTCCTG
Smt	GATGATCGGGCTCAAGCTGG	TTGATGTGCGCCACCTT
DP1	CTGTACCTGCAGGACATGG	GAAACAGCTTGGTCTCGCT
MAT3	GAGGTCAACAGCAAGGTGTA	AGCATGATCTGGTCGATGTG
ALD	AAGGCCAACTCGGACGCTCA	GCTGGCGACCAGCAATTTCG
HRP3	AGCGTGAGCGCTGTCATC	GCAGCGCTTTCTTGATGTTGGC

$$F_x = \omega^2 r \cos \omega t$$

$$F_y = \omega^2 r \sin \omega t$$

, where ω is the angular velocity (rad/s); *r* is the radius of the orbital shaker, and *t* is the run duration (s). In this work, *r* was set as 0.010 m. No slip wall boundary conditions were applied for all boundaries of the domain.

4.2.5 Construction of the GFP-expressing Strain

CC-2653 (nonsense mutation in rbcL) and a P-67 plasmid (p-67 cpDNA EcoRI 14) were purchased from *Chlamydomonas Center*. The P-67 plasmid was modified by inserting the *SacI*/*NotI* restriction enzyme sites between the psaB terminator and tRNA terminator. Then, the chloroplast codon-optimized GFP gene (customized by Thermo Fisher) tagged with the HA epitope (human influenza glycoprotein peptide) with the psbD promoter (the light inducible promoter) and rbcL terminator region was ligated into the restriction enzyme sites shown in Figure 4.8 (a). As previously described [51], gene bombardment (BioRad, Biolistic PDS-1000/He Particle Delivery System) was used to transform the plasmid into the cells. Then, the genomic DNA of every GFP integrated-transformant was extracted and screened by PCR using primers for homoplasmy & integration tests (Figure 4.8 (b)). Afterwards, the

transformants were cultivated in TAP+N medium in a dark condition until reaching late exponential phase and then diluted into fresh TAP+N medium at a concentration of 8×10^5 cells/ml. After one day of cultivation, they were incubated in a continuous light condition for additional 24 h to induce the expression of GFP. Then, 200 µl of the cell suspensions were transferred to the wells of a flat bottom, 96-well microplate (Thermo, Cat. No.:167008) and to a solid black microtiter plate (Corning, Cat. No.:3915) to measure the cell density and GFP fluorescence intensity, respectively. The optical density was measured at 750 nm using a microplate spectrophotometer (BioTek, Epoch). The fluorescence intensities of the GFP were measured at excitation/emission wavelengths of 488/515 nm by fluorometry (Perkin Elmer, LS-50B). Specific fluorescence was calculated by normalizing the fluorescence intensity to the optical density (Figure 4.9 (a)). The higher intensities of the transformants compared to the control intensity indicated that the cells expressed the GFP protein [147].

4.2.6 Sampling

After about a 9-day dark cultivation in the baffled flasks, cells just in the stationary phase were cultivated in an additional one-day cultivation in a light condition (50

μE). The dark condition drove the cells to grow primarily and the light condition was necessary to induce the transgenic microalgae to express recombinant protein, GFP-3HA. Then, the cells were harvested: 25 ml for biomass measurements and 3 ml for GFP yield measurements.

4.2.6.1 Biomass Measurement

The cells were harvested in glass test tubes with a centrifuge (Eppendorf, Cat. No.:5810R) at 3,000 rpm for 10 min. Their supernatants were removed, and the pellets were dried in a 70℃ oven for 5 days.

4.2.6.2 Protein preparation and Western Blot Analysis

The cells were suspended in 100 μl of lysis buffer [2 mM Tris-HCl (pH 8.0), 40 mM NaCl, 0.2% SDS, and 2 mM EDTA]. After adding chelex resin (BioRad, Cat. No.:C7901), the mixture was vortexed for 20 s and incubated at 95 ℃ for 10 min. Afterwards, they were additionally incubated in ice for 5 min. After centrifuging at 14,000 rpm at 4℃ for 10 min., the supernatants were quantified by the Bradford

assay. Then, 20 μg of lysates were separated by 12.5% SDS-PAGE gel and analyzed by western blotting with an anti-HA antibody (Santa Cruz, Cat. No.: sc-7392).

4.3 Results and Discussion

4.3.1 Microalgal Stress Responses to Mechanical Stimulus with Vibrational Frequencies

For the G-force measurement, the vibrational frequency was set at 0, 10, 30, and 100 Hz at 0.5 G. *C. reinhardtii* was exposed to up/down vibration with the different frequencies for 72 h. Then, the cells were harvested for RNA preparation and cDNA synthesis. Real-time PCR was used to measure the expression levels of several mechanoreceptors (*TRP11*, *CAV2*, *ADF1*, and *MSC1*). The RNA levels of *TRP11*, *CAV2*, and *ADF1* in the 10 Hz-treated microalgal cells increased 1.94, 2.23, and 1.87-fold compared to that in the non-treated microalgal cells, respectively, while the 30 and 100 Hz treatments had almost the same or less RNA levels (Figure 4.4). It means that 10 Hz could be a significant frequency for inducing mechanical stress responses.

Because Ca^{2+} is a second messenger for the general CSR, it could be deduced that the mechanotransduction pathway became activated by the changes in expression of the mechanoreceptors [77,78]. MSC1, however, was not expressed in the vibration-treated cells. Considering that MSC1 is known to open for a large

intensity mechanical stimulus and has a hysteresis for it, the vibrational intensities used in this study were not enough to activate the MSC1 channel and to respond to the stimulus [76,144].

Moreover, how high microalgal cells move in the vibration system could be measured using the equation for sinusoidal motion shown below.

$$D = \frac{V}{\pi F} = \frac{GA}{2\pi^2 F^2} = \frac{ZV^2}{GA}$$

If any two of the four variables are known, the other two can be calculated; D is the displacement of the cells; V is the velocity of the cell movement; A is the acceleration of the vibration, and F is the frequency of the vibration. The microalgal cells moved 2.484, 0.276, and 0.025 mm/peak-to-peak for 10, 30, and 100 Hz, respectively. About 2 mm seems to be the threshold displacement for cells to experience stress from the vibrational effect.

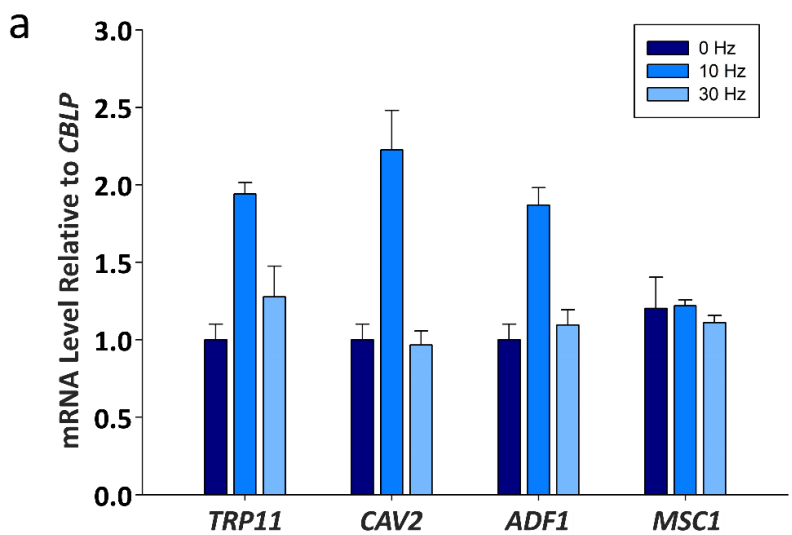

Figure 4.4 Real-time PCR measuring the change in expression of four mechanosensitive mRNAs (*TRP11*, *CAV2*, *ADF1*, and *MSC1*) relative to *CBLP* in vibrational conditions with different frequencies (0, 10, and 30 Hz) at a fixed magnitude (0.5 G). Error bars represent standard deviation (SD) from three biological replicates.

4.3.2 Microalgal Stress Responses to Mechanical Stimulus with Vibrational Magnitudes

Based on the 10 Hz effect on the vibrational mechanical response, different vibrational magnitudes (0, 0.15, 0.30, and 0.45 G) at 10 Hz were additionally assessed for their effects on the mechanotransductory mRNA expression in microalgae. In contrast to the results in Fig. 2a, all the RNA levels were roughly equal to each other with almost the same expression levels regardless of the magnitude (Figure 4.5 (a)). In this study, 0.15 G was set as the optimal condition to make cells respond to up/down vibration because the vibrational pretreatment with 0.15 G uses less energy when stimulating microalgal cells, and this would be more efficient than that of the other magnitudes.

Cellular response to stress changes chromatin substructures and the concomitant transcriptional network. These epigenetic changes result in cells preparing for stress environments. Because the RNA microarray under mechanical stress confirmed that RNA expression changes were overlapped under abiotic or biotic stress, it could be deduced that TRP11, CAV2, and ADF1 from the up/down vibrational stress also use the general downstream CSR and its resultant physiological phenotypes associated with those stresses. Hence, wide transcriptome

analysis is needed for a more extensive study on the up/down vibration-induced mechanotransductory signaling pathway. Thus, the stress priming of cells is expected to put the cells into a prepared state by increasing other global RNA levels.

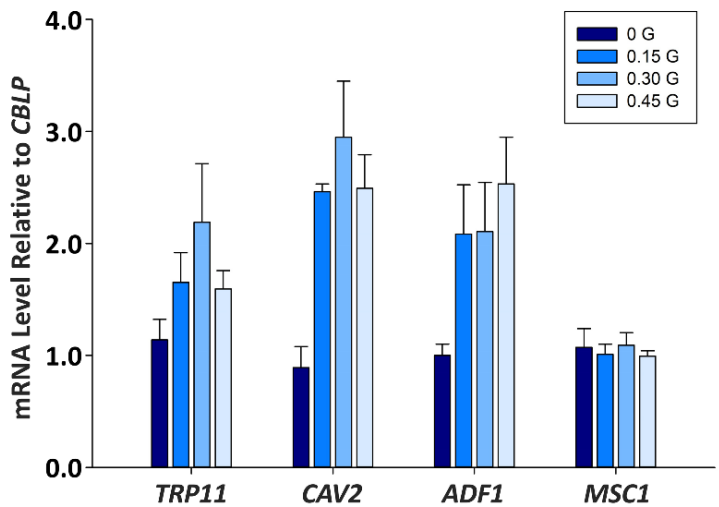

Figure 4.5 Real-time PCR measuring the change in expression of four mechanosensitive mRNAs (*TRP11*, *CAV2*, *ADF1*, and *MSC1*) relative to *CBLP* in vibrational conditions with different magnitudes (0, 0.15, 0.30, and 0.45 G) at a fixed frequency (10 Hz). Error bars represent standard deviation (SD) from three biological replicates.

4.3.3 Shear Strain Rate (SSR) and Wall Shear Force (WSF) in Baffled Flasks

Although several studies have reported on the different types of shear stress from large scale bioreactor operations, the average shear stress in a large-scale bioreactor is chosen as a key parameter to describe how harsh the bioreactor environment is [146]. The parameter ranges from 2 to 2×10^5 s^{-1}, and such a shear force was enough to damage cells cultivated in such an industrial bioreactor embedding apparatus like stirring panels, agitators, or a baffled block and to consequently reduce the biomass yield [148].

The equation $\tau_\omega = r_o \times \sqrt{\rho\nu(2\pi f)^3}$ is used to calculate the orbital shear stress (OSS) that adherent animal cells experience. Here, τ_ω is the orbital shear stress at a specific point away from the center of the flask (r_o); ρ is the density of the medium; ν is the viscosity of the medium, and f is the shaking speed of the orbital rotation [149]. This equation, however, cannot be applied to a three-dimensional cultivation in a flask because the cells do not stick to the bottom but instead are suspended in the culture medium which limits its use with baffled flasks to just two-dimensional animal dishes.

Therefore, there is a need to simulate computational fluid dynamics (CFD) in a baffled flask to extract values for mechanical forces such as the average shear

strain rate (aveSSR) or average wall shear force (aveWSF). Figure 4.6 (a) shows the volumetric fraction of the medium as well as its turbulence stream. It was confirmed that this simulation could achieve a similar motion to that of the medium over time. Velocities or stress forces from numerous points would describe how exposed the cells are; however, the aveWSF and aveSSR in the baffled flasks were evaluated in 3-dimensional motion and were calculated as 0.292 Pa and 184 s^{-1} after 0.25 s for one rotation, respectively. These values correspond to the range of the shear forces found in a large scale operation [148] which are mimicked in the baffled flasks as a large-scale hydrodynamic mimetic environment (Figure 4.6 (b) and (c)).

In addition, mechanical stimulation receptors were analyzed with real-time PCR. The mRNA levels of *CAV2* and *MSC1* were opposite based on the vibration-treatment with *CAV2* and *MSC1* showing no change and 3.8-fold in expression, respectively; however, the *TRP11* mRNA expression was also 2.6-fold increased quite more compared to that in the non-treated cells (Figure 4.7). This means that *TRP11* is cross-activated linking both up/down compression/tension stress and shear stress; thus, the TRP11 mechanosensitive receptor might be able to induce a cross-adaptation to other types of mechanical stresses [150].

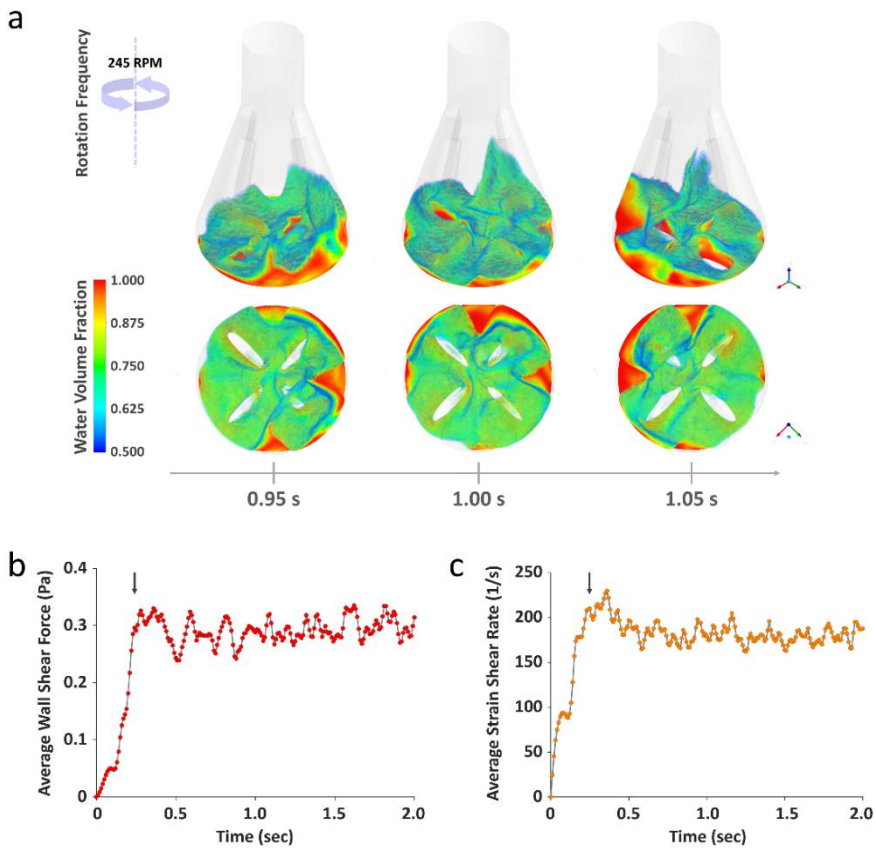

Figure 4.6 Simulation of the hydrodynamic shear force field in baffled flasks.

(a) Computational fluid dynamics (CFD) simulation of the medium at a rotational speed of 245 RPM at 0.95, 1.00, and 1.05 s, (b) average wall shear force (aveWSF) and (c) average strain shear rate (aveSSR) calculated by CFD with time intervals (0.01 s) (arrows indicate 0.25 s for one rotation)

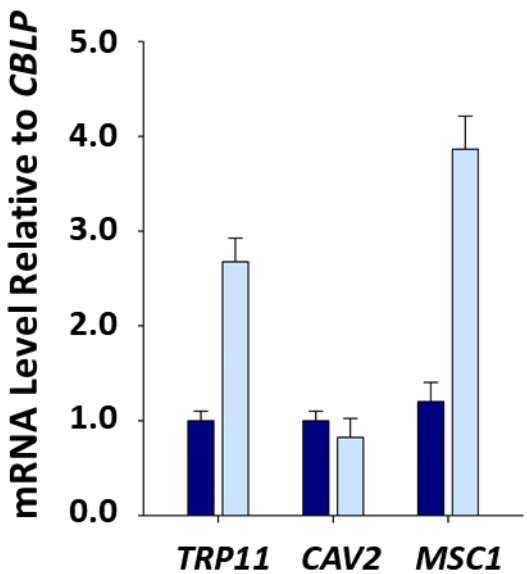

Figure 4.7 Changes in the mRNA expression levels in baffled flask cultivation.

RT-PCR measuring the change in expression of three mechanosensitive mRNAs (*TRP11*, *CAV2*, and *MSC1*) relative to *CBLP* during cultivation in the baffled flasks. Error bars represent standard deviation (SD) from three biological replicates.

4.3.4 Priming Effects on Microalgal Biomass and Corresponding Productivity

To verify whether this vibration pre-treatment could have a positive priming effect on transgenic microalgae, a strain was developed that constitutively expresses GFP-3HA in chloroplast (Figure 4.9 (a)), and the cells were either primed or not primed. They were cultivated by orbital shaking for 10 days (9 days in dark for cell growth and one day in light for the recombinant GFP-3HA protein expression), for which the intensity of the shear force was already simulated to be enough to trigger a microalgal mechanical stress response. The number of microalgae in the shaking baffled flasks was measured and plotted over time. The vibration-treated primed microalgae grew faster until the end of the exponential phase (Figure 4.9 (b)). Microalgae in the primed state weighed 27.38% more than the microalgae in the non-primed state (Figure 4.9 (c)). Volumetric productivities were relatively quantified by western blotting using the HA antibody. The GFP protein production was enhanced by 39.05% in the primed cells compared to that of the non-primed cells (Figure 4.9 (d)).

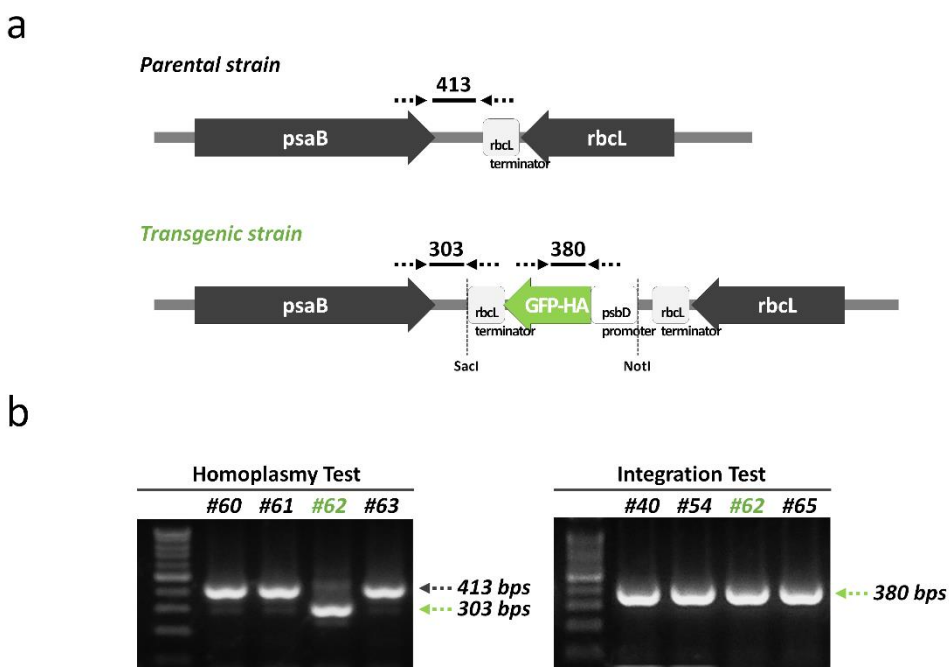

Figure 4.8 Vector construction and its integration into plastome. (a) chloroplast codon-optimized GFP gene integrated into the plastome compared to the plastome of the parental strain, (b) homoplasmy test to check that all copies of the plastome were substituted with the GFP-gene construct and integration test for GFP insertion.

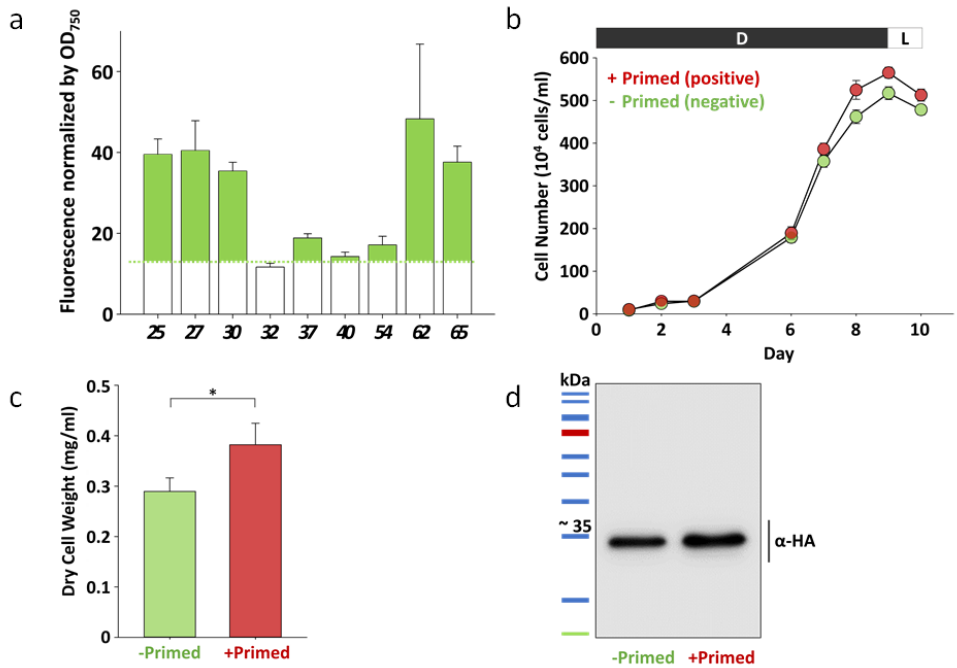

Figure 4.9 Priming effect on the productivity of the transgenic microalgae. (a) screening the transformants by GFP fluorescence intensity, (b) growth curve of (−) primed and (+) primed GFP transgenic Chlamydomonas reinhardtii for 10 days, (c) biomass measurement (Student's t-test, $P < 0.05$) and (d) GFP volumetric productivity comparison by western blotting from the (−) primed and (+) primed cells. Error bars represent standard deviation (SD) from three biological replicates.

Priming encompasses a lag or memory phase in which the priming event is separated from the second stress event. Based on studies that showed epigenetic modulation could be maintained for several generations from the initial state of the parental strains and stress-responsive metabolites and proteins exist distributed to each progeny over the generations [151,152], it could be deduced that the up/down vibration treated microalgal cells that already expressed more TRP11 responded to and adapted more easily to the harsh shear force field that mimics the conditions of a large-scale cultivation compared to the non-treated cells. In plant, calmodulin binding transcription factors (CAMTA) translates Ca^{2+} signals into transcriptional regulation, where typically master regulator CBF/DREB1 is expressed to respond to abiotic stresses. *Chlamydomonas* would also activate specific pathways similar to CBF/DREB1-mediated signalling pathways against mechanical stimuli; however, there have been few studies about Ca^{2+}-signalling pathways in *Chlamydomonas*.

In terms of cost analysis, power consumption can be estimated with proportion of mass between seed culture and industrial cultivation: 100-1000 times less power. When the same frequency and amplitude as in this study are applied to industrial scale, energy or work required to generate the vibrational force would be consumed proportionally to the mass of a batch process unit. This is because the energy that generates vibration is equal to the power that subjects are forced by.

Therefore, considering that the volume of the large scale is more than tons of batches and enough amount of primed microalgae should be secured for operation, this approach can save 100-1000 times power supply compared with traditional methods. In addition to that, microalgal biomass increase that results from vibration-induced priming could be also beneficial for environment and profit. Around 25% increase by priming has a positive effect on reducing the number of the processes to four batches compared to five batch process without priming. This drop in batch number can give rise to less wastewater at the end of each operation. Moreover, this makes more profits by saving electricity usage and operation costs in relation to not only batch process reduction but also initial cost expenditure for vibration-generating facility suitable for industrial scale process.

This approach could be applied to numerous large-scale cultivations with primed cells that experience different stresses other than mechanical stresses. In view of the cross adaptation, when cells are cultivated at a non-optimal temperature, this temperature gap also prepares the cells to be in a primed state and is applicable to the industrial process operations with the harsh hydrodynamic field. Many countries in addition to Australia and the Western United States have distinct seasons with large temperature changes which makes maintaining optimal conditions for outdoor microalgae cultivation difficult. From an engineering perspective, when cells are

pre-exposed to stressors before a large-scale cultivation, a shorter batch process could be feasible and advantageous for a larger biomass yield during the same period.

Microalgae can be presented as a better alternative for plants with more biomass with less time and less need for labour and costs. Especially, the biomass of edible *Nannochloropsis sp.* or *Chlorella sp.* are well-known to consist of up to 70% macronutrients, but they have not been genetically transformed to increase their biomass due to their inherent genetic characteristics. When large scale bioreactors are operated to cultivate primed *Nannochloropsis sp.* or *Chlorella sp.*, it is expected that a larger amount of algae-based food would be harvested, and thus, this method of priming microalgae to increase their biomass could be a potential solution to meeting the global food demand providing an alternative sustainable protein source other than plant-based foods.

4.4 Conclusions

When microalgal cells were exposed to up/down vibration at 10 Hz and 0.15 G, they recognized it as one of the mechanical stressors and were primed with 1.65, 2.46, and 2.08-fold increase in mechanosensitive *TRP11*, *CAV2*, and *ADF1* RNA levels. When these primed cells were cultivated in a triggering environment in which baffles caused hydrodynamic shear fields similar to the ones in large-scale bioreactors: 0.292 Pa for the average wall shear force (aveWSF) and 184 s^{-1} for the average shear strain rate (aveSSR), the primed microalgal biomass and volumetric product yield were increased by 27% and 39% more than non-primed cells, respectively. There is a need to understand how Ca^{2+}-signaling pathways are cross-talked with vibrational stress responses and stress priming, but stress priming of microalgae could contribute to better bio-productivity through a more efficient operation that requires less energy and costs in industrial applications.

Chapter 5

Chloroplastic Malate Synthase Expression for Microalgal Growth by Upregulating TCA cycle

5.1 Introduction

For photosynthetic organisms, among other cellular organelles, the chloroplast is a significant organelle not only for various anabolic metabolisms but also for energy conversion. High photon energy excites electrons to be available as reduced ferredoxin and NADPH, and the photon gradient during electron transport generates ATP. These reducing energy carriers are primarily for not only fixing CO_2 via the Calvin cycle but also for converting their cellular energy into net biomass or for proliferation [153,154].

Communication between organelles is vital for the survival of photosynthetic organisms, preventing the chloroplasts from being over-reduced by high intensity of light. Typical interactions between the chloroplast and the mitochondria are carried out by the transfer of reducing equivalents as well as metabolites, affecting gene expression and the production and utilization of ATP. During the communication, however, the energy carriers are not directly transported across the chloroplastic envelope or other organelle membranes, but transported in the form of metabolites. This is because their pool sizes are limited and have to be intricately regulated to be delivered to other compartments at the required rates. Their indirect transport from the chloroplast can be achieved by malate-

oxaloacetate(OAA) shuttles for NADPH as well as the dihydroxyacetone 3–phosphate (DHAP)/3–phosphoglycerate (3–PGA) shuttle for ATP [9,10].

The malate/OAA shuttle helps to regulate the $NADPH/NADP^+$ in chloroplast or the $NADH/NAD^+$ ratio in mitochondria and to control the availability of the reducing equivalents with ATP synthesis, where malate is used as an indirect hydrogen carrier replacing NADPH or NADH [9,10]. Exported malate, as an ubiquitous substrate for several types of malate-dehydrogenase (MDH) enzymes, malic enzyme (MME) or pyruvate dehydrogenase complex (PDH) spanning organelles is exploited in a variety of ways: *i)* it can serve as a source for NADH in the cytosol, *ii)* can be metabolized in the mitochondria for ATP production, *iii)* can be used as a carrier for CO_2 in the chloroplast, and *iv)* can be consumed in the alternative pathway of respiration without ATP generation [10] like in microbodies containing the glyoxylate shunt cycle [153,155].

The decreasing activity of mitochondrial malate dehydrogenase (mMDH) was reported in Tomato enhanced photosynthetic performance and plant growth. The CO_2 assimilation rates and total plant dry weight were about 11% and 19% improved in the transgenics compared with the wild-type [156]. Genetic manipulation targeting a specific malate dehydrogenase, however, could rather lead to other phenotypes dependent on the growth phase or organ and probably have a deteriorated capacity

to control redox balancing. It was also likely that low malate contents in leaves meant that accumulated malate in leaves has a significant role as a reducing equivalent valve to transport its energy potential to other organs like fruits and stems on a whole plant basis.

Considering the fact that malate is a multipurpose metabolite in energy production and that integration of transgenes to microalgae chloroplast enables a high level of expression by many gene copy numbers without gene silencing [5], distribution of more malate produced in the chloroplast to energy or macromolecule-producing organelles such as the mitochondria could be a more effective way for achieving a higher biomass yield, helping more malate to be utilized in each specific metabolic pathway. In this study, the *glcB* gene encoding malate synthase derived from *E.coli* was integrated into the plastome of *Chlamydomonas reinhardtii*, a model microalgae, and changes in the primary metabolism-related RNA levels and metabolites were analyzed. It was confirmed that malate could be involved in the increase of the microalgal biomass production.

5.2 Materials and Methods

5.2.1 Construction of the Expression Vectors for the Transformations

5.2.1.1 Recombinant Plasmid for E.coli Transformation

Malate Synthase G encoding *glcB* gene from *Escherichia coli str. K-12 substr. MG1655* (NCBI Reference Sequence: NC_000913.3) with the HA epitope (human influenza glycoprotein peptide) was codon-optimized synthesized based on the *Chlamydomonas* chloroplast codon usage (customized by Thermo Fisher). The *Cr.glcB*-HA gene was amplified with *EcoRI* and *NotI* sites flanking both sides and ligated into the pET-22b(+) vector. The recombinant malate synthase G was tagged with 6× His as well as HA for double conformation and easy purification with Ni-NTA resin (Thermo, Cat.No.:88221) (Figure 5.1).

5.2.1.2 Recombinant Plasmid for Chlamydomonas Chloroplast Transformation

CC-2653 (a point-nonsense mutation in rbcL) and a P-67 plasmid (p-67 cpDNA EcoRI 14) were obtained from the *Chlamydomonas Center*. As described in [53],

several nucleotides between the psaB terminator and the tRNA G genes of the P-67 plasmid were modified by inserting SacI/NotI restriction enzyme sites, which was a negative control. The *Cr.glcB*-HA gene flanked with the constitutive psbD promoter [50] and rbcL terminator was ligated into the restriction enzyme sites shown in Figure 5.2.

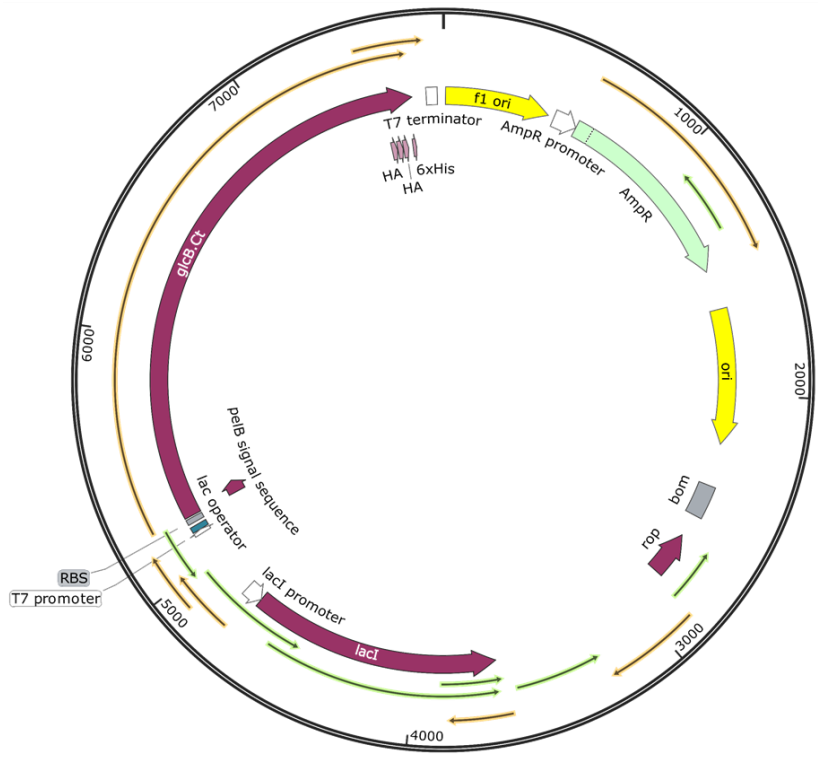

Figure 5.1 Schematic of recombinant plasmid for *E.coli* transformation.

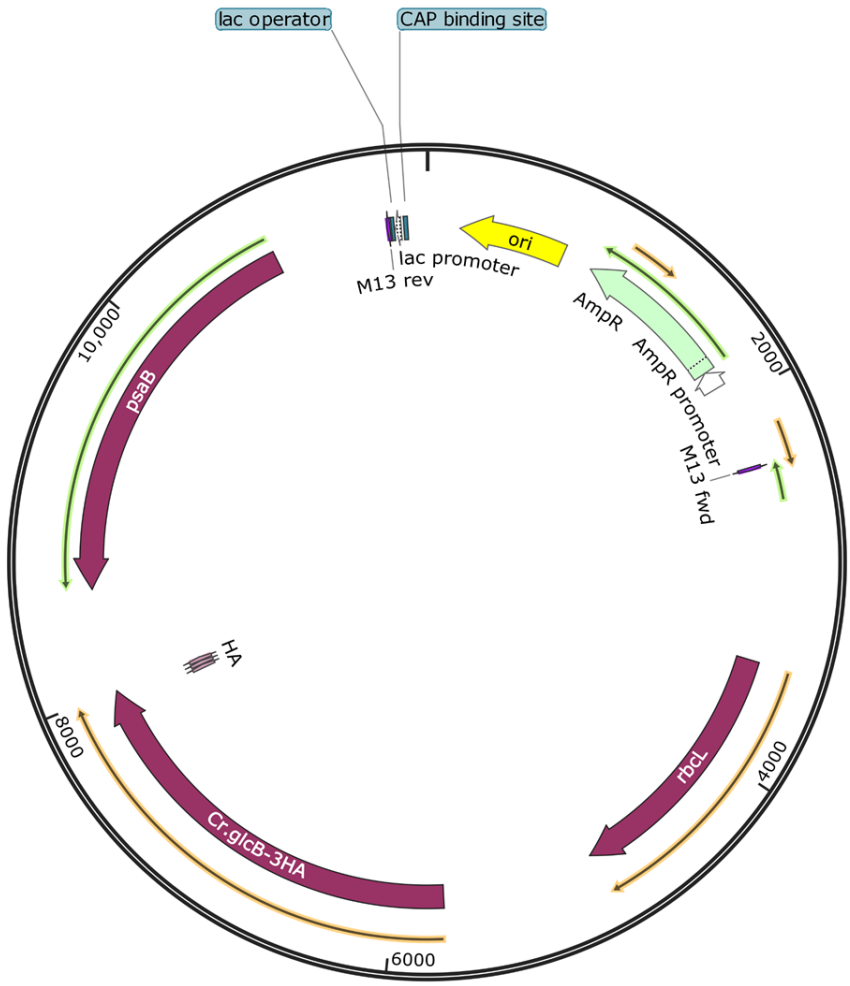

Figure 5.2 Schematic of recombinant plasmid for *Chlamydomonas* transformation.

5.2.2 Protein Purification

BL21(DE3) transformed with pET-22b(+)-*Cr.glcB*-HA-His6 was second inoculated into 250 ml LB containing 500 μg of ampicillin. When the culture reached an OD_{600} of 0.4 , it was treated with 1 mM IPTG to induce the expression of malate synthase and cultivated for another 24 h at 16 ℃ with a final OD_{600} of 1.2 . The cells were harvested and stored in a -80 ℃ deep freezer. All steps for the purification were performed with 700 ul of Ni-NTA resin (Thermo) following the manufacturer's instructions. Briefly, the cells were resuspended in 25 ml of PBS containing PIC (1:1000) and lysed by sonication (on/off cycle of 5/15 sec for 30 min). The lysate was loaded into a column packed with Ni-NTA resin already equilibrated with equilibration buffer. Wash buffer at two times the volume of the resin was poured into the column to wash out non-specific proteins, and then, the column was eluted with 200 ul of PBS containing 250 mM imidazole (pH 7.4) followed by dialysis with 10 mM K-phosphate buffer (pH 8.0) and 10% glycerol. The purified protein was resolved on a 7.5% SDS-PAGE gel and confirmed by Coomassie Brilliant Blue staining and Western Blotting using the HA antibody (Santa Cruz, Cat. No.: sc-7392) and His6 antibody (Abcam, Cat.No.: ab137839) (Figure 5.3).

A

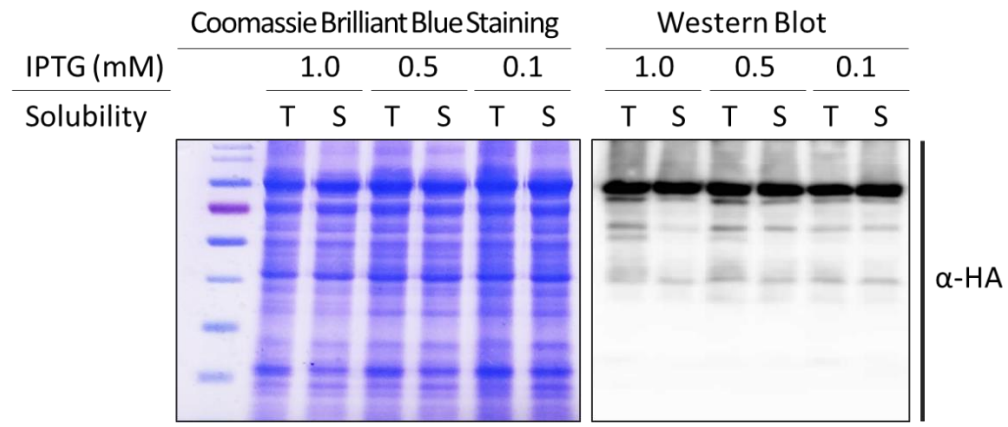

B C D

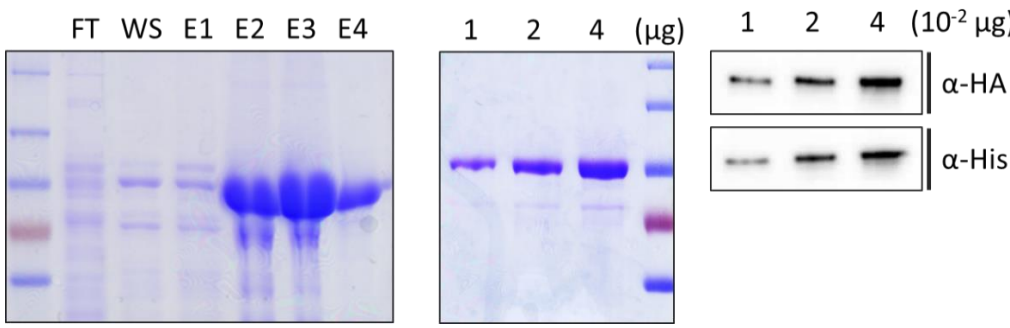

Figure 5.3 Purification of the recombinant malate synthase tagged with the HA epitope and 6×Histidine. A) expression test with 1.0, 0.5, and 0.1 mM IPTG and solubility test for the malate synthase, B) recombinant malate synthase was prepared from the E2 to E4 elution after Immobilized Metal Affinity Chromatography (IMAC), C) respective quantity of the purified malate synthase was checked by Coomassie Blue Brilliant (CBB) staining and D) Western Blotting (WB).

5.2.3 in vitro Malate Synthase Activity Test

The manufacturer's instructions (Sigma Aldrich) were followed for the enzymatic assay of malate synthase. Thus, 90 ul of a mixture of 50 mM K-phosphate buffer (pH 8.0), 10 mM MgCl2, 0.25 mM acetyl-CoA, 1 mM glyoxylate, and 0.2 mM 5,5'-dithio-bis(2-nitrobenzoic acid) was stabilized in a 96-well plate (Corning® UV-Transparent Microplates, Cat.No.: CLS3635S) for 40 min and then measured at 412 nm using a microplate spectrophotometer (BioTek, Epoch). Just after the addition of 0.8 µg of the purified recombinant malate synthase, the amount of TNB was kinetically measured for 60 sec by the absorbance at 412 nm, where the free thiol groups of CoA-SH released react with the DTNB and TNB as a product can absorb the 412 nm wavelength light.

5.2.4 Particle Bombardment

Gene bombardment (BioRad, Biolistic PDS-1000/He Particle Delivery System) was used to transform the plasmid into cells- 1,100 psi rupture disks were used to shot gold particles coated with the recombinant plasmids linearized with the restriction enzyme SalI to 6 cm below the HS agar plate where the CC-2653 cells were spread

[51,53]. About two weeks later, transformants were inoculated into 96-well plates filled with TAP+N medium for screening.

5.2.5 PCR for Screening Transformants

Following the experimental procedure for colony PCR suitable for *Chlamydomonas reinhardtii*, the genomic DNA of every candidate was screened by PCR using primers for the homoplasmy test and the integration test to check whether all copies of the plastome were complemented with the rescuing rbcL gene and inserted with the *Cr.glcB* gene in the specific proper position, respectively (Fig. 5.5 and Fig 5.6).

5.2.6 Southern Blot

The purified genomic DNA of the transgenic *Chlamydomonas reinhardtii* (20 μg) was digested with EcoRI and SacI, separated in a 0.8% agarose gel, and capillary force-transferred to a Hybond™-N+ membrane (Amersham, Dayton, TN, USA). Using as a probe the *Cr.glcB* gene fragment amplified by specific primers, southern blotting was performed by following the manufacturer's instructions

(Amersham Gene Images AlkPhos Direct Labelling and Detection System, Cat.No.: RPN3680).

5.2.7 Chloroplastic Malate Synthase Expression Test

Transformants were cultivated in TAP+N medium in dark condition until reaching late exponential phase, and then, they were inoculated into fresh TAP+N medium at a concentration of 5×10^5 cells/ml. After one day of cultivation, some cells were exposed to and some cells were not exposed to light for additional 24 h and 48 h to induce the expression of chloroplastic malate synthase.

5.2.8 Transgenic Microalgae Cultivation and Measurement of Cell Number and Biomass

After the initial inoculation of the cells into TAP+N medium in dark condition, they were inoculated into fresh TAP+N medium with 0.25 mM glyoxylate (pH 7.0) in a continuous light condition (60 µE), for which the initial cell number was 5×10^4 cells/ml. A hemocytometer was used to count the cells at each time point. 10 ml of

microalgal suspension was centrifugated in a glass test tube and dried in a 65 ℃ oven for about 4-5 days.

5.2.9 RNA Preparation and Analysis

Relative mRNA changes were determined as described [53]. Briefly, the traditional PCI method was used to extract the mRNA, and then, 1 μg of mRNA was used for cDNA synthesis using reverse transcriptase (Thermo Scientific, Cat. No.: EP0441) with an oligo dT_{15} (IDT) primer and dNTPs. Then, 5 μl of cDNA (diluted 1:5) were amplified by the SYBR Green I master mix (Roche Applied Science, Cat. No.: 04 707 516 001) using 5 pmol of each specific primer (45 cycles of 95 °C for 20 s, 60 °C for 20 s, and 72 °C for 8 s on a Lightcycler 480 II System (Roche Applied Science)). Relative mRNA levels to CBLP (*Chlamydomonas* β subunit-like polypeptide) were represented as normalized target/reference ratios.

5.2.10 PAM (Pulse-Amplitude-Modifier) Measurement

F_v/F_m measures the intrinsic quantum yield of PSII, and as such, it should correlate with the maximum quantum yield of photosynthetic gas exchange (CO_2 or O_2). Thus,

3×10^7 cells were filtered carefully using a manual filtration system and placed on a 1.5% agar plate. After a 15 min. dark adaptation of the cells, the parameter was measured.

5.3 Results and Discussion

5.3.1 in vitro Recombinant Malate Synthase Activity

Prior to the *Chlamydomonas* transformation, the chloroplast codon optimized malate synthase with 3×HA epitopes and 6×His was overexpressed in *E.coli* enabling a rapid *in vitro* enzymatic activity assay for the malate synthase. This *Cr.glcB* gene encoding an ~87 kDa malate synthase was transferred to the bacterial expression vector pET22(b) downstream of the *pelB* leader peptide using *EcoRI* and *NotI* restriction sites. Purified engineered malate synthase was tested for its activity, and BSA was used as the control. The recombinant engineered malate synthase exhibited the same activity as the wild type malate synthase condensing glyoxylate with acetyl CoA to produce malate while the BSA exhibited no activity. This confirmed that tagging with the HA epitopes as well as 6×His did not affect the activity of this recombinant engineered malate synthase (Figure 5.4).

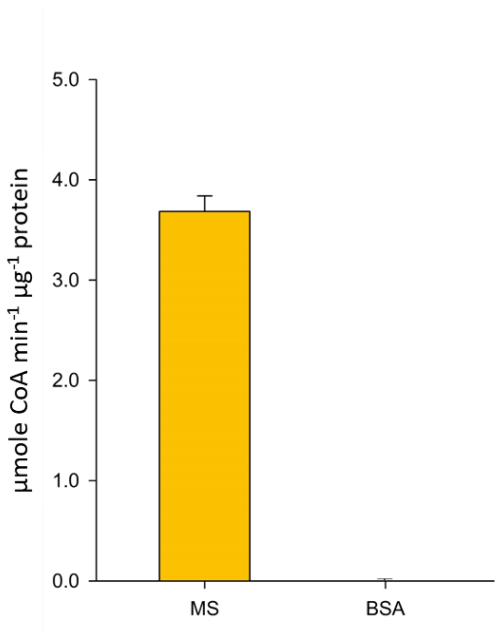

Figure 5.4 *in vitro* recombinant malate synthase, BSA as a negative control.

5.3.2 Analysis of Chloroplast Transgenic Microalgae Expressing Malate Synthase

86 putative transformants were first tested by genomic PCR analysis to check whether all copies of the chloroplast genome were transformed and that homologous recombination had worked. A specific pair of primers, one binding to the psaB terminator and the other to the rbcL terminator, was used to test the homoplasmy of the chloroplastic genome. Generation of a 413 bp product indicates that not all the chloroplast DNA copies were transformed with the *Cr.glcB* gene construct; wild-type copies of the CC2653 parental strain would generate only an amplicon of 413 bp, but the recombinant plasmid containing the *Cr.glcB* gene construct would only generate an amplicon of 303 bp. 10 of the 86 transgenic lines showed one a single product size of 303 bp which indicates the homoplasmy of their chloroplast DNA; however, the others generated both 413 and 303 bp products or just the 413 bp band (Figure 5.5). The integration PCR test was additionally carried out to further check that the *Cr.glcB* transgene was also integrated into the plastome. Comparing the band pattern derived from the DNA of the CC2653 parental strain, half of the putative transformants screened had the proper amplicon size of 499 bp (Figure 5.6).

Because there is a chance of false positive in the transformants, and

unknown regulatory mechanisms could interfere with the chloroplastic expression of the transgene, the transgene protein accumulation of 5 putative transformants was verified by western blot analysis. Using a HA epitope specific monoclonal antibody, recombinant malate synthase with a molecular weight of 84 kDa was detected only in the B-69 line, but the others had no malate synthase derived from E.coli. When the B-69 line initially adapted to a dark condition was inoculated and cultivated for 24 h and 48 h in either a continuous light condition or a dark condition, it maintained the expression of the recombinant malate synthase for that period. The lower level of expression in the first 24 h in continuous light could be due to the cellular adaptation to light; thus, it might take more time to express the protein (Figure 5.7).

Gene expression in plastids is regulated at both the transcriptional and post-transcriptional levels. Protein levels in chloroplasts depend on the mRNA abundance, which is determined by the promoter strength and mRNA stability. However, high mRNA levels do not necessarily result in high levels of protein accumulation because posttranscriptional processes ultimately determine the levels of foreign proteins within transgenic chloroplasts [157].

Even though two PCR tests and an expression test of the chloroplastic recombinant malate synthase were performed to screen for the transgenic cell line, rigorous molecular and biochemical analysis should be done for the homoplasmic

transformant B-69. This is because non-integrated copies might recover other copies transformed with malate synthase with serial inoculations. Southern blot analysis was used to make sure that the whole transgene expression cassette was integrated into the plastome of B-69. The wild-type strain CC-2653 and just a restriction enzyme site-integrated but rbcL rescued cell line R-10 were also included in this analysis as controls. Genomic DNA was digested with EcoRI and SacI. One probe was used to target the middle domain of rbcL, and the resultant DNA fragments should be 5,995, 2,887, and 5,905 bp, respectively. As shown in Fig 5.8, it was observed that the probe hybridized to each proper fragment, indicating that all the copies of the chloroplast genome of B-69 were integrated with the malate synthase in the targeted position (Figure 5.8).

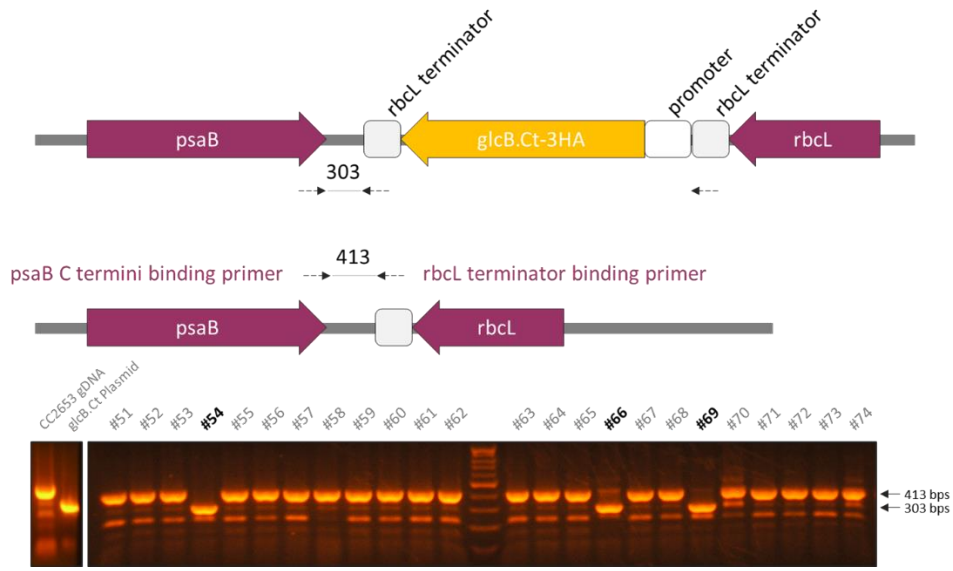

Figure 5.5 Homoplasmy test for screening malate synthase transgenic *Chlamydomonas.*

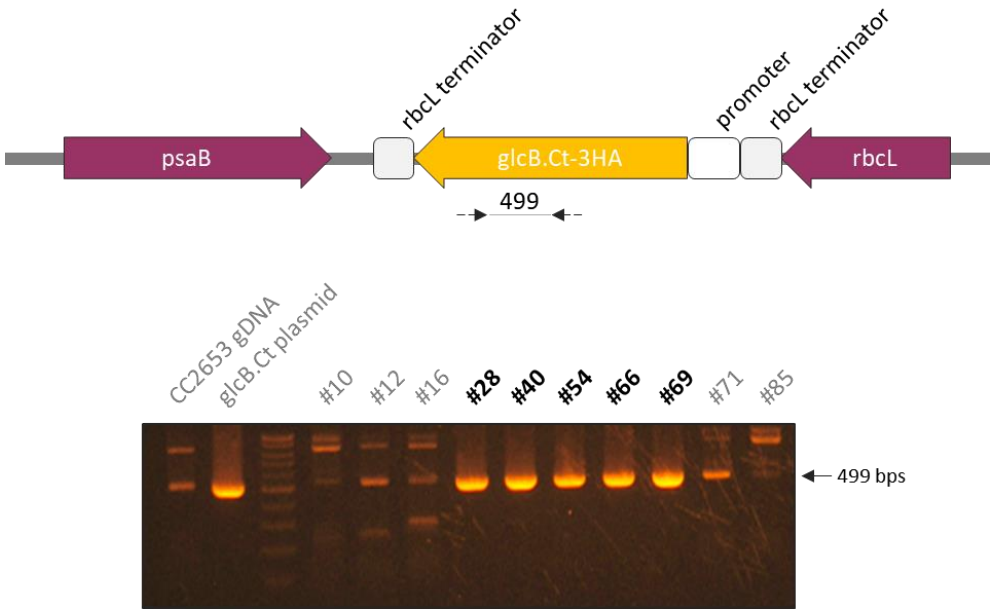

Figure 5.6 Transgene MS integration test for screening malate synthase transgenic *Chlamydomonas.*

A

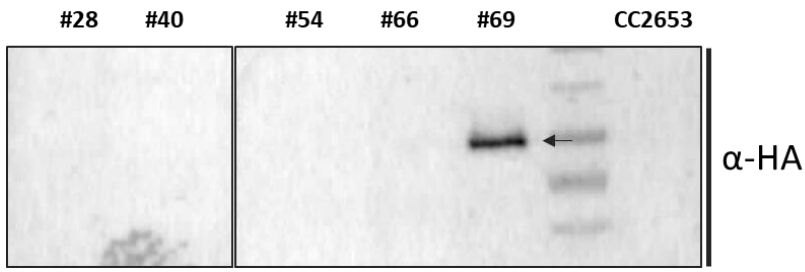

B

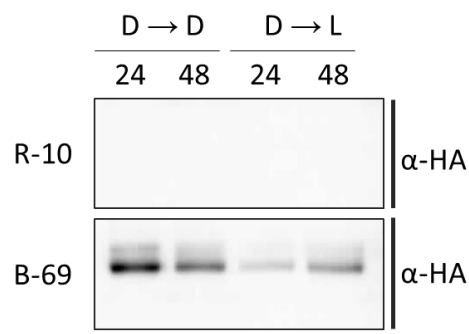

Figure 5.7 Chloroplastic transgene expression test from five putative candidates.

After their expression were checked (A), cultivation condition could affect the expression of malate synthase in chloroplast via Western Blotting analysis (B).

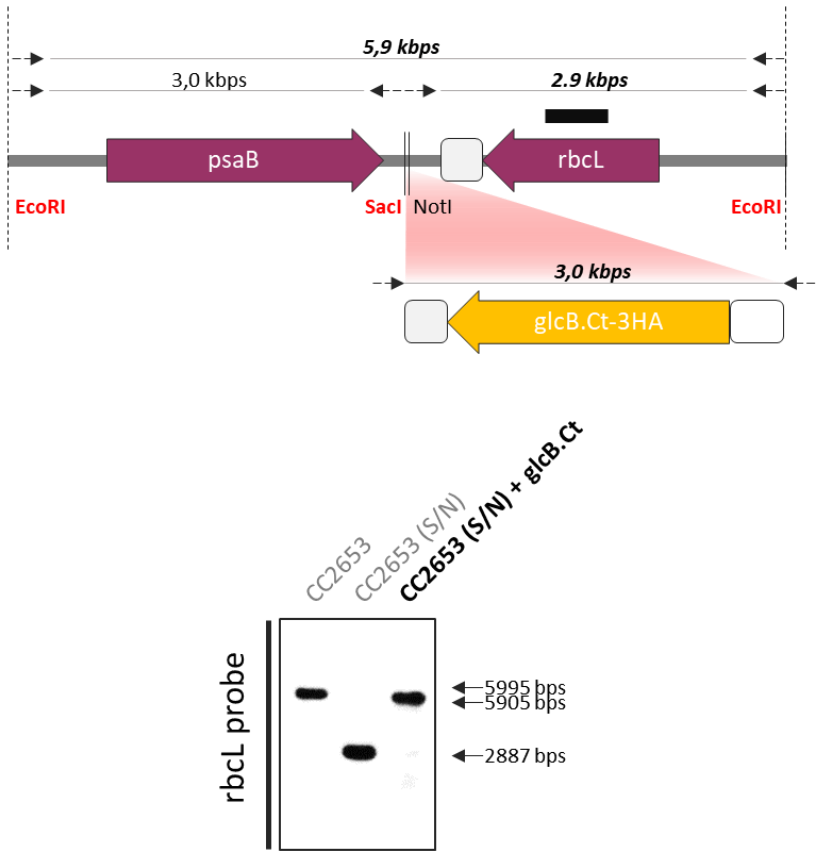

Figure 5.8 Southern blot for rigorous confirmation of their homoplasy of plastome copies.

5.3.3 Malate Synthase Changes the Parameters of Microalgal Growth

After dark adaptation, each cell line, R-10 and B-69, was cultivated in a continuous light condition, and the number of cells at each time point was counted until reaching their stationary phase. the B-69 mutant was confirmed to express the recombinant malate synthase at the early-, mid-, and late exponential phases (36, 60, 84 h, respectively). Proliferation of the transgenic B-69 line appeared to be almost the same as the R-10 control (Figure 5.9). Meanwhile, the dry cell weight of the B-69 line was 19% more, and the individual microalgae of the transgenic cell line weighed 12% more than that of the wild-type cell line, R-10 (Figure 5.10). As microalgal growth at 60 h after cultivation was highest in both cell lines, cells at this phase were prepared for further RNA analysis.

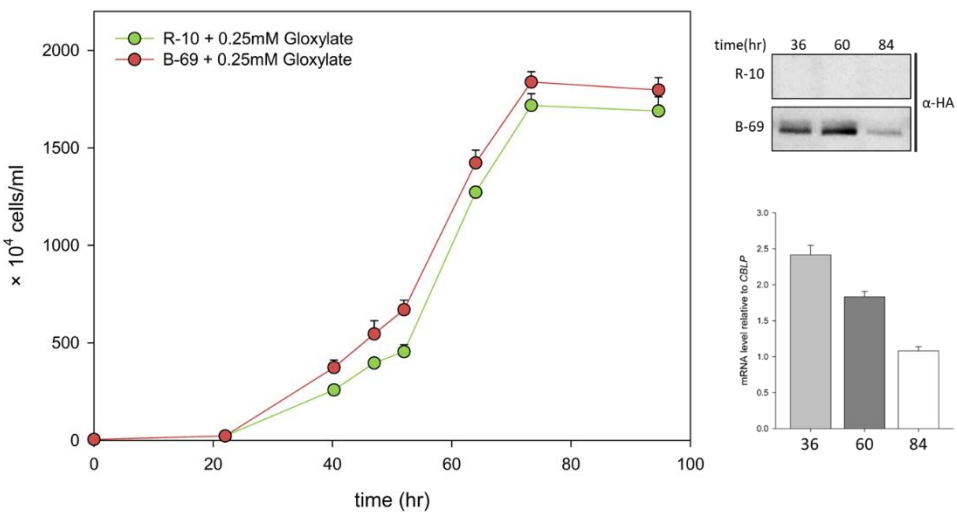

Figure 5.9 Growth curve of wild-type (R-10) and transgenic *C. reinhardtii* (B-69) line and its expression of malate synthase.

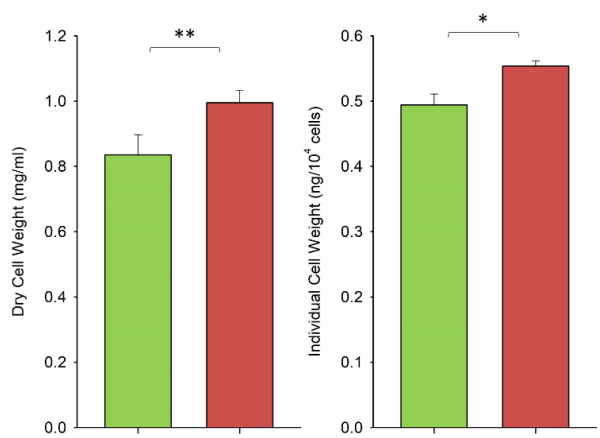

Figure 5.10 Growth parameters of WT (R-10) and transgenic *C. reinhardtii* (B-69). (A) dry cell weight (mg/ml), and (B) individual cell weight (ng/10^4 cells).

5.3.4 Malate-related Transcripts Changes Under Glyoxylate Treatment

To understand which factors contribute to the increase in the microalgal biomass, RNA transcripts that are relevant to malate were first analyzed.

In the chloroplast, malate can be utilized in two different ways: $NADP^+$-dependent malate dehydrogenase (MDH1) that reversely converts malate into oxaloacetate with the release of NADPH and malic enzyme (MME4) that produces pyruvate releasing one NADPH and one CO_2. It was demonstrated that the *MDH1* transcript was increased by 7%, but the expression of the *MME4* transcript in the B-69 line was 10% less than that of R-10, although the difference between the values was very small. The maximum intrinsic quantum yield of PSII (F_v/F_m) in B-69 was slightly lower (Figure 5.11), but both cell lines at exponential phase exhibited active photosynthesis.

The RNA levels of the TCA cycle enzymes were measured to check whether this malate import could have an upregulating impact on the energy producing TCA cycle. Although not all the transcripts of the TCA cycle related enzymes were analyzed, the *MDH4* level was increased by 18% (Figure 5.11).

While transcripts of malate dehydrogenases in microbodies containing glyoxylate cycle were shown not to significantly change, isocitrate lyase transcript,

ICL1, and malate synthase transcript, *MAS1*, were upregulated by 25% and 19%, respectively. These two enzymes are crucial key enzymes of the glyoxylate cycle to metabolize acetate for producing energy.

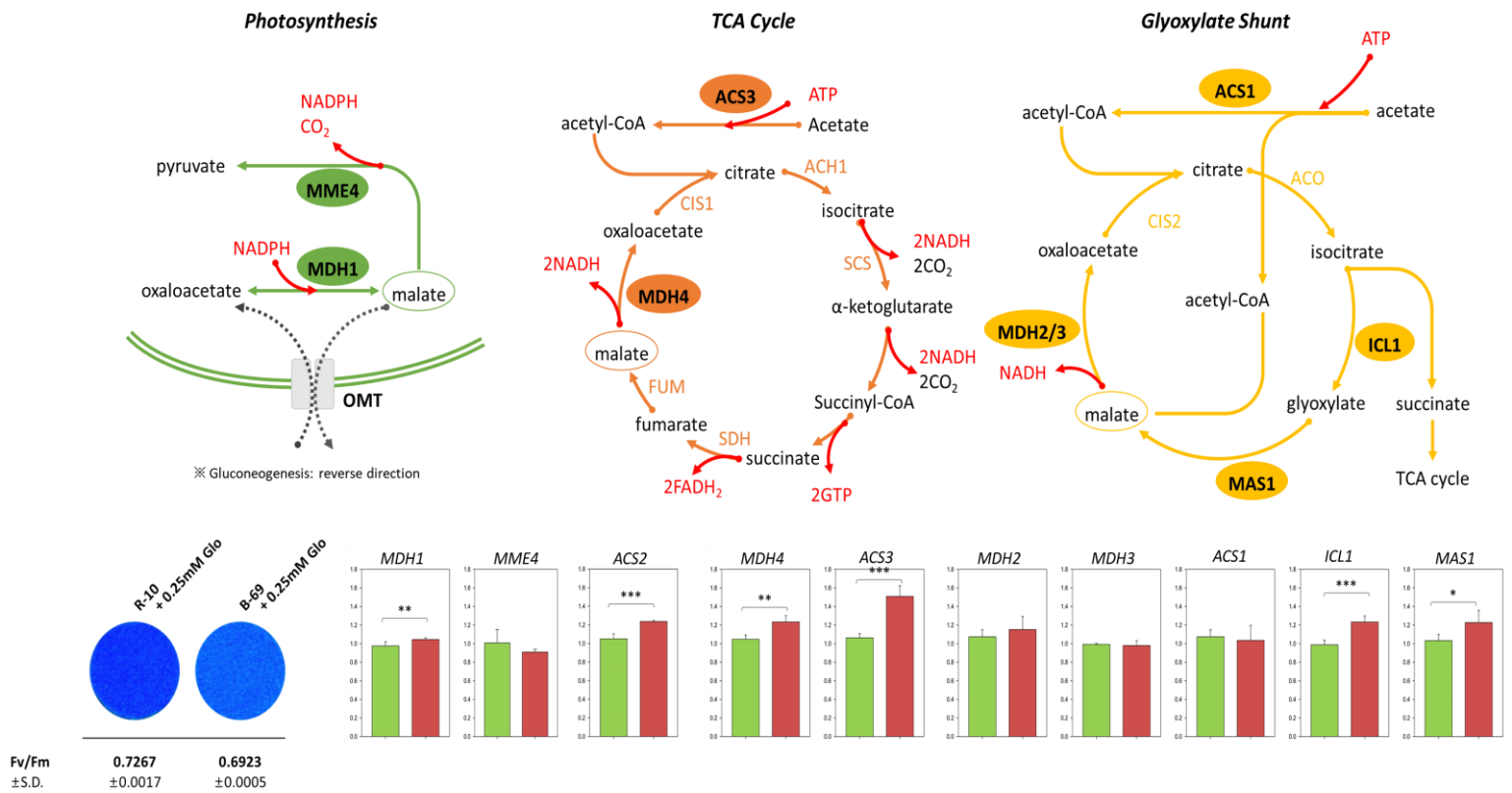

Figure 5.11 Changes in levels of transcripts in chloroplast (a), mitochondria (b), and microbodies (c).

5.3.5 Acetate-related Transcripts Changes Under Glyoxylate Treatment

It was shown in glyoxylate-treated B-69 that the transcript levels of *ACS2* in the chloroplast and *ACS3* in the mitochondria were additionally upregulated by 18% and 42%, respectively. Acetate fed as nutrient was converted into acetyl-CoA in chloroplast as a substrate for recombinant malate synthase and even in mitochondria as a precursor for metabolizing TCA cycle or acetate assimilation.

Meanwhile, transcript level of *ACS1* of glyoxylate cycle was not changed. *Chlamydomonas* is also reported to possess microbodies that contain the components of the glyoxylate cycle [153,155], enabling growth on acetate as a sole carbon source. In addition to that, the glyoxylate cycle has a role in the anabolic pathway, centering on the conversion of acetyl-CoA to succinate for the synthesis of carbohydrates. The glyoxylate non-treated R-10 was confirmed to grow on acetate as a sole carbon source with all primary transcripts upregulated (data not shown), where NADH and succinate were supposed to be involved in TCA cycle. Especially, *ACS1* was expressed 1.95-fold more. Glyoxylate treated B-69, however, showed almost the same level of *ACS1* transcript with glyoxylate treated R-10. Taken together, this means that glyoxylate as well as acetate was also used as another carbon source and

that glyoxylate cycle had less capacity to utilize acetyl-CoA from acetate (Figure 5.11).

Glyoxylate treated B-69, however, meaningfully upregulated isocitrate lyase, producing succinate that enters the TCA cycle. It could be expected that succinate is metabolized for further metabolism. To demonstrate which pathways were activated in detail, transcriptome analysis should be carried out comparing B-69 with R-10 under glyoxylate treatment.

5.4 Conclusions

Transgenic *Chlamydomonas reinhardtii* expressing malate synthase showed an increase of 19% in microalgal biomass compared to cells without malate synthase. Malate produced in chloroplast likely entered the mitochondria by the malate/OAA shuttle and upregulated *MDH4* (malate dehydrogenase) transcript. In addition, the transgenic microalgae with malate synthase under glyoxylate treatment was demonstrated to increase as well as drive acetate feeding into TCA cycle rather than into glyoxylate cycle, compared to wild type. Both the increased exportation of malate into the mitochondria and the increased acetate utilization in the TCA cycle seemed to contribute to TCA energy production, which is closely related with the increase in microalgal biomass.

Chapter 6

Overall Conclusion

In this dissertation, in order to enhance microalgal biomass through overcoming limitations in industrial cultivation, several strategies, including stable low concentration of nutrient feeding, stress priming, and metabolic engineering, were represented to increase microalgal biomass productivity, especially for *Chlamydomonas reinhardtii*. It is expected that this study will provide a feasible approaches for operating industrial scale bioprocess.

In the first part, a continuous cultivation process that provides stable flow of low concentration nutrient medium was developed. The cells in the system produced TAG and also proliferate although being supplied with only slightly higher than an absolutely deplete one (particularly 7.5% of NH_4^+/ 7.5% of PO_4^{2-}). This can suggest that a continuous, stable flow of a low concentration of nutrient can not only starve cells but also boost them to proliferate at a minimum growth rate, enhancing total TAG yield per batch.

In the second part, stress priming induced by vibration with low amplitude and low frequency was applied. When microalgal cells were pre-treated by up/down vibration (10 Hz and 0.15 G), they responded to it as one of the mechanical stressors and get to be in a primed state with about 2-fold increase in mechanosensitive RNA transcript, *TRP11*, *CAV2*, and *ADF1*. When they were cultivated in a environment with hydrodynamic shear fields similar in large-scale bioreactors, the microalgal

biomass and volumetric yield of bioproduct were increased by 27% and 39% more than non-primed cells, respectively. Through a more efficient operation by less energy and costs, stress priming effect can contribute to better bio-productivity in industrial applications.

In the third part, transgenic microalgae of which chloroplast genome was integrated with malate synthase was developed. Malate synthase expression of transgenic *Chlamydomonas* contributed to increase microalgal biomass by 19% more, comparing to wild-type cells. Chloroplastic malate entered mitochondria by malate/OAA shuttle and upregulated *MDH4* transcript. Moreover, glyoxylate treatment was demonstrated that the transgenic cell more drove acetate from nutrient medium into TCA cycle than into glyoxylate cycle. Both more malate export to mitochondria and its consumption in TCA cycle were supposed to lead to TCA energy production.

Bibliography

[1] United Nations Population Division, 2017. World Population Prospects: the 2017 Revision, Online at. https://esa.un.org/unpd/wpp/Publications/Files/WPP2017_KeyFindings.pdf

[2] United Nations Food and Agriculture Organization (FAO), 2017, The State of Food and Agriculture. Online at http://www.fao.org/3/a-I7658e.pdf

[3] Smetana, S., Sandmann, M., Rohn, S., Pleissner, D., Heinz, V., 2017. Autotrophic and heterotrophic microalgae and cyanobacteria cultivation for food and feed: life cycle assessment. *Bioresour. Technol. 245(Part A)*, 162–170.

[4] Hartmann, C., Siegrist, M., 2017. Consumer perception and behaviour regarding sustainable protein consumption: a systematic review. *Trends Food Sci. Technol. 61*, 11–25.

[5] León-Bañares, R., González-Ballester, D., Galván, A., Fernández, E., 2004. Transgenic microalgae as green cell-factories. *Trends Biotechnol. 22*, 45–52.

[6] Radakovits, R., Jinkerson, R.E., Darzins, A., Posewitz, M.C., 2010. Genetic engineering of algae for enhanced biofuel production. *Eukaryot. Cell 9*, 486–501.

[7] Wang, Z.T., Ullrich, N., Joo, S., Waffenschmidt, S., Goodenough, U., 2009. Algal lipid bodies: stress induction, purification, and biochemical characterization in wildtype and starchless *Chlamydomonas reinhardtii*. *Eukaryot. Cell 8*, 1856–1868.

[8] Gallardo-Rodríguez, J.J., López-Rosales, L., Sánchez-Mirón, A., García-Camacho, F., Molina-Grima, E., Chalmers, J.J., 2016. New insights into shear-sensitivity in dinoflagellate microalgae. *Bioresour. Technol. 200*, 699–705.

[9] Fernie, A.R., Carrari, F., Sweetlove, L.J., 2004, Respiratory metabolism: glycolysis, the TCA cycle and mitochondrial electron transport. *Curr. Opin. Plant Biol. 7*, 254–261.

[10] Scheibe, R., 2004, Malate valves to balance cellular energy supply. *Physiol. Plantarum 120*, 21-26.

[11] IPCC(Intergovernmental Panel on Climate Change), 2014, IPCC(Intergovernmental Panel on Climate Change) Fifth Assessment Report. Online at. http://www.ipcc.ch/pdf/assessment-report/ar5/wg3/ipcc_wg3_ar5_full.pdf

[12] UNFCCC, 2015, Report of the conference of the parties on its twenty-first session, held in Paris from 30 November to 13 December 2015. Addendum Part two: Action taken by the Conference of the Parties at its twenty-first session. Online at. http://https://unfccc.int/resource/docs/2015/cop21/eng/10a01.pdf

[13] Global Harvest Initiative, 2016. Global Agricultural Productivity Report. Online at. http://www.globalharvestinitiative.org/GAP/2016_GAP_Report.pdf

[14] A. Demirbas, M. Fatih Demirbas, 2011, Importance of algae oil as a source of biodiesel: Energy Conversion and Management. *Energ. Convers. Manage. 52*, 163-170.

[15] Cristiane Mesquita da Silva Gorgônio, Donato Alexandre Gomes Aranda, Sônia Couri, 2013, Morphological and chemical aspects of *Chlorella pyrenoidosa*, *Dunaliella tertiolecta*, Isochrysis *galbana* and *Tetraselmis gracilis* microalgae. *Natural Science 5(7)*, 783-791.

[16] Chisti, Y., 2007, Biodiesel from microalgae. *Biotechnol. Adv. 25*, 294-306.

[17] Menetrez, M.Y., 2012, An overview of algae biofuel production and potential environmental impact. *Enviorn. Sci. Technol. 46*, 7073-7085.

[18] Becker, 2007, Micro-algae as a source of protein. *Biotechnol. Adv. 25*, 207-210

[19] Hu, Q., Sommerfeld, M., Jarvis, E., Ghirardi, M., Posewitz, M., Seibert, M., Darzins, A., 2008, Microalgal triacylglycerols as feedstocks for biofuel production: perspectives and advances. *Plant J. 54*, 621-639.

[20] Wijffels, R.H., Barbosa, M.J., 2010, An Outlook on Microalgal Biofuels. *Science 329*, 796-799.

[21] Zeng, X., Danquah, M.K., Chen, X.D., Lu, Y., 2011, Microalgae bioengineering: From CO_2 fixation to biofuel production. *Renew. Sust. Energ. Rev. 15*, 3252-3260.

[22] Melis, A., 2009, Solar energy conversion efficiencies in photosynthesis: Minimizing the chlorophyll antennae to maximize efficiency. *Plant Sci. 177*, 272-280.

[23] Zhang, X., Rong, J., Chen, H., He, C., Wang, Q., 2014, Current status and outlook in the application of microalgae in biodiesel production and environmental protection. *Front. Energ. Res. 2(32)*, 1-15.

[24] Lauersen, K.J., Huber, I., Wichmann, J., Baier, T., Leiter, A., Gaukel, V., Kartushin, V., Rattenholl, A., Steinweg, C., Riesen, L.V., Posten, C., Gudermann, F., Lütkemeyer, D., Mussgnug, J.H., Kruse, O., 2015, Investigating the dynamics of recombinant protein secretion from a microalgal host. *J. Biotechnol. 215*, 62-71.

[25] Siaut, M., Cuiné, S., Cagnon, C., Fessler, B., Nguyen, M., Carrier, P., Beyly, A., Beisson, F., Triantaphylidès, C., Li-Beisson, Y., Peltier, G., 2011, Oil accumulation in the model green alga *Chlamydomonas reinhardtii*: characterization, variability between common laboratory strains and relationship with starch reserves. *BMC Biotechnol. 11(7)*, 1-15.

[26] Gallaher, S.D., Fitz-Gibbon, S.T., Glaesener, A.G., Pellegrini, M., Merchanta, S.S., 2015, *Chlamydomonas* Genome Resource for Laboratory Strains Reveals a Mosaic of Sequence Variation, Identifies True Strain Histories, and Enables Strain-Specific Studies. *Plant Cell 27*, 2335-2352.

[27] Scaife, M.A., Nguyen, G.T.D.T., Rico, J., Lambert, D., Helliwell, K.E., Smith, A.G., 2015, Establishing *Chlamydomonas reinhardtii* as an industrial biotechnology host. *Plant J. 82*, 532-546.

[28] Almaraz-Delgado, A.L., Flores-Uribe, J., Pérez-España, V.H., Salgado-Manjarrez, E., Badillo-Corona, J.A., 2014, Production of therapeutic proteins in the chloroplast of *Chlamydomonas reinhardtii*. *AMB Express 4(57)*, 1-9.

[29] Lauersen, K.J., Kruse, O., Mussgnug, J.H., 2015, Targeted expression of nuclear transgenes in *Chlamydomonas reinhardtii* with a versatile, modular vector toolkit. *Appl. Microbiol. Biot. 99(8)*, 3491-3503.

[30] Sun, M., Qian, K., Su, N., Chang, H., Liu, J., Chen, G., 2003, Foot-and-mouth disease virus VP1 protein fused with cholera toxin B subunit expressed in *Chlamydomonas reinhardtii* chloroplast. *Biotechnol. Lett. 25*, 1087-1092.

[31] Mayfield, S.P., Franklin, S.E., Lerner, R.A., 2003, Expression and assembly of a fully active antibody in algae. *Proc. Natl. Acad. Sci. 100(2)*, 438-442.

[32] Zongqi, Y., Yinü, L., Feng, C., Dong, L., Zhifang, Z., Yanxin, L., Dexian, Z., Yong, W., Guifang, S., 2006, Expression of human soluble TRAIL in *Chlamydomonas reinhardtii* chloroplast. *Sci. Bull. 51(14)*, 1703-1709.

[33] Manuell, A.L., Beligni, M.V., Elder, J.H., Siefker, D.T., Tran, M., Weber, A., McDonald, T.L., Mayfield, S.P., 2007, Robust expression of a bioactive mammalian protein in *Chlamydomonas* chloroplast. *Plant Biotechnol. J. 5*, 402-412.

[34] He, D-M., Qian, K-X., Shen, G-F., Zhang, Z-F., Li, Y-N., Su, Z-L., Shao, H-B., 2007, Recombination and expression of classical swine fever virus (CSFV) structural protein E2 gene in *Chlamydomonas reinhardtii* chroloplasts. *Colloids Surf. B. 55*, 26-30.

[35] Wang, X., Brandsma, M., Tremblay, R., Maxwell, D., Jevnikar, A.M., Huner, N., Ma, S., 2008, A novel expression platform for the production of diabetes-associated autoantigen human glutamic acid decarboxylase (hGAD65). *BMC Biotechnol. 8(87)*, 1-13.

[36] Surzycki, R., Greenham, K., Kitayama, K., Dibal, F., Wagner, R., Rochaix, J.D., Ajam, T., Surzycki, S., 2009, Factors effecting expression of vaccines in microalgae. *Biologicals 37*, 133-138.

[37] Tran, M., Zhou, B., Pettersson, P.L., Gonzalez, M.J., Mayfield, S.P., 2009, Synthesis and Assembly of a Full-Length Human Monoclonal Antibody in Algal Chloroplasts. *Biotechnol. Bioeng. 104(4)*, 663-673.

[38] Dreesen, I.A.J., Hamri, G.C.E., Fussenegger, M., 2010, Heat-stable oral alga-based vaccine protects mice from *Staphylococcus aureus* infection. *J. Biotechnol. 145*, 273-280.

[39] Rasala, B.A., Muto, M., Lee, P.A., Jager, M., Cardoso, R.M.F, Behnke, C.A., Kirk, P., Hokanson, C.A., Crea, R., Mendez, M., Mayfield, S.P., 2010,

Production of therapeutic proteins in algae, analysis of expression of seven human proteins in the chloroplast of *Chlamydomonas reinhardtii*. *Plant Biotechnol. J. 8*, 719-733.

[40] Michelet, L., Lefebvre-Legendre, L., Burr, S.E., Rochaix, J.D., Goldschmidt-Clermont, M., 2011, Enhanced chloroplast transgene expression in a nuclear mutant of *Chlamydomonas*. *Plant Biotechnol J. 9(5)*, 565-574.

[41] Yoon, SM., Kim, SY., Li, K.F., Yoon B.H., Choe, S., Kuo, M.M.C., 2011, Transgenic microalgae expressing *Escherichia coli* AppA phytase as feed additive to reduce phytate excretion in the manure of young broiler chicks. *Appl. Microbiol. Biotechnol. 91(3)*, 553-563.

[42] Gregory, J.A., Li, F., Tomosada, L.M., Cox, C.J., Topol, A.B., Vinetz, J.M., Mayfield, S., 2012, Algae-Produced Pfs25 Elicits Antibodies That Inhibit Malaria Transmission. *PLoS One 7(5)*, e37179.

[43] Tran, M., Van, C., Barrera, D.J., Pettersson, P.L., Peinado, C.D., Bui, J., Mayfield, S.P., 2013, Production of unique immunotoxin cancer therapeutics in algal chloroplasts. *Proc. Natl. Acad. Sci. 110(1)*, E15-22.

[44] Gregory, J.A., Topol, A.B., Doerner, D.Z., Mayfield, S., 2013, Alga-Produced Cholera Toxin-Pfs25 Fusion Proteins as Oral Vaccines. *Appl. Environ. Microbiol. 79(13)*, 3917-3925.

[45] Tran, M., Henry, R.E., Siefker, D., Van, C., Newkirk, G., Kim, J., Bui, J., Mayfield, S.P., 2013, Production of Anti-Cancer Immunotoxins in Algae: Ribosome Inactivating Proteins as Fusion Partners. *Biotechnol. Bioeng. 110(11)*, 2826-2835.

[46] Stoffels, L., Taunt, H.N., Charalambous, B., Purton, S., 2017, Synthesis of bacteriophage lytic proteins against *Streptococcus pneumoniae* in the chloroplast of *Chlamydomonas reinhardtii*. *Plant Biotechnol. J. 15(9)*. 1130-1140.

[47] Young, R.E.B., Purton, S., 2014, Cytosine deaminase as a negative selectable marker for the microalgal chloroplast: a strategy for the isolation of nuclear mutations that affect chloroplast gene expression. *Plant J. 80*, 915-925.

[48] Bertalan, I., Munder, M.C., Weiß, C., Kopf, J., Fischer, D., Johanningmeier, U., 2015, A rapid, modular and marker-free chloroplast expression system for the green alga *Chlamydomonas reinhardtii*. *J. Biotechnol. 195*, 60-66.

[49] Rasala, B.A., Muto, M., Sullivan, J. Mayfield, S.P., 2011, Improved heterologous protein expression in the chloroplast of *Chlamydomonas reinhardtii* through promoter and 5' untranslated region optimization. *Plant Biotechnol. J. 9*, 674-683.

[50] Barnes, D., Franklin, S., Schultz, J., Henry, R., Brown, E., Coragliotti, A., Mayfield, S.P., 2005, Contribution of 5'- and 3'-untranslated regions of plastid mRNAs to the expression of *Chlamydomonas reinhardtii* chloroplast genes. *Mol. Gen. Genomics 274*, 625-636.

[51] Chen, H.C., Melis, A., Marker-free genetic engineering of the chloroplast in the green microalga *Chlamydomonas reinhardtii*. *Plant Biotechnol. J. 11*, 818-828.

[52] Yamaoka, Y., Achard, D., Jang, S., Legeret, B., Kamisuki, S., Ko, D., Schulz-Raffelt, M., Kim, Y., Song, W.Y., Nishida, I., Li-Beisson, Y., Lee, Y., 2016, Identification of a *Chlamydomonas* plastidial 2-lysophosphatidic acid acyltransferase and its use to engineer microalgae with increased oil content. *Plant Biotechnol. J. 14*, 2158-2167.

[53] Paik, S.M., Jin, E., Sim, S.J., Jeon, N.L., 2018, Vibration-induced stress priming during seed culture increases microalgal biomass in high shear field-cultivation. *Bioresour. Technol. 254*, 340-346.

[54] Rosales-Mendoza, S., Paz-Maldonado, L.M.T., Soria-Guerra R.E., 2012, *Chlamydomonas reinhardtii* as a viable platform for the production of recombinant proteins: current status and perspectives. *Plant Cell Rep. 31*, 479-494.

[55] Newman, S.M., Boynton, J.E., Gillham, N.W., Randolph-Anderson, B.L., Johnson, A.M., Harris, E.H., 1990, Transformation of Chloroplast Ribosomal RNA Genes in *Chlamydomonas*: Molecular and Genetic Characterization of Integration Event. *Genetics 126*, 875-888.

[56] Melis, A., Chen, H.C., 2013, Method of microalgal chloroplast transformation using functional selection in the absence of antibiotics. US Patent 2013/0302812 A1, November 14, 2013.

[57] Wobbe, L., Remacle, C., 2015, Improving the sunlight-to-biomass conversion efficiency in microalgal biofactories. *J. Biotechnol. 201*, 28-42.

[58] Polle, J.E.W., Kanakagiri, S.D., Melis, A., 2003, *tla1*, a DNA insertional transformant of the green alga *Chlamydomonas reinhardtii* with a truncated light-harvesting chlorophyll antenna size. *Planta 217*, 49-59.

[59] Mitra, M., Kirst, H., Dewez, D., Melis, A., 2012, Modulation of the light-harvesting chlorophyll antenna size in *Chlamydomonas reinhardtii* by TLA1 gene over-expression and RNA interference. *Philos. Trans. R. Soc. Lond. B. Biol. Sci. 367(1608)*, 3430-3443.

[60] Kirst, H., Garcia-Cerdan, J.G., Zurbriggen, A., Ruehle, T., Melis, A., 2012, Truncated Photosystem Chlorophyll antenna size in the green microalga *Chlamydomonas reinhardtii* upon deletion of the TLA3-CpSRP43 Gene. *Plant Physiol. 160(4)*, 2251-2260.

[61] Bonente, G., Ballottari, M., Truong, T.B., Morosinotto, T., Ahn, T.K., Fleming, G.R., Niyogi, K.K., Bassi, R., 2011, Analysis of LhcSR3, a protein essential for feedback de-excitation in the green alga *Chlamydomonas reinhardtii*. *PLoS Biol. 9*, e10005777.

[62] Mussgnug, J.H., Thomas-Hall, S., Rupprecht, J., Foo, A., Klassen, V., McDowall, A., Schenk, P.M., Kruse, O., Hankamer, B., 2007, Engineering photosynthetic light capture: impacts on improved solar energy to biomass conversion. *Plant Biotechnol. J. 5(6)*, 802-814.

[63] Oey, M., Ross, I.L., Stephens, E., Steinbeck, J., Wolf, J., Radzun, K.A., Kügler, J., Ringsmuth, A.K., Kruse, O., Hankamer, B., 2013, RNAi knock-down of LHCBM1, 2 and 3 increases photosynthetic H_2 production efficiency of the green alga *Chlamydomonas reinhardtii*. *PLoS ONE 8*, e61375.

[64] Beckmann, J., Lehr, F., Finazzi, G., Hankamer, B., Posten, C., Wobbe, L., Kruse, O., 2009, Improvement of light to biomass conversion by de-regulation

of light-harvesting protein translation in *Chlamydomonas reinhardtii*. *J. Biotechnol. 142*, 70-77.

[65] Jeong, J., Baek, K., Kirst, H., Melis, A., Jin, ES., 2017, Loss of CpSRP54 function leads to a truncated light-harvesting antenna size in *Chlamydomonas reinhardtii*. *Biochim. Biophys. Acta. 1858*, 45-55.

[66] de Bianchi, S., Ballottari, M., Dall'osto, L., Bassi, R., 2010, Regulation of plant light harvesting by thermal dissipation of excess energy. *Biochem. Soc. Trans. 38(2)*, 651-660.

[67] Krieger-Liszka, A., 2004, Singlet oxygen production in photosynthesis. *J. Exp. Bot. 56(411)*, 337-346.

[68] Johnson, X., Alrica, J., 2013, Central carbon metabolism and electron transport in *Chlamydomonas reinhardtii*: metabolic constraints for carbon partitioning between oil and starch. *Eukaryot. Cell. 12(6)*, 776-793.

[69] Wheeler, G.L.. Calcium-Dependent Signalling Processes in *Chlamydomonas*. In *Chlamydomonas*: Molecular Genetics and Physiology: Michael Hippler, *Ed*.; Springer: Münster, 2017; pp 233-255.

[70] McAinsh, M.R., Pittman, J.K., 2008, Shaping the calcium signature. *New Phytologist 181*, 275-294.

[71] Edel, K.H., Kudla, J., 2015, Increasing complexity and versatility: How the calcium signaling toolkit was shaped during plant land colonization. *Cell Calcium 57(3)*, 231-246.

[72] Zhu, X., Dunand, C., Snedden, W., Galaud, J.P., 2015, CaM and CML emergence in the green lineage. *Trends Plant Sci. 20*, 483-489.

[73] Finkler, A., Ashery-Padan, R., Fromm, H., 2007, CAMTAs: Calmodulin-binding transcription activators from plants to human. *FEBS Lett. 581(21)*, 3893-3898.

[74] Finkler, A., Kaplan, B., Fromm, H., 2007, Ca^{2+}-responsive *cis*-elements in plants. *Plant Signal. Behav. 2(1)*, 17-19.

[75] Kudla, J., Batistic, O., Hashimoto, K., 2010, Calcium signals: the lead currency of plant information processing. *Plant Cell 22*, 541-563.

[76] Yoshimura, K.. Stimulus Perception and Membrane Excitation in Unicellular Alga *Chlamydomonas*. In Coding and Decoding of Calcium Signals in Plants: Sheng Luan, *Ed.*; Springer: Verlag Berlin Heidelberg, 2011; pp 79-91.

[77] Fujiu, K., Nakayama, Y., Iida, H., Sokabe, M., Yoshimura, K., 2011, Mechanoreception in motile flagella of *Chlamydomonas*. *Nat. Cell Biol. 13*, 630–632.

[78] Fujiu, K., Nakayama, Y., Sokabe, M., Yoshimura, K., 2009, *Chlamydomonas* CAV2 encodes a voltage-dependent calcium channel required for the flagellar waveform conversion. *Curr Biol. 19*, 133–139.

[79] Hille, B., 2011, Ion channels of excitable membranes. 3rd Ed. Sinauer Associates, Sunderland.

[80] Gu, S., Zhang, Y., Wu, Y., 2016, Effects of sound exposure on the growth and intracellular macromolecular synthesis of *E. coli* k-12, *PeerJ 4*, e1920.

[81] Marycz, K., Lewandowski, D., Tomaszewski, K.A., Henry, B.M., Golec, E.B., Mardziak, B., 2016, Low-frequency, low-magnitude vibrations (LFLM) enhances chondrogenic differentiation potential of human adipose derived mesenchymal stromal stem cells (hASCs). *PeerJ 4*, e1637.

[82] Tirkkonen, L., Halonen, H., Hyttinen, J., Kuokkanen, H., Sieva¨nen, H., Koivisto, A.M., Mannerstro¨m, B., Sa´ndor, G.K.B., Suuronen, R., Miettinen, S., Haimi, S., The effects of vibration loading on adipose stem cell number, viability and differentiation towards bone-forming cells. *J. Royal Soc. Interface 8*, 1736–1747.

[83] Han, F., Pei, H., Hu, W., Jiang, L., Cheng, J., Zhang, L., 2016. Beneficial changes in biomass and lipid of microalgae Anabaena variabilis facing the ultrasonic stress environment. *Bioresour. Technol. 209*, 16–22.

[84] Ghosh, R., Mishra, R.C., Choi, B., Kwon, Y.S., Bae, D.W., Park, S.C., Jeong, M.J., Bae, H., 2016. Exposure to sound vibrations lead to transcriptomic, proteomic and hormonal changes in *Arabidopsis*. *Sci. Rep. 6*, 33370.

[85] Fukuda, H., Kondo, A., Noda, H., 2001, Biodiesel fuel production by transesterification of oils. *J. Biosci. Bioeng. 92*, 405–416.

[86] Kajikawa, M., Abe, T., Ifuku, K., Furutani, K., Yan, D., Okuda, T., Ando, A., Kishino, S., Ogawa, J., Fukuzawa, H., 2016. Production of ricinoleic acid containing monoestolide triacylglycerides in an oleaginous diatom, *Chaetoceros gracilis. Sci. Rep. 6*, 36809.

[87] Li-Beisson, Y., Beisson, F., Riekhof, W., 2015, Metabolism of acyl-lipids in *Chlamydomonas reinhardtii*. *Plant J. 82*, 504-522.

[88] Wase, N., Black, P.N., Stanley, B.A., DiRusso, C.C., 2014, Integrated Quantitative Analysis of Nitrogen Stress Response in *Chlamydomonas reinhardtii* Using Metabolite and Protein Profiling. *J. Proteome Res. 13,* 1373-1396.

[89] Michelet, L., Lefebvre-Legendre, L., Burr, S.E., Rochaix, J.D., Goldschmidt-Clermont, M., 2011, Enhanced chloroplast transgene expression in a nuclear mutant of *Chlamydomonas*. *Plant Biotech. J. 9*, 565–574.

[90] Boyle, N.R., Page, M.D., Liu, B., 2012, Three acyltransferases and nitrogen-responsive regulator are implicated in nitrogen starvation induced triacylglycerol accumulation in *Chlamydomonas. J. Biol. Chem. 287*, 15811–15825.

[91] Ng, I.S., Tan, S.I., Kao, P.H., Chang, Y.K., Chang, J.S., 2017, Recent Developments on Genetic Engineering of Microalgae for Biofuels and Bio-Based Chemicals. *Biotechnol. J. 12*, 1600644.

[92] Page, R.A., Okada, S., Harwood, J.L., 1994, Acetyl-CoA carboxylase exerts strong flux control over lipid synthesis in plants. *Biochim. Biophys. Acta. 1210(3)*, 369-372.

[93] Ahmad, I., Sharma, A.K., Daniell, H., Kumar, S., 2015, Altered lipid composition and enhanced lipid production in green microalga by introduction of brassica diacylglycerol acyltransferase 2. *Plant Biotechnol. J. 13(4)*, 540-550.

[94] Niu, Y.F., Zhang, M.H., Li, D.W., Yang, W.D., Liu, J.S., Bai, W.B., Li, H.Y., 2013, Improvement of Neutral Lipid and Polyunsaturated Fatty Acid Biosynthesis by Overexpressing a Type 2 Diacylglycerol Acyltransferase in Marine Diatom *Phaeodactylum tricornutum*. *Mar. Drugs 11(11)*, 4558-4569.

[95] Deng, X., Cai, J., Li, Y., Fei, X., 2014, Expression and knockdown of the PEPC1 gene affect carbon flux in the biosynthesis of triacylglycerols by the green alga *Chlamydomonas reinhardtii*. *Biotechnol. Lett. 36(11)*, 2199-2208.

[96] Yang, J., Pan, Y., Bowler, C., Zhang, L., Hu, H., 2016, Knockdown of phosphoenolpyruvate carboxykinase increases carbon flux to lipid synthesis in *Phaeodactylum tricornutum*. *Algal Res. 15*, 50-58.

[97] Dunahay, T.G., Jarvis, E.E., Roessler, P.G., 1995, Genetic transformation of the diatoms *Cyclotella cryptica* and *Navicula saprophila*. *J. Phycol. 31(6)*, 1004-1011.

[98] Klaus, D., Ohlrogge, J.B., Neuhaus, H.E., Dörmann, P., 2004, Increased fatty acid production in potato by engineering of acetyl-CoA carboxylase. *Planta 219*, 389-396.

[99] Roesler, K., Shintani, D., Savage, L., Boddupalli, S., Ohlrogge, J., 1997, Targeting of the *Arabidopsis* homomeric acetyl-coenzyme A carboxylase to plastids of rapeseeds. *Plant Physiol. 113*, 75-81.

[100] Dehesh, K., Tai, H., Edwards, P., Byrne, J., Jaworski, J.G., 2001, Overexpression of 3-ketoacyl-acyl-carrier protein synthase IIIs in plants reduces the rate of lipid synthesis. *Plant Physiol. 125*, 1103-1114.

[101] Vigeolas, H., Waldeck, P., Zank, T., Geigenberger, P., 2007, Increasing seed oil content in oil-seed rape (*Brassica napus L.*) by over-expression of a yeast glycerol-3-phosphate dehydrogenase under the control of a seed-specific promoter. *Plant Biotechnol. J. 5(3)*, 431-441.

[102] Jain, R.K., Coffey, M., Lai, K., Kumar, A., MacKenzie, S. L., 2000, Enhancement of seed oil content by expression of glycerol-3-phosphate acyltransferase genes. *Biochem. Soc. Trans. 28(6)*, 958-961.

[103] Zou, J., Katavic, V., Giblin, E.M., Barton, D.L., MacKenzie, S.L., Keller, W.A., Hu, X., Taylor, D.C., 1997, Modification of seed oil content and acyl composition in the *brassicaceae* by expression of a yeast sn-2 acyltransferase gene. *Plant Cell 9*, 909-923.

[104] Lardizabal, K., Effertz, R., Levering, C., Mai, J., Pedroso, M.C., Jury, T., Aasen, E., Gruys, K., Bennett, K., 2008, Expression of *Umbelopsis*

ramanniana DGAT2A in Seed Increases Oil in Soybean. *Plant Physiol. 148*, 89-96.

[105] Work, V.H., Radakovits, R., Jinkerson, R.E., Meuser, J.E., Elliott, L.G., Vinyard, D.J., Laurens, L.M.L, Dismukes, G.C., Posewitz, M.C., 2010, Increased Lipid Accumulation in the *Chlamydomonas reinhardtii sta7-10* Starchless Isoamylase Mutant and Increased Carbohydrate Synthesis in Complemented Strains. *Eukaryot. Cell 9(8)*, 1251-1261.

[106] Ramazanov, A., Ramazanov, Z., 2006, Isolation and characterization of a starchless mutant of *Chlorella pyrenoidosa* STL-PI with a high growth rate, and high protein and polyunsaturated fatty acid content. *Phycol. Res. 54*, 255-259.

[107] Lu, X., Vora, H., Khosla, C., 2008, Overproduction of free fatty acids in *E. coli*: Implications for biodiesel production. *Metabol. Eng. 10(6)*, 333-339.

[108] Fulda, M., Schnurr, J., Abbadi, A., Heinz, E., Browse, J., 2004, Peroxisomal Acyl-CoA Synthetase Activity Is Essential for Seedling Development in *Arabidopsis thaliana*. *Plant Cell 16*, 394-405.

[109] Germain, V., Rylott, E.L., Larson, T.R., Sherson, S.M., Bechtold, N., Carde, J.P., Bryce, J.H., Graham, I.A., Smith, S.M., 2001, Requirement for 3-ketoacyl-CoA thiolase-2 in peroxisome development, fatty acid β-oxidation and breakdown of triacylglycerol in lipid bodies of *Arabidopsis* seedlings. *Plant J. 28(1)*, 1-12.

[110] Rylott, E.L., Rogers, C.A., Gilday, A.D., Edgell, T., Larson, T.R., Graham, I.A., 2003, *Arabidopsis* Mutants in Short- and Medium-chain Acyl-CoA Oxidase Activities Accumulate Acyl-CoAs and Reveal That Fatty Acid β-Oxidation Is Essential for Embryo Development. *J. Biol. Chem. 278(24)*, 21370-21377.

[111] Voelker, T.A., Worrell, A.C., Anderson, L., Bleibaum, J., Fan, C., Hawkins, D.J., Radke, S.E., Davies, H.M., 1992, Fatty acid biosynthesis redirected to medium chains in transgenic oilseed plants. *Science 257(5066)*, 72-73.

[112] Voelker, T.A., Davies, H.M., 1994, Alteration of the Specificity and Regulation of Fatty Acid Synthesis of Escherichia coli by Expression of a

Plant Medium-Chain Acyl-Acyl Carrier Protein Thioesterase. *J. Bacteriol. 176(23)*, 7320-7327.

[113] Nawabi, P., Bauer, S., Kyrpides, N., Lykidis, A., 2011, Engineering Escherichia coli for Biodiesel Production Utilizing a Bacterial Fatty Acid Methyltransferase. *Appl. Environ. Microbiol. 77(22)*, 8052-8061.

[114] Dehesh, K., Edwards, P., Fillatti, J., Slabaugh, M., Byrne, J., 2002, KAS IV: a 3-ketoacyl-ACP synthase from *Cuphea sp.* is a medium chain specific condensing enzyme. *Plant J. 15(3)*, 383-390.

[115] Sheehan, J., Dunahay, T., Benemann, J., Roessler, P., A look back at the U.S. Department of Energy's Aquatic Species Program—biodiesel from algae. National Renewable Energy Laboratory, Golden, CO; 1998. Report NREL/TP-580–24190.

[116] Adams, C., Godfrey, V., Wahlen, B., Seefeldt, L., Bugbee, B., 2013, Understanding precision nitrogen stress to optimize the growth and lipid content tradeoff in oleaginous green microalgae. *Bioresour. Technol. 131*, 188-194.

[117] Quinn, J.M., Merchant, S., 1995, Two Copper-Responsive Elements Associated with the *Chlamydomonas* Cyc6 Gene Function as Targets for Transcriptional Activators. *Plant Cell 7*, 623-638.

[118] Arora, N., Patel, A., Pruthi, P.A., Pruthi, V., 2016, Synergistic dynamics of nitrogen and phosphorous influences lipid productivity in *Chlorella minutissima* for biodiesel production. *Bioresour. Technol. 213*, 79-87.

[119] Tevatia, R., Demirel, Y., Blum, P., 2012, Kinetic modeling of photoautotropic growth and neutral lipid accumulation in terms of ammonium concentration in *Chlamydomonas reinhardtii*. *Bioresour. Technol. 119*, 419-424.

[120] Dénervaud, N., Becker, J., Delgado-Gonzalo, R., Damay, P., Rajkumar, AS., Unser, M., Shore, D., Naef, F., Maerkl, SJ., 2013. A chemostat array enables the spatio-temporal analysis of the yeast proteome. *Proc. Natl. Acad. Sci. 110*, 15842–15847.

[121] Gardner, RD., Lohman, E., Gerlach, R., Cooksey, KE., Peyton, BM., 2013. Comparison of CO_2 and bicarbonate as inorganic carbon sources for

triacylglycerol and starch accumulation in *Chlamydomonas reinhardtii*. *Biotechnol, Bioeng. 110*, 87-96.

[122] Kamalanathan, M., Pierangelini, M., Shearman, LA., Gleadow, R., Beardall, J., 2016. Impacts of nitrogen and phosphorus starvation on the physiology of *Chlamydomonas reinhardtii. J. Appl. Phycol. 28*, 1509-1520.

[123] Lee, DY., Fiehn, O., 2008. High quality metabolomic data for *Chlamydomonas reinhardtii*. *Plant Methods 28*, 4-7.

[124] Tevatia, R., Allen, J., Blum, P., Demirel, Y., Black, P., 2014. Modeling of rhythmic behavior in neutral lipid production due to continuous supply of limited nitrogen: mutual growth and lipid accumulation in microalgae. *Bioresour. Technol. 170*, 152-159.

[125] Park, J., Wu, J., Polymenis, M., Han, A., 2013. Microchemostat array with small-volume fraction replenishment for steady-state microbial culture. *Lab. Chip. 7*, 4217-4224.

[126] Dusny, C., Grünberger, A., Probst, C., Wiechert, W., Kohlheyer, D., Schmid, A., 2015. Technical bias of microcultivation environments on single-cell physiology. *Lab. Chip. 15*, 1822-1834.

[127] Garbayo, I., Forján, E., Salguero, A., Cuaresma, M., Vega, JM., Vílchez, C., 2005. Enhancement of photorespiration in immobilized *Chlamydomonas reinhardtii* cells. *Biotechnol Lett. 27*, 265-267.

[128] Feng, C., Wei, J., Li, Y., Yang, Y., Wang, Y., Lu, L., Zheng, G., 2016. An on-chip pollutant toxicity determination based on marine microalgal swimming inhibition. *Analyst. 141*, 1761-1771.

[129] Zheng, G., Wang, Y., Wang, Z., Zhong, W., Wang, H., Li, Y., 2013. An integrated microfluidic device in marine microalgae culture for toxicity screening application. *Mar. Pollut. Bull. 72(1)*, 231-243.

[130] Zheng, G., Zhang, X., Yang, Y., Zeng, S., Wei, J., Wang, Y., Li, Y., 2014. An integrated microfludic device for culturing and screening of *Giardia lamblia*. *Exp. Parasitol. 137*, 1–7.

[131] Lee, S., Spencer, ND., 2008. Adsorption properties of poly(l-lysine)-graft-poly(ethylene glycol) (PLL-g-PEG) at a hydrophobic interface: influence of

tribological stress, pH, salt concentration, and polymer molecular weight. *Langmuir. 24*, 9479-9488.

[132] Govender, T., Ramanna, L., Rawat, I., Bux, F., 2012. BODIPY staining, an alternative to the Nile Red fluorescence method for the evaluation of intracellular lipids in microalgae. *Bioresour. Technol. 114*, 507-511.

[133] Lazazzera, BA., 2000. Quorum sensing and starvation: signals for entry into stationary phase. *Curr. Opin. Microbiol. 3*, 177–182.

[134] Caicedo, HH., Brady, ST., 2016. Microfluidics: The Challenge Is to Bridge the Gap Instead of Looking for a 'Killer App'. *Trends Biotechnol. 34*, 1-3.

[135] Savchenko, O., Xing, J., Yang, X., Gu, Q., Shaheen, M., Huang, M., Yu, X., Burrell, R., Patra, P., Chen, J., 2017, Algal Cell Response to Pulsed Waved Stimulation and Its Application to Increase Algal Lipid Production. *Sci. Rep. 7*, 42003.

[136] Scharlemann, J.P.W., Laurance, W.F., 2008. How green are biofuels?. *Science 319(5859)*, 43-44.

[137] Martinez-Medina, A., Flors, V., Heil, M., Mauch-Mani, B., Pieterse, C.M.J., Pozo, M.J., Ton, J., van Dam, N.M., Conrath, U., 2016, Recognizing Plant Defense Priming. *Trends Plant Sci. 21(10)*, 818-822.

[138] Andrade-Linares, D.R., Lehmann, A., Rillig, M.C., 2016a. Microbial stress priming: a meta-analysis. *Environ. Microbiol. 18*, 1277-1288.

[139] Balmer, A., Pastor, V., Gamir, J., Flors, V., Mauch-Mani, B., 2015, The 'prime-ome': towards a holistic approach to priming. *Trends Plant Sci. 20(7)*, 443-452.

[140] Savvides, A., Ali, S., Tester, M., Fotopoulos, V., 2015, Chemical Priming of Plants Against Multiple Abiotic Stresses: Mission Possible?. *Trends Plant Sci. 21(4)*, 329-340.

[141] Hilker, M., Schwachtje, J., Baier, M., Balazadeh, S., Bäurle, I., Geiselhardt, S., Hincha, D. K., Kunze, R., Mueller-Roeber, B., Rilling, M. C., Rolff, J., Romeis, T., Schmülling, T., Steppuhn, A., Dongen, J. V., Whitcomb, S. J., Wurst, S. W., Zuther, E., Kopka, J., 2016. Priming and memory of stress responses in organisms lacking a nervous system. *Biol. Rev. 91*, 1118–1133.

[142] Appel, H. M., Cocroft, R. B., 2014. Plants respond to leaf vibrations caused by insect herbivore chewing. *Oecologia 175*, 1257-1266.

[143] Andrade-Linares, D. R., Veresoglou, S. D., Rillig, M. C., 2016b. Temperature priming and memory in soil filamentous fungi. *Fungal Ecol. 21*, 10-15.

[144] Nakayama, Y., Fujiu, K., Sokabe, M., Yoshimura, K., 2007. Molecular and electrophysiological characterization of a mechanosensitive channel expressed in the chloroplasts of *Chlamydomonas*. *Proc. Natl. Acad. Sci. 104(14)*, 5883-5888.

[145] Paik, S. M., Sim, S. J., Jeon, N. L., 2017. Microfluidic perfusion bioreactor for optimization of microalgal lipid productivity. *Bioresour. Technol. 233*, 433-437.

[146] Liua, Y., Wang, Z.J., Zhanga, J.W., Xia J., Chu, J., Zhang, S.L., Zhuang, Y.P., 2016. Quantitative evaluation of the shear threshold on *Carthamus tinctorius L.* cell growth with computational fluid dynamics in shaken flask bioreactors. *Biochem. Eng. J. 113*, 66–76.

[147] Lauersen, K.J., Baier, T., Wichmann, J., Wördenweber, R., Mussgnug, J.H., Hübner, W., Huser, T., Kruse, O., 2016. Efficient phototrophic production of a high-value sesquiterpenoid from the eukaryotic microalga *Chlamydomonas reinhardtii*. *Metabol. Eng. 38*, 331-343.

[148] Garcia Camacho, F., Gallardo Rodriguez, J.J., Sanchez Miron, A., Ceron Garcia, M.C., Belarbi, E.H., Molina Grima, E., 2007. Determination of shear stress thresholds in toxic dinoflagellates cultured in shaken flasks Implications in bioprocess engineering. *Process Biochem. 42*, 1506–1515.

[149] Dardik, A., Chen, L., Frattini, J., Asada, H., Aziz, F., Kudo, F.A., Sumpio, B.E., 2005. Differential effects of orbital and laminar shear stress on endothelial cells. *J. Vasc. Surg. 41(5)*, 869-880.

[150] Li, Z-G., Gong, M., 2011. Mechanical stimulation-induced cross-adaptation in plants: An overview. *J. Plant Biol. 54*, 358-364.

[151] Probst, A.V., Mittelsten, S. O., 2015. Stress-induced structural changes in plant chromatin. *Curr. Opin. Plant Biol. 27*, 8–16.

[152] Lämke, J., Bäurle, I., 2017, Epigenetic and chromatin-based mechanisms in environmental stress adaptation and stress memory in plants. *Genome Biol. 18*, 124-135.

[153] Yang, W., Catalanotti, C., Wittkopp, T.M., Posewitz, M.C., Grossman, A.R., 2015, Algae after dark: mechanisms to cope with anoxic/hypoxic conditions. *Plant J. 82*, 481–503.

[154] Johnson, X., Alric, J., 2013, Central Carbon Metabolism and Electron Transport in *Chlamydomonas reinhardtii*: Metabolic Constraints for Carbon Partitioning between Oil and Starch. *Eukaryot. Cell 12(6)*, 776-793.

[155] Hayashi, Y., Shinozaki, A., 2012, Visualization of microbodies in *Chlamydomonas reinhardtii*. *J. Plant Res. 125(4)*, 579-586.

[156] Nunes-Nesi, A., Carrari, F., Lytovchenko, A., Smith, A.M.O., Loureiro, M.E., Ratcliffe, R.G., Sweetlove, L.J., Fernie, A.R., 2005, Enhanced Photosynthetic Performance and Growth as a Consequence of Decreasing Mitochondrial Malate Dehydrogenase Activity in Transgenic Tomato Plants. *Plant Physiol. 137(3)*, 611-622.

[157] Verma, D., Samson, N.P., Koya, V., Daniell, H., 2008, A protocol for expression of foreign genes in chloroplasts. *Nat. Protoc. 3*, 739-758.

Abstract in Korean

국 문 초 록

광합성 미생물인 미세조류는 이산화탄소 저감 능력과 식량 자원으로의 활용성으로 최근 주목받고 있다. 인류의 식량안보와 에너지문제를 보다 효과적으로 해결할 수 있기 때문이다. 이로 인해 효율적인 공정 운영을 통한 미세조류의 대량 생산은 중요한 화두로 떠오르고 있다. 본 학위논문에서는 산업 공정에서 미세조류의 생산성 증대를 위해 필요한 실질적인 세가지 전략을 제시하였다.

첫번째는 불균형한 C/N 비율 유지 배양법이다. 미세조류 유래의 2차 대사산물은 항산화제 (루테인, 아스타잔틴 등) 및 중성지질 (TAG)로, 대부분이 유용물질이다. 이 물질들은 영양분이 고갈된 환경 하에 배양되는 미세조류 내에서 생성이 된다. 총 생산성을 향상시켜 경제성을 높이기 위해서는 세포 내 함량과 더불어 공정 당 생체량의 증가도 함께 수반되어야 한다는 점에서, 생체량 증가가 일어나지 않는 기존의 영양분 고갈법은 더 이상 현실적인 방안이 될 수 없다. TAG 생산의 경우, 최근 제시된 불균형한 C/N 비율 유도법을 통해 TAG 생산과 일정 수준 이상의 생체량 증가가 동시에 유도되는 현상이 확인되었다. 그러나, 이러한 회분식 공정 배양도 영양분이 고갈되는 순간이 존재하며, 영양분 고갈법과 마찬가지로 생체량 증가가 없는 일정 수준 이하의 TAG 가 생산된다. 본 연구에서는 연속식 배양 공정을 통해 영양분 고갈이 없는 불균형한 C/N 비율 유지 배양법을 제시하였다. 연속식 배양 공정과 농도 구배 생성이 가능한 미세유체 칩을 제작하였고, 낮은 농도의 인산염, 암모늄 용액을 유입시켜 높은 C/N 비율 혹은 Redfield 비율을 일정하게 유지시켜 배양하였다. 기존 대비 7.5%의 영양분 농도에서, 세포 내 TAG 함량에는 영향 없이 3 배의 생체량 증가가 유도되었고, 이는 총 TAG 생산성을 3 배 향상시킬 수 있다는

결론을 도출할 수 있다. 최종적으로 불균형한 C/N 비율을 유지시키면 생체량 증가에 의한 총 TAG 의 생산성을 향상시킬 수 있다는 것을 확인하였다.

두번째는 Stress priming 을 통한 세포의 배양기 내 난류에 대한 반응성 향상 유도법이다. 산업 규모의 배양기 내 교반기는 영양분의 공급을 원활하고 균일하게 한다. 하지만 교반기에 의해 유발되는 높은 전단응력은 세포의 생존율을 감소시켜 생체량 확보에 부정적인 영향을 미친다. 물리적 자극으로 세포의 분열을 촉진시키는 방법이 제시되었지만, 대규모 배양기 적용 시 소요될 설비비용과 예상되는 실질적인 효과를 고려하면 한계가 있다. 본 연구에서는 stress priming 효과를 적용하였다. 약한 스트레스로 스트레스 반응성이 준활성화된 primed 상태의 세포는 강한 스트레스 환경 내에서 생존율이 향상된다. 배양기 내 전단응력장 내 세포 생존율을 높이기 위해 세기가 덜한 진동 자극으로 미세조류를 전처리하여 stress priming 을 유도하였다. 높은 전단응력 환경 하에서 27%의 생체량 증가와 39% 단백질 생산성이 향상되는 것이 확인되었다. TRP11 은 스트레스 반응 Ca^{2+} 이온 채널로 진동과 배양기내 전단응력에 공통으로 발현됨이 확인되었다. 식물의 경우, Ca^{2+} 신호 전달 체계는 스트레스 반응성과 밀접한 관계가 있으며 CAMTA 에 의해 마스터 전사조절인자인 CBF/CREB1 가 발현되어 스트레스 반응을 하는 것으로 알려져 있다. 이와 달리 *C. reinhardtii* 내 신호전달체계가 밝혀지지 않았지만, stress priming 효과로 TRP11 이하의 신호전달 체계와 기계적 자극에 대한 스트레스 반응성이 활성화되어 대규모 배양 시 생체량을 증가시킬 수 있다는 것을 짐작할 수 있었다.

세번째는 malate 를 통한 세포 자체의 대사 활성화 촉진 방법이다. Malate 는 생체량 증가와 밀접한 관계가 있다. 고농도의 malate 처리 시 세포 내로 흡수되는 malate 의 양이 증가되며 성장 관련 인자의 요소가 증가된다는 보고가 있다. 또한 세포 내

malate 의 세포소기관 분배에 따라 생체량에 변화가 생기게 된다. 광합성 생물은 계속적인 빛에 노출되면 조효소인 NADPH 를 과생성하여 과환원상태의 엽록체를 유발할 수 있기 때문에, 엽록체 내 산화-환원 균형을 유지해야 한다. 각 세포소기관 내 조효소의 pool 을 유지하면서 NADPH 의 에너지는 대사 물질인 malate 로 전달되고, malate 는 다른 세포소기관으로 이동 · 분배가 된다. 그러면 에너지 분배를 통해 효율적인 대사가 일어나며, 식물의 경우 생체량 증가를 수반한다는 것이 밝혀졌다. 본 연구에서는 엽록체 내 malate 를 과생성하는 형질 전환 균주를 개발하여 malate 의 생체량 영향성을 검증하였다. 안정적인 malate 합성 효소의 발현을 위해 엽록체 형질 전환을 수행하였으며, 과생성되는 malate 의 자연스런 분배를 유도하였다. 엽록체 내 Malate 합성효소를 과발현하는 균주의 생체량이 기존 야생형 균주 대비 19% 증가하였다. 생체량 증가 현상을 이해하기 위해 수행한 RT-PCR 분석 결과, malate 와 연관되는 TCA 회로의 malate dehydrogenase (*MDH4*), acetate 동화대사와 관련된 TCA 회로의 acetyl-CoA synthetase (*ACS3*), 그리고 glyoxylate 회로의 isocitrate lyase (*ICL1*) 및 malate synthase(*MAS1*)의 RNA level 이 유의미하게 증가되었다. 대사유입분석(Flux Balance Analysis)에 따르면 혼합영양배양 시 위의 transcript 의 양이 증가한다는 보고가 있다. 좀 더 면밀한 분석이 필요하겠지만, Malate 합성 효소 과발현 균주 내 대사 과정은 혼합영양배양 시 광합성에 의한 에너지 생산보다는 TCA 회로 및 glyoxylate 회로를 통한 에너지 생산이 좀 더 효율적으로 이뤄져 생체량 증가가 가능했던 것으로 추측된다.

주 요 어: 미세조류, 미세조류 생체량, 중성지질, 관류형 미세유체 배양기, 스트레스 프라이밍, 말릭산 합성효소

학 번:. 2013-30302